Titre: Title:	Experimental and finite element dynamic response analyses of a human lumbar motion segment
Auteur: Author:	Mehran Kasra
Date:	1991
Type:	Mémoire ou thèse / Dissertation or Thesis
Référence: Citation:	Kasra, M. (1991). Experimental and finite element dynamic response analyses of a human lumbar motion segment [Ph.D. thesis, Polytechnique de Montréal]. PolyPublie. https://www.proquest.com/docview/231014607

UNIVERSITE DE MONTREAL

EXPERIMENTAL AND FINITE ELEMENT DYNAMIC RESPONSE ANALYSES OF A HUMAN LUMBAR MOTION SEGMENT

Par

Mehran KASRA

DEPARTEMENT DE GENIE MECANIQUE

ECOLE POLYTECHNIQUE

THESE PRESENTEE EN VUE DE L'OBTENTION

DU GRADE DE PHILOSOPHIAE DOCTOR (Ph.D.)

(GENIE MECANIQUE)

Mars 1991

UNIVERSITE DE MONTREAL

ECOLE POLYTECHNIQUE

Cette thèse intitulée :

EXPERIMENTAL AND FINITE ELEMENT DYNAMIC RESPONSE ANALYSES OF A HUMAN LUMBAR MOTION SEGMENT

Présenté par : Mehran Kasra

en vue de l'obtention du grade de : Ph. D.

a été dûment acceptée par le jury d'examen constitué de :

M. Jean Rousselet....., Ph.D., président

M. Aboulfazl Shirazi-Adl....., Ph.D.

M. Gilbert Drouin....., Ph.D.

M. Hocine Yahia....., Ph.D.

M. Malcolm H. Pope....., Ph.D.

ABSTRACT

In order to improve our understanding of the dynamic characteristics of the human lumbar spine, both experimental and finite element methods are called for. In the experimental part, using a MTS Bionix testing machine, the axial steady state response, resonant frequencies, and damping of seven lumbar motion segments are measured under an upper body mass of 40 Kg. The influence of the presence of posterior elements and different magnitudes of compression preload on the response is also studied.

To supplement the measurements, using the ADINA program, linear and nonlinear, axisymmetric and 3-D finite element models of a L2-L3 disc-vertebra unit are developed to predict the free and forced vibration response. The step and harmonic loadings in axial direction are considered for the forced vibration analysis. The effects of the presence of the body mass and compression preloads are also examined. In the axisymmetric model, the annulus is represented as a homogeneous orthotropic mixture of fibres and matrix. A nonhomogeneous composite of collagenous fibres embedded in a matrix of ground substance is however taken for the 3-D modelling. The nucleus, in both models, is simulated by either displacement-based or potential-based fluid ele-

ments.

The results of experimental and finite element studies appear to be in good agreement with each other. They indicate that the system resonant frequencies are reduced considerably with the addition of a body mass of 40 Kg and increase significantly ($p<.005$) as the compression preload increases. The compliance at both low and resonant frequencies decrease with increasing compression preload. Removal of the facet joints tend to slightly decrease the segmental resonant frequencies irrespective of the magnitude of compression preload ($p<.1$).

The finite element model studies show quasi-static response under harmonic loads with periods much larger than the fundamental period of the segment and under ramp loads with slow rising times. Under a step load without the body mass, the nucleus pressure varies with both location and time and reaches a maximum of about 2.7 times that under equivalent static load. Addition of a 40 Kg mass, in this case, renders a single degree-of-freedom response with the pressure nearly remaining constant with location inside the nucleus. The stresses and strains throughout the segment in this case increase by about twice in comparison with equivalent static values.

The effect of the disc degeneration on the resonant frequency is also studied by reducing the value of the nucleus bulk modulus and nucleotomy in the finite element models. The results predict a decrease in the resonant frequency by removing the nucleus or reducing its bulk modulus value.

The results indicate that the most vulnerable element under axial vibration loads is the cancellous bone adjacent to the nucleus space. Fatigue fracture of bone as a cumulative trauma and the subsequent loss of nucleus content likely initiate or accelerate the segmental degenerative processes. The annulus fibres do not appear to be vulnerable to rupture when the segment is subjected to pure axial vibration.

RÉSUMÉ

Les maux de dos constituent la deuxiéme cause d'absentéisme au niveau des accidents de travail en Amérique du nord. Il a été rapporté que les maux de dos, les blessures et les maladies dégénératives de la colonne vertébrale se retrouvent le plus fréquemment chez les personnes sujettes à des chargements dynamiques (choc et vibration).

Les vibrations généralement rencontrées, notamment dans l'industrie, sont d'origines diverses et peuvent être classées en quatre catégories : vibrations produites par un processus de transformation, vibrations liées aux modes de fonctionnement des machines et matériels, vibrations dues à des défauts de machines ou à de mauvais fonctionnements, vibrations résultant de phénomènes naturels (comme, le vent, la houle et les séismes).

Dans le cas de vibrations produites par un processus de transformation ou de vibrations transmises à l'ensemble du corps, les symptômes pathologiques les plus courants se situent au niveau de la colonne vertébrale, assez fréquemment chez les conducteurs de tracteurs agricoles, de camion, de pilotes d'hélicoptères, etc. Lombalgies,

lombosciatiques, cervicalgies, hernies et pincements discaux sont les troubles les plus souvent cités. Ils apparaissent après un certain temps d'exposition aux vibrations; de plus, les vibrations sont souvent un facteur d'aggravation de lésions rachidiennes pré-existantes.

Pour étudier le comportement de la colonne vertébrale, on considère habituellement un ensemble vertèbre-disque-vertèbre. Cet ensemble est appelé segment fonctionnel ou unité fonctionnelle. Le disque intervertébral est essentiel pour assurer le maintien et la mobilité de la colonne vertébrale. Agissant comme une sorte de joint universel, il permet des mouvements dans plusieurs directions. Lors d'une activité normale, le disque est soumis à des contraintes mécaniques considérables. Cette situation répetée des centaines de milliers de fois tout au long d'une vie, peut être la cause de dégénération, d'hernie ou de déplacement du disque et peut entraîner des blessures chroniques de la colonne vertébrale.

Afin d'améliorer notre compréhension de la caractéristique dynamique de la région lombaire de la colonne vertébrale de l'être humain, une étude expérimentale ainsi qu'une méthode d'éléments finis ont été utilisées. Dans l' etude expérimentale, la réponse axiale sta-

tionnaire, la fréquence de résonance et l'amortissement de sept segments fonctionnels de la région lombaire ont été mesurés, sous une masse de 40 kg et à l'aide d'une machine MTS bionix. L'influence de la présence des facettes articulaires et de différents niveaux de compression initiale sur la réponse est aussi etudiée.

Pour compléter les mesures expérimentales, des modéles linéaire et non linéaire, axisymétriques et tridimensionnels d'une unité vertèbre-disque-vertèbre L2-L3, sont utilisés pour prédire les réponses des vibrations libres et forcées. Les chargements en échelon et sinusoïdal sont considérés pour l'analyse de la vibration forcée. Les effets dûs à la présence de la masse corporelle et de la compression initiale sont aussi examinés.

Pour le modèle axisymétrique, l'anneau fibreux est representé par un modèle orthotropique homogène et pour le modéle en trois dimensions, il est representé par un matériel non homogène de fibres collagènes dans une substance matricielle. Le noyau dans les deux modèles est simulé par les élément fluides.

Les résultats d'études expérimentales et d'éléments finis semblent bien concorder. Ils indiquent que les

fréquences de résonance du système sont diminuées nettement avec l'addition de la masse corporelle (40 Kg) et augmentent de facon significative ($p < 0.005$) avec la charge initiale. La compliance et l'amortissement interne (hystérésis) à des fréquences beaucoup plus basses que la frequénce de résonance diminuent avec l'augmentation de la charge initiale.

En l'absence des facettes articulaires la fréquence de résonance du segment fonctionnel diminue un peu, et ce résultat n'est pas influencé par l'ampleur de la charge initiale ($P < 0.1$).

Le taux d'amortissement visqueux à la fréquence de résonance est mesurée par trois méthodes différentes (Méthode-"$\sqrt{2}$", Méthode d'amplification, la perte d'énergie par cycle). Sa valeur varie entre 0.05 et 0.13 et l'effet de la charge initiale n'est pas significatif.

Les études des modèles d'éléments finis indiquent une réponse quasi-statique sous une charge sinusoïdale avec des périodes beaucoup plus grandes que la période fondamentale du segment fonctionnel et sous une charge en rampe avec un temps d'élévation lent. Sous une charge en échelon sans la masse corporelle, la distribution de pression dans

le noyau change avec le temps, et elle atteint une valeur maximale, d'environ 2.7 fois la valeur atteinte dans le cas statique. Avec l'addition d'une masse de 40 Kg, la réponse du système est celle d'un système à un degré de liberté, et la distribution de pression est constante dans l'anneau. Les contraintes et les déformations dans ce cas sont cependant deux fois plus élévées que dans le cas statique équivalent.

L'effet de dégénération du disque sur la fréquence de résonance est representée par la réduction de la valeur de module de volume du noyau pulpeux dans les modèles d'éléments finis. Les résultats prédisent une diminution de fréquence de résonance avec la réduction de la valeur de module de volume.

Si l'on étudie par éléments finis l'état des contraintes et des déformations dans le corps vertébrale, les résultats indiquent que l'élément le plus vulnérable sous une charge (axiale et vibratoire) est l'os spongieux près de l'anneau. La fracture de l'os spongieux et une perte de matière du noyau pulpeux peut-être le commencement de la dégénération du segment fonctionnel. De plus les résultats indiquent que l'anneau fibreux est moins susceptible aux vibrations axiales.

ACKNOWLEDGEMENTS

The author would like to take this opportunity to express his sincere thanks to professor A. Shirazi-Adl (Department of Mechanical Engineering) for his guidance, particularly with respect to the analytical and clinical aspects of the present work, as well as continual encouragement throughout this investigation. Equal gratitude is also extended to professor G. Drouin (Institute of biomedical Engineering) for his precious advice concerning the experimental aspect of this study and for his constant encouragement as well.

Finally, the financial assistant provided by the NSERC and the MRC (Canada) is gratefully acknowledged.

LIST OF CONTENTS

LIST OF FIGURES

LIST OF TABLES

LIST OF APPENDICES

CHAPTER 1

INTRODUCTION

1.1 GENERAL

Disorders of the lumbar spine are among the most common medical problems in western countries which affect from 50 to 80% of the population [34,108]. Besides the grave human suffering involved, the economical impact of low-back pain on society is enormous. It has been estimated that the total economic burden of this disorder in the United States exceeds $10 billion annually [108]. It is further reported that, among chronic conditions in the United States, impairments of the back and spine are the most frequent cause of activity limitation in persons under age 45 years [61].

In spite of considerable effort by a large number of researchers, the determination of the causes of low-back pain in the majority of cases continues to remain a formidable challenge. In many instances, the exact cause of low-back pain cannot be determined despite thorough evaluation of the patient by a capable clinician [108]. In order to advance the understanding and treatment of this problem, the need for multi-disciplinary investigation in the areas such as epidemiology, anatomy, biochemistry, neuromechanics and biomechanics has been recognized [108]. Although the

natural history of disc disorders is a matter of uncertainty, epidemiological and biomechanical studies indicate that mechanical factors (such as; heavy manual handling, vibration and impact) play a prominent role [14,18,21,33, 43,44,58,80,99,107,108].

The human spine is a complicated dynamic system which during daily activities is exposed to static loadings with vibration and impact superimposed. Previous epidemiological studies have suggested an increased risk of low-back pain in truck drivers, bus drivers, air crew and generally in people with occupations involving vibration and multiple impacts [17,21,25,32,43,44,81]. It is therefore difficult to minimize the need for consideration of the mechanical factors when dealing with low-back disorders. Consequently, the biomechanical aspects of the lumbar joint have been the subject of considerable experimental and mathematical investigation. The majority of the investigations, experimental as well as mathematical aim at analysing the behaviour of the spinal segments under static or quasi-static loadings. Compare to static analyses, the reported literatures on the dynamic analysis of the motion segments are a few, and the biomechanics of the spinal segments under dynamic loadings still needs to be further clarified.

1.2 PREVIOUS EXPERIMENTAL STUDIES

Under static loadings, there has been many experimental investigations reported on the measurements of the state of deformation in various joint components [7,8,28,65,75,79,100,104] and the intradiscal pressure [57,66,102].

In experimental dynamic analysis of the spine, considering the likely role of vibrational environments in the causation of the low-back pain and spinal disorders, there has been a considerable interest in the measurement of the whole body vibration response. In these tests, the subject is usually seated in various postures, and accelerations at the lumbar level and/or head are recorded while the seat is subjected to vertical impact or vibrations [11,13,36,37,65,69,70,71,72,74,84,85,111]. These in-vivo studies have demonstrated that the resonant frequency of the body in the axial direction is at about 4-6 Hz which is noted to be in the range of frequencies at which many vehicles operate [43,44,111]. This emphasizes the need to modify the seat design and the posture in order to avoid potentially harmful frequencies and hence reduce risk of injury.

A number of in-vitro experiments on the single or multi-motion segments of the spine have been carried out in

order to better understand the dynamic charateristics of the intervertebral joints. Hirsch [28] performed impact tests on lumbar discs by free falling weights and analysed the effect of preload and falling height on the segmental response. For a constant falling height, he noted a decrease in the initial shock compression as the preload increased. This stiffening behaviour of the motion segments due to an increase in the preload was also reported by Kazarian [30]. In his studies, Kazarian measured steady state impedance data (magnitude and phase angle) for different motion segments under axial compression at a frequency range of 5 to 50 Hz. The recorded quasi-static response under these frequencies demonstrated that motion segments should have higher fundamental frequency. Some L5-S1 specimens, however, appeared to have resonant frequencies at about 30 to 40 Hz. Assuming a single degree-of-freedom system, Markolf [53] carried out axial resonant tests to evaluate the equivalent axial damping factor. A resonant frequency of about 240 Hz was found in the presence of an added mass (simulating the head) on top of the segment. Long-term vibration response analyses of the motion segment have shown an increase in the segmental stiffness [94] and creep rate [110] and a decrease in the hysteretic damping [94]. Koeller et al [38] studied the segmental response to axial dynamic compression as a function of the age. They found however that the age of subjects markedly influences

the disc biomechanics so far as the axial deformability and creep response are concerned.

1.3 PREVIOUS FINITE ELEMENT STUDIES

To supplement the foregoing experimental investigations, a number of researchers have carried out finite element studies. Due to the inhomogeneous structure of the lumbar joints with highly irregular geometry, the classical stress analysis is unsuitable. Hence, the finite element method of structural analysis becomes a particularly appropriate technique to evaluate the state of strain and stress in such a body with complex shape, loading and material behaviour. In response to the need for investigation in the areas such as artificial joint replacement, fracture fixation methods, and lumbar disc disorders, the finite element method has long proved its usefulness and potential as a tool in orthopaedic biomechanics. For the purpose of the present project, only those analyses related to the single or multi-motion segments of the spine are intended to be discussed and evaluated.

Various finite element models have been developed for the study of spinal motion segments which are based on elastic, viscoelastic and poroelastic response [4,22,40,41, 48,87,89,92,93,96]. In static analyses, Considering the elastic models, an oversimplified axisymmetric finite ele-

ment model of the disc-vertebra unit taking annulus as a linear homogeneous isotropic material was reported by Spilker et al [95]. The nucleus was assumed as an incompressible inviscid fluid with its generated pressure taken as an unknown. The model was used to examine the effect of gross disc geometry and material properties on the predicted intradiscal pressure, radial disc bulge, and vertical deflection under compressive load of 400 N. The first detailed report of an elastic finite element model of the disc-vertebra unit is by Belytschko et al [4]. These authors modelled the unit as an axisymmetric body, the annulus as layers of homogeneous linear orthotropic material and the nucleus pulposus was assumed to be an incompressible inviscid fluid. Since then more progress has been made such that the report by Shirazi-Adl et al [89] contains the details of a nonlinear three-dimensional model where the annulus has been represented as a composite of collagenous fibres embeded in a matrix of ground substance.

Liu and Ray [48] reported a linear viscoelastic axisymmetric finite element model of an intervertebral joint in order to predict the creep response under constant compression load.

For finite element dynamic response analysis, Hakim and King [22] used a linear three-dimensional model of a

vertebra-disc unit in which the disc was represented by a number of uniaxial elements. They computed a fundamental frequency of 846 Hz for the unit. A nonlinear three dimensional axial dynamic response analysis of a disc-vertebra unit was performed by Natali and Merio [60]. Under the axial load considered in their study, the model predicted a quasi-static response with a time variation similar to that of the applied axial load. Simon et al [92,93] studied the steady state response of an axisymmetric model of the disc-vertebra unit in which the tissues were modelled as linear poroelastic materials. For frequencies about and above 1 Hz, they concluded that the pore fluid remained trapped inside the solid phase resulting in no relative fluid-solid motion. They compared their computed results with the quasi-static experimental data of intervertebral discs reported by Kazarian [30]. Goel et al [20] used a linear three-dimensional finite element model for frequency analysis of the lumbosacral spine and predicted a resonance frequency of about 5.8 Hz. The experimental results of the same segments reported by Kazarian [30] however showed higher resonance frequencies (30 to 40 Hz). There are also some other dynamic models of the spine reported in the litrature [26,39,49,73,112]. These models study the overall response of the spine and do not give any information about the state of stress and strain in the intervertebral discs.

1.4 PRESENT STUDY AND ITS OBJECTIVES

In the foregoing studies, for example, the presence of the upper body mass has often been neglected. Apart from the mass, the effect of the presence of facet joints and that of various magnitudes of the compression preload on the response need also to be considered. These factors influence the stiffness of the system and hence its time-dependent characteristics. Moreover, in some studies, the rising time or the vibration period of the applied compression load is much larger than the fundamental periods of vibration of the intervertebral discs. These cases require only a quasi-static analysis in which the inertia and damping effects are negligible and the time variation of the predicted results closely resembles that of the applied load. It is therefore clear that there is a need for further detailed experimental and finite element investigations on the dynamic behaviour of spinal motion segments.

The objectives of the present research work have been set as follows: (1) Experimental measurement of the basic dynamic characteristics (such as: steady state response, resonant frequencies, damping) of spinal motion segments in the axial direction. The mass of the upper body is accounted for in the tests, and the role of the posterior elements, in particular facet joints, on the response is examined by repeating the tests following the removal of

these elements. Moreover, the response is measured under different magnitudes of the compression preload to evaluate the influence of upper-body weight, external loads carried, and muscle contraction forces on segmental dynamics; (2) Linear and nonlinear, dynamic, axisymmetric and three-dimensional finite element model studies of a L2-L3 disc-vertebra unit. The model studies are performed to supplement the experimental part (with the posterior elements removed). Both frequency and forced response analyses are performed. In the frequency response analyses of the models, natural frequencies and corresponding mode shapes are computed, these results are then used to predict the forced vibration responses of the models.

1.5 ORGANIZATION OF THE PRESENT REPORT

General scope of the problem, reported experimental studies, previous finite element models of the lumbar joint and objectives of this study have already been dealt with in this chapter.

A short review of the literature relating to the anatomy and structure of a lumbar intervertebral joint including its various components and loading is presented in chapter 2.

Chapter 3 presents experimental and finite element

methods. Experimental method describes specimen preparation, test equipment, and test procedure. The methods used to measure the system damping is also explained in this section. In describing the finite element method, first a brief discussion about the problem formulation (fluid-solid interaction) is presented. This is then followed by discussing the developement of the axisymmetric and three-dimensional models.

The experimental measurements of static deformations, resonance frequencies, steady state response, damping, and their corresponding finite element predictions under different preloads are presented and discussed in chapter 4. The finite element predictions also include the variation of intradiscal pressure, and stresses at different parts of the joint.

Chapter 5 deals with the in-depth discussion of the results of the analyses presented in the previous chapter. This includes comparison of the experimental and finite element results with each other and with those of previous works, and discussions on frequency response, damping characteristics, effect of the posterior elements, and finite element models. The vulnerable sites of the lumbar joint under different loadings are also identified and correlated with the results of clinical studies.

Chapter 6 provides a short summary of the prominent features of the analyses, conclusions, and some directions for further research.

CHAPTER 2

GENERAL ANATOMY AND STRUCTURE OF THE LUMBAR INTERVERTEBRAL JOINTS

2.1 INTRODUCTION

This chapter presents a short review of the literature relating to the anatomy and structure of the intervertebral joints [89]. Familiarity with the content of this chapter will prove helpfull in comprehension of succeeding ones.

The vertebral column, having a length of about 70 cm, consists of seven cervical vertebrae, twelve thoracic vertebrae, five lumbar vertebrae, five fused sacral vertebrae and three to four fused coccygeal segments. The anterior and lateral views of a vertebral column are shown in Fig. 2.1. The vertebrae are joined by the intervertebral ligaments and the intervertebral discs. The discs are 23 in number and constitute about 25% of the column length. This ligamentous column, then, is markedly stiffened by the rib cage and the trunk muscles.

2.2 A LUMBAR INTERVERTEBRAL JOINT

As is shown in Fig. 2.1, the lumbar spine is that part of the spine located in between the thoracic and the sacrum regions and is distinguished by its sagittal curva-

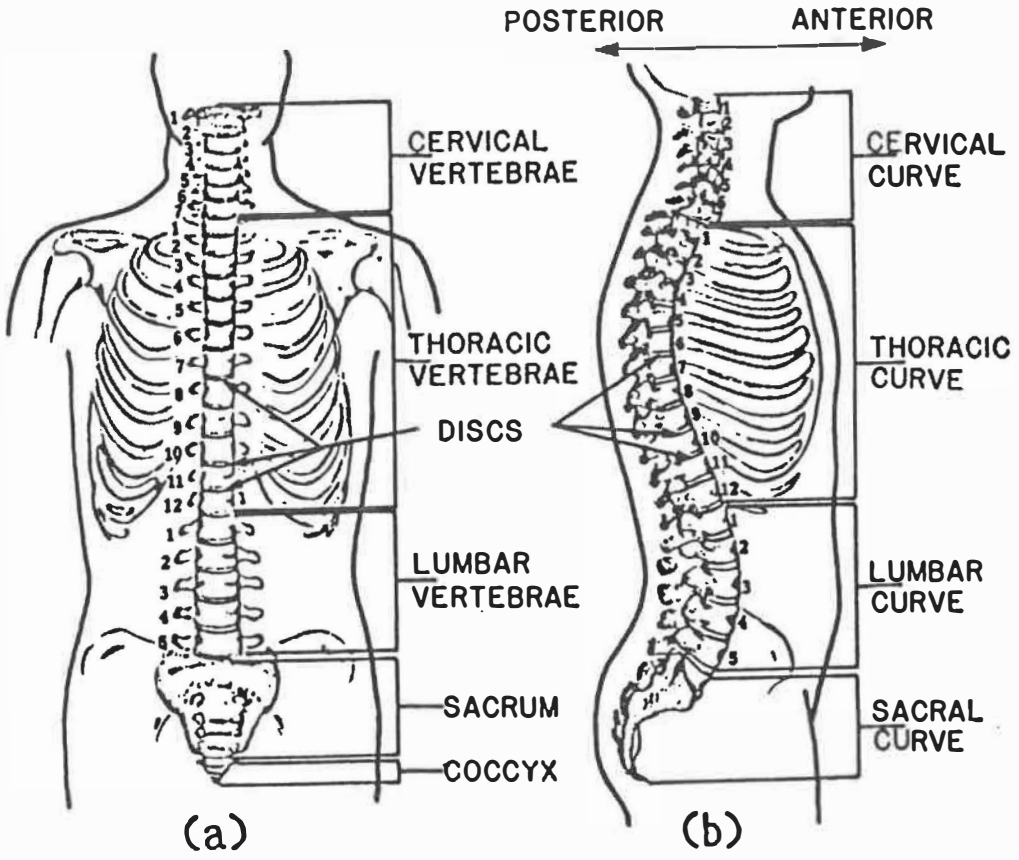

Fig. 2.1 Vertebral column. (a) Anterior or frontal view, (b) Lateral or sagittal view [89,101].

ture referred to as lumbar lordosis. The designations of the lumbar vertebrae from top to bottom are usually L1, L2, L3, L4 and L5 respectively while those of the lumbar discs are L1-L2, L2-L3, L3-L4, L4-L5 and L5-S1 respectively.

A lumbar intervertebral joint is defined to consist of two adjacent vertebrae including the bony posterior elements together with the interconnecting disc and ligaments. However, neglecting the bony posterior elements and ligaments, the remaining structure is referred to as the disc-body unit.

Although the exact geometrical characteristics of the joint components are subject to some variations in different lumbar levels, their basic shape remains essentially unaltered. The following sections present discussions of each of the constituent components of a typical lumbar intervertebral joints.

2.2.1 Lumbar Vertebrae

Superior and lateral views of a lumbar vertebra are shown in Fig. 2.2. Each vertebra consists of an anterior body which is cylindrical in shape and a posterior ring, known as the neural arch. The neural arch consists of two pedicles and two laminae, from which arises articular, transverse and spinous processes. The superior and inferior

surfaces of a vertebral body, being slightly concave, are the vertebral end-plates. The whole vertebra is a mass of cancellous bone contained in a relatively thin shell of cortical bone. The central part of the vertebral end-plate is composed of a thin plate of hyaline cartilage separating the central portion of the disc from the adjacent cancellous bone of the vertebral body. However, with advancing age the central cartilage undergoes calcification and replacement by bone [103].

The posterior articulating processes of two adjacent vertebrae, known as facets, together with their cartilaginous articular surfaces and capsular ligaments form posterior joints which are often refered to as the facet joints. The articulating surfaces of the facet joints are usually curved, the inferior ones being convex, and the superior ones concave. There is considerable variation in orientation of the facet joints in different levels of the lumbar spine.

2.2.2 Lumbar Discs

The lumbar intervertebral discs are subjected to a variety of loadings during physiological activities. Due to its structural characteristics, the disc provides sufficient flexibility to the trunk and hence, under various loadings, it undergoes relatively large deformations.

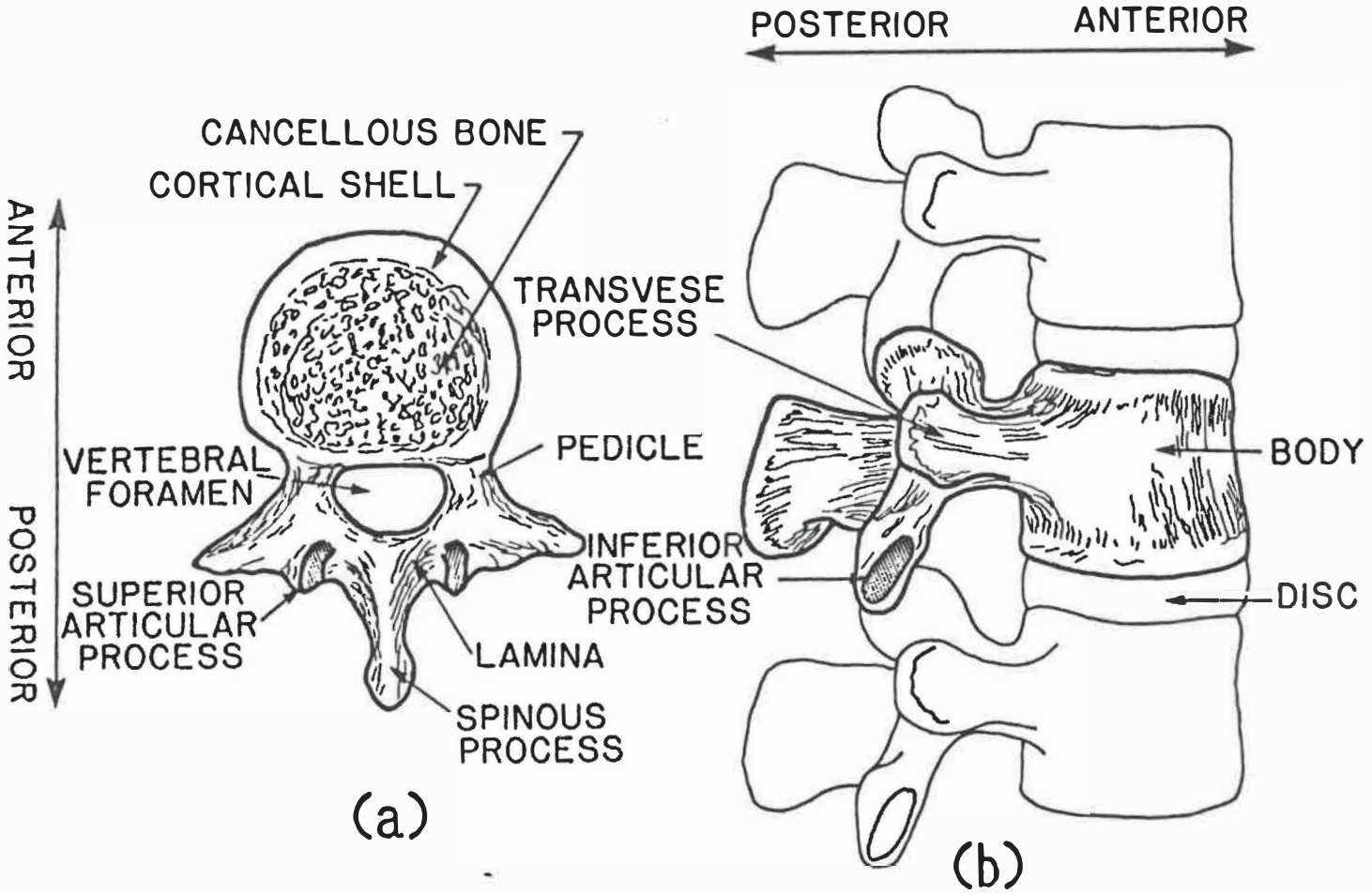

Fig. 2.2 Lumbar vertebrae. (a) Superior view, (b) Right lateral view [89,101]

The intervertebral disc is comprised of three distinct parts, the nucleus pulposus, the annulus fibrosus, and the cartilaginous end-plates. As is illustrated in Fig. 2.3, the nucleus pulposus is located nearly in the central portion of the disc, occupying about 30 to 60 percent of its cross-sectional area [53,55,109]. The nucleus pulposus of the normal or slightly degenerated discs, having water content of 80 to 90 percent, is generally confirmed to act as an incompressible fluid [55,56,103]. This has been done by both biochemical analyses of the constituent materials of the nucleus and direct measurements of the intradiscal pressure at different locations inside the nucleus. The nucleus water content is highest at birth and decreases with age, reaching a minimum of about 70 percent. After middle life, with a loss of water and an increase in collagen, the normal gelatinous nucleus becomes semi-solid and exhibits a fibrous viscous structure. Therefore, although at young age the annulus and nucleus are quite distinct, with advancing age they tend to merge with a less distinct transitional zone so that it becomes nearly impossible to ascertain where the nucleus ends and annulus begins [77,83].

The annulus fibrosus, illustrated in Fig. 2.3, gradually becomes differentiated from nucleus and forms the outer boundary of the disc. This structure is comprised of

a series of concentric laminated bands. Each band or layer contains strong collagenous fibres embedded in an amorphous ground substance [19], referred to as annulus bulk. These fibres are inclined with respect to the horizontal plane of the disc, the angle of inclination changing alternately from one band to the next. The range of variation of this angle is reported to be from 24 deg. to 45 deg., with an average value of 29 deg. to 30 deg [14,19,109]. Since the ground substance is a relatively soft material, the deformation behaviour of the annulus in tensile loadings can be expected to be dependent directly upon the amount of collagenous fibres present in the annulus. Therefore, on the basis of comparison of the strengths of the annulus samples with those of isolated collagenous fibres, Galante [19] suggested a collagen fibre content of about 16% of the volume of the annulus. This value is in general agreement with biochemical investigations [24,98]. It has been reported that the collagenous fibres are present mainly in the outer layers of the annulus [98]. Because of their high tensile strength, the collagen fibres appear inextensible relative to the deformation of the ground substance. The pure collagenous fibre first behaves elastically with a Young's modulus of up to 1000 MPa or more [24,82], and then begins to soften as strains increase beyond 3 to 7 percent [76,106], reaching an ultimate tensile strength of about 100 MPa or more [24,82]. On the basis of the foregoing, it

appears clear that the fibres of the annulus, because of their strength and orientation, play a major role in determining the deformation response of the disc.

In the inner zone, the annulus fibres are attached to the cartilaginous end-plates, while in the more peripheral zone they attach directly to the vertebral bodies. The outer attachment to the vertebrae, as expected, are stronger than the more central ones. The water content of the annulus is lower than that of the nucleus and with advancing age reduces slightly to 70 percent by middle age.

The cartilaginous end-plate is composed of a thin plate of hyaline cartilage separating the central portion of the disc from the adjacent cancellous bone of the vertebral body. As noted earlier, with advancing age this structure undergoes calcification and replacement by bone.

2.2.3 Lumbar Ligaments

The main constituents of ligaments are collagen and ground substance. Ligaments as uniaxial structures are most effective in carrying tensile loads along the direction of their fibres. The seven ligaments that connect two adjacent lumbar vertebrae together with their fibre directions are shown in Fig. 2.4. Due to their material characteristics, initially, ligaments are easily stretched and, therefore,

allow adequate motions during physiological activities. However, at larger tensile strains, they become increasingly stiffer and thereby perform their protective function of limiting the deformations in traumatic situations.

The most anteriorly located ligaments are called the anterior longitudinal ligaments which are wide fibrous sheets and are attached to the anterior surfaces of the vertebral bodies. At the disc level, they blend with the outer fibres of the discs. The posterior longitudinal ligaments are also blended intimately with the outer layers of the discs and are attached strongly to the posterior edges of the vertebrae, but very poorly to the posterior surfaces of the vertebrae. The intertransverse ligaments pass between the transverse processes. The adjacent spinous processes, from root to the apex, are connected by the interspinous ligaments while their tips are attached by the supraspinous ligaments. The capsular ligaments attach the articular processes, while the ligamenta flava extend from the edges of the upper laminae to those of lower laminae and bridge the intervening gaps.

2.3 INNERVATION OF LUMBAR SPINE

The lumbar spine, protecting the crucial spinal cord, is itself supplied with nerves branching out of the cord. It is evident that any element of lumbar spine which

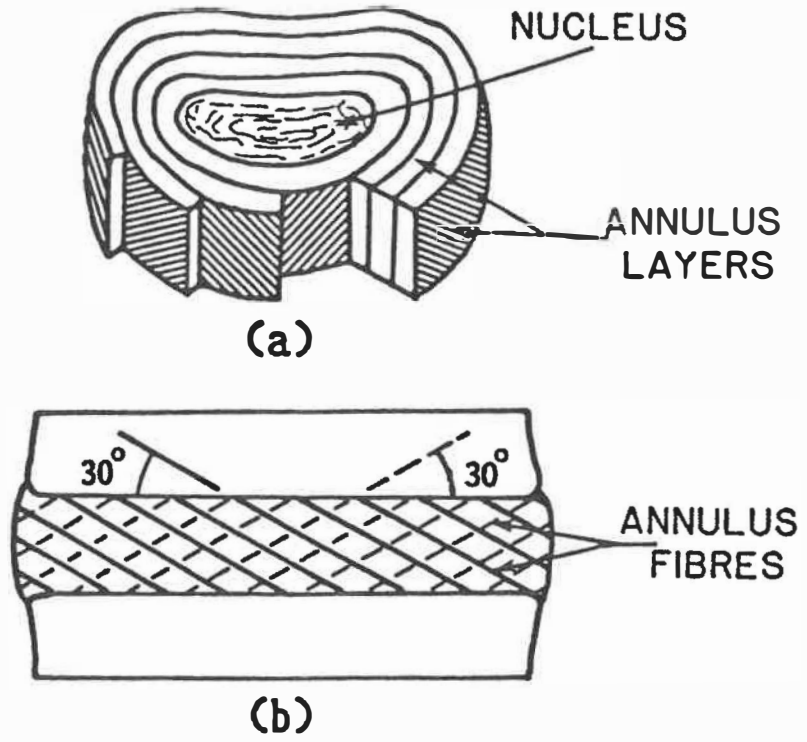

Fig. 2.3 Intervertebral disc. (a) Nucleus pulposus surrounded by the annulus layers, (b) Fibre orientations [89,109].

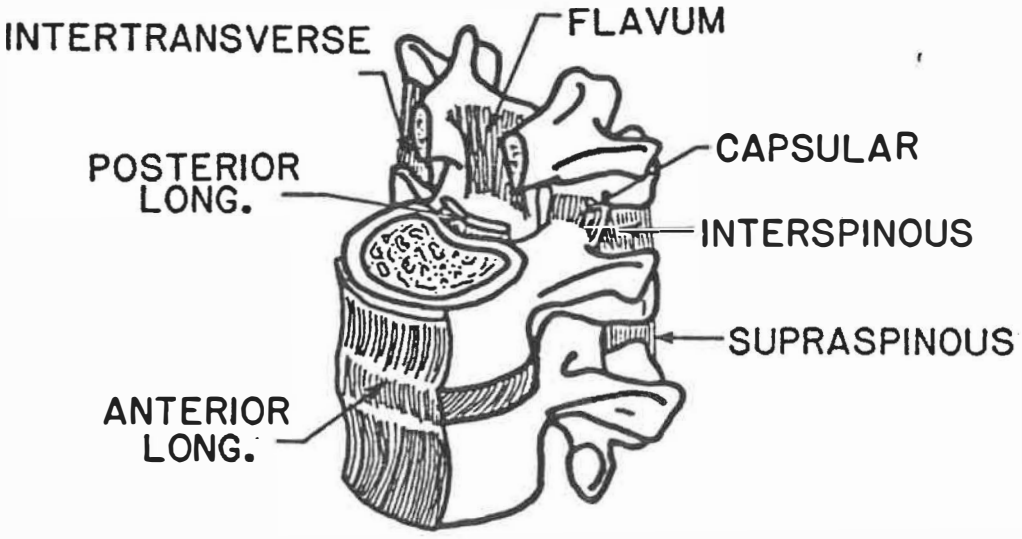

Fig. 2.4 Ligaments of lumbar intervertebral joints [89,109]

is innervated, may well be a potential source of pain. A knowledge of the lumbar innervation is thus of fundamental importance in the diagnosis and treatment of low-back pain. The innervation of the lumbar spine has been studied by various investigators [14,51,59,103,114,116]. These studies indicate the presence of the nerve endings in cartilaginous and ligamentous tissues as well as bony elements of the lumbar joints. In terms of the discs, recent studies [116] have supported the earlier reports [51] that the disc annulus is innervated at its outer layers. The inner layers of the annulus as well as the nucleus pulposus are generally believed to be devoid of nerve endings.

2.4 DYNAMIC LOADINGS ON LUMBAR SPINE

The lumbar spine during the course of daily activity is subjected to a variety of static and dynamic loadings consisting mainly of axial compression.

Dynamic loads on the spine are mainly, either in the form of compressive impacts (for example, due to a car accident, falling, pilot ejection) or whole-body vibrations which are caused by driving motor vehicles or operating industrial machineries [21,43,44]. These vibrations are mainly vertical with different basic frequency bands. Most of the large motor vehicles possess similar vibration spectral shape characteristics. For example, The basic truck

vibrations are in the 0 to 10 Hz frequency band while the basic bus vibrations are in the 0 to 15 Hz band. Mean acceleration levels typically range from 0.03 to 0.3g [21]. Whole-body vibration is most likely to be applied to vehicle operators in the vertical direction. Studies of the mechanical response of the human body in the vertical (seat to head) direction have shown that the major whole-body mechanical effects are produced in the frequency range 3 to 7 Hz, with the whole-body resonance occuring around 5 Hz [21]. At this frequency, the human body being vibrated in the sitting erect position absorbs more mechanical energy than at any other frequency.

CHAPTER 3

MATERIALS AND METHODS

3.1 INTRODUCTION

This section presents both the experimental procedure and the finite element model used in this study. The experimental part deals with the application of an axial sinusoidal force to the lumbar motion segments (with a mass of 40 Kg on top) under different compression preloads, with and without the posterior elements, in order to investigate their steady state compliance response and damping characteristics. Mechanical compliance is defined as the complex ratio of the resulting displacement to the applied sinusoidal force where the force and displacement are taken in the same direction and at the same point. The finite element part, on the other hand, presents the details of a number of axisymmetric and three dimensional models employed to predict the linear and nonlinear response of a disc-body unit under impact and vibration.

3.2 EXPERIMENTAL INVESTIGATION

3.2.1 Preparation and Evaluation of Specimens

One thoracolumbar (T12-L1) and six lumbar (L2-L3) motion segments have been removed from 6 fresh human cadaveric columns. The subject sex, age, cause of death, and

disc degeneration rating are listed in Table 3.1. The specimens are dissected free from surrounding soft muscular structures while the posterior structures (facet joints and ligaments) are left intact. After dissection, each specimen is wrapped in a saline soaked bandage and inserted into a plastic bag. The bag is then vacumed, sealed, labelled and placed in the deep freeze. Prior to testing, specimens are removed from the freezer and thawed for about 14 hours in a refrigerator. Throughout the thawing period the specimens have remained sealed in their plastic bag. Prior to testing, the distal and proximal vertebrae of the thawed specimens are firmly embedded in two aluminium cups (upper and lower cups) using formatray powder and three side screws for each cup (Figs. 3.1-3.2). The specimens are positioned in the cups in a manner that the horizontal surfaces of the cups and the disc horizontal mid-planes remain perpendicular to the axis of the actuator. The specimens are kept moist during the preparation and testing procedure by using liberal amount of saline solution. At the end of all the tests, the intervertebral discs are sliced at the mid-height plane. The degeneration rating is then done by the visual inspection according to the following conventional classification system [16,31].

Grade 0: Disks without changes visible to the unaided eye and with gelatinous shiny nucleus pulposus which

can easily be distinguished from the grossly unruptured annulus.

Grade 1: Disks with the nucleus pulposus somewhat more fibrosus but still clearly distingushible from the intact annulus fibrosus.

Grade 2: Discs with gross changes in both the nucleus pulposus and annulus fibrosus. In this case the nucleus is fibrotic but still soft, and the annulus has some fissures. The two are less clearly, yet perceptibly, demarcated.

Grade 3: Discs with marked gross changes in the form of fissures or cavities in both the nucleus pulposus and the annulus fibrosus.

Scores of 2 or 3 were taken as evidence of disc degeneration. The photographs of the gross appearance of the cut surfaces of the discs are shown in Figs. I.1-I.7 of Appendix I.

Table 3.1. Test specimens

Specimen No.	Cadaver No.	Sex	Age	Disc level	Disc grade	Cause of death
1	1	M	65	L2-L3	0	Cardiac failure
2	1	M	65	T12-L1	2	Cardiac failure
3	2	M	62	L2-L3	1	Cardiac Failure
4	3	M	41	L2-L3	0	NA
5	4	M	65	L2-L3	2	Cardiac Failure
6	5	F	85	L2-L3	1	NA
7	6	F	65	L2-L3	2	NA

3.2.2 Test Equipment

The test apparatus used in this study is shown in Fig. 3.3 and consists of a MTS Model 858 Bionix Low-Force Mechanical Test System (A). The applied force is measured by a MTS load cell (B), with a range of +/- 2500 N, which records only the axial loads. The load cell is installed on the MTS actuator (C) in order to measure the driving force to generate a force feedback signal for a force control test. A linear variable differential transducer (LVDT) on the actuator supplies the stroke feedback signals to the system electronic control console (D). The actuator motion is controlled by the console which consists of an AC controller for displacement control and a DC controller for force control. The load cell and displacement transducer readings are recorded and stored using a PC computer and related hardwares (E) with the Assyst data acquisition

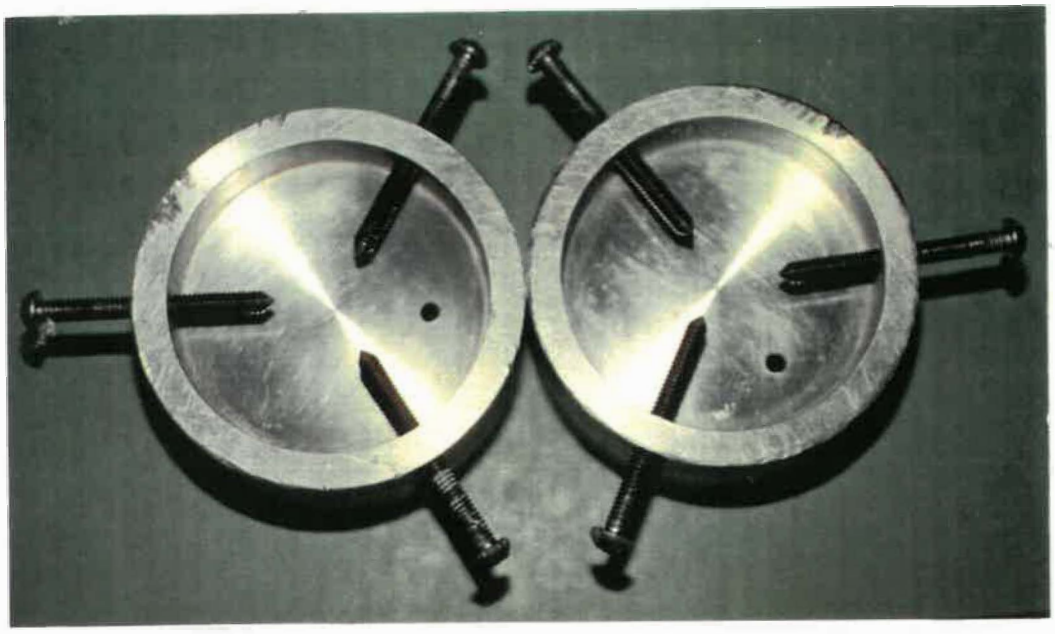

Fig. 3.1 Upper and lower cups with the side screws.

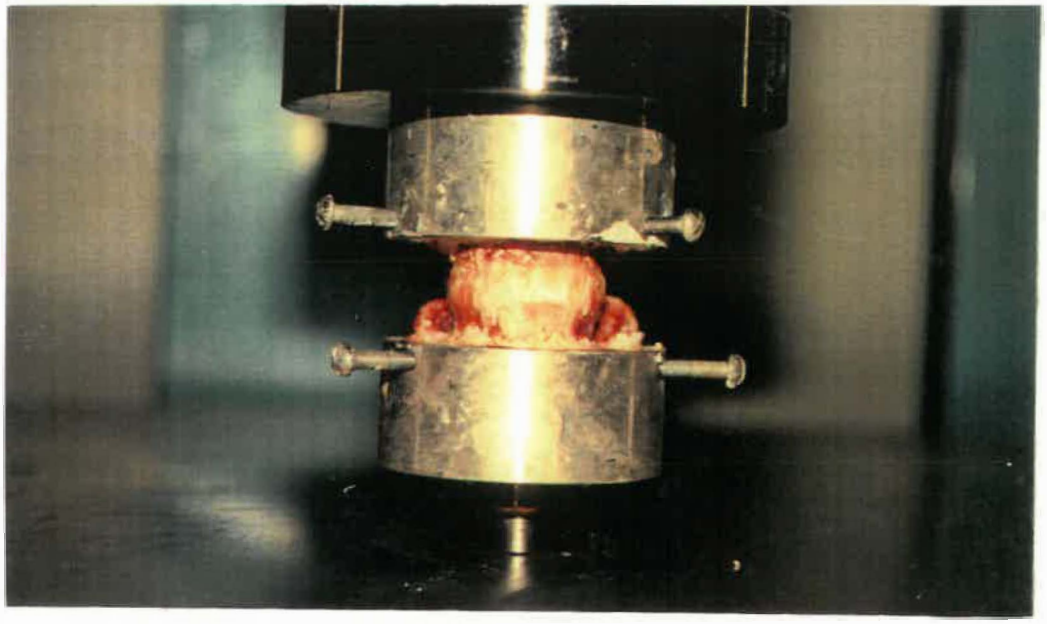

Fig. 3.2 Front view of the motion segment fixed in the upper and lower cups.

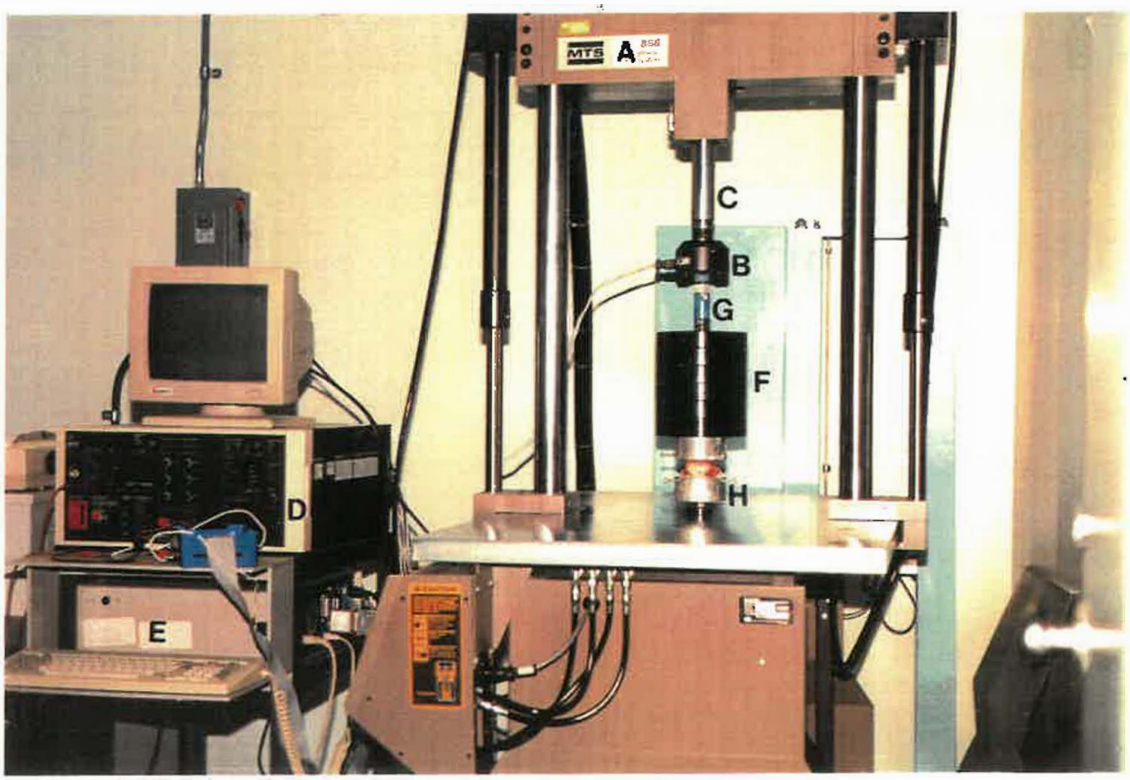

Fig. 3.3 Test apparatus used in the experimental studies.

software. They have also been monitored on the MTS micro-console display.

The mass of the upper body has been represented by 6 metal plates (F) with a total of about 38.5 Kg weight which are connected together by 3 screws and spring washers. Taking also into account the mass of connections, upper cup and that of the load cell below its sensing part, the total vibrating mass on top of the upper vertebra reaches a value of about 40 Kg. The added mass is connected to the load cell at top (top constraint) by a connecting assembly (G). The bottom of the lower cup is fixed to the MTS base (H) (bottom constraint).

3.2.3 Test Procedure

For positioning the specimens into the cups, first the superior end of the top vertebra is fixed and casted into the upper cup in a way that the bottom surface of the cup is parallel to the horizontal midplane of the disc. Then the assembly is inverted and installed on the actuator. By lowering the actuator gently, the inferior end of the bottom vertebra is placed into the lower cup which is secured on the base. It is then fixed by the screws and casted. In this way, the top surface of the upper cup and the bottom surface of the lower cup and the disc horizontal midplane are parallel to each other and perpendicular to

the axis of the actuator. After the cast is solidified and the actuator is released from the upper cup, the steel plates constituting the upper body mass are mounted on the upper cup and they are fixed to the load cell at top through the connecting assembly. The time required to install the steel plate is about 10 minutes. Prior to testing, the weight of the added mass on top of the specimen is counterbalanced by applying a tensile force (in the upward direction). After 15 minutes (the time allowing the specimen to recoil after installation), this loading condition is then chosen as the experiment base-line from which the compressive preload on the motion segment is measured.

The intact specimens are subjected to axial sinusoidal force with frequencies ranging from 0.5 to 50 Hz. The amplitude of the applied force is kept low (an average of about 20 N) in order to generate a linear response. A frequency sweep technique is employed to collect compliance data. Data are recorded at 1 to 5 Hz frequency intervals at frequencies distant from the resonant frequency and at 0.5 Hz intervals at frequencies approaching the resonant frequency. The above procedure is performed at different compression preloads of 30 N, 230 N, 390 N, 530 N and 680 N. After these tests the loading is set to the base-line and creep tests are performed for three of the specimens under a compression force of 400 N and for a period of 60 minu-

tes. The posterior elements including the facet joints are then removed, the system loading is set to the base-line and the entire foregoing test procedure is repeated. This time at the end of the tests each specimen is creep tested for periods of 20 or 60 minutes.

For each preload, after its application, there is a waiting period of about 10 minutes in order to have a relatively stable displacement reading. The time needed to collect the data at each compression preload is about 15 minutes. A recovery period of about 90 minutes is considered each time the system loading is set to the base-line. That is before the creep tests of intact specimens and the tests with no posterior elements. These recovery periods are expected to diminish the possible role of creep on the vibration measurements. These experiments have been designed to examine the role of both compression force carried by the spine and the presence of facet joints on the dynamics of motion segments.

3.2.4 Damping Measurements

In view of the viscoelastic behaviour of intervertebral joints, the segmental damping character involves both hysteretic and viscous energy losses. The level of energy dissipated in a segment at low frequencies (1 Hz in this analysis) is determined using hysteresis curves of the

load-displacement data. The ratio of the dissipated energy divided by the amount of energy input during each loading cycle is defined as the hysteresis value. Figure 3.4 shows a typical hysteresis loop in these experiments in which the loop area A is equivalent to the lost energy and the area (A + B) is the energy input into the specimen during a loading cycle [38,95]. In this figure the dynamic stiffness of joint is estimated from the change in force DF divided by the change in displacement DD.

For linear, single degree-of-freedom systems with a small amount of viscous damping, equivalent viscous damping ratio could be evaluated from the normalized frequency-response curves using either of the following methods: free-vibration decay, resonant amplification, half-power (bandwidth), or energy loss per cycle at resonant frequency [3]. In the present work, the latter three methods are used to calculate damping. For the use in the finite element analysis, the equivalent viscous damping defined in terms of the energy loss per cycle at resonance is chosen. This method provides a reasonable approximation of experimental results [3], since the energy loss is measured directly from the force-displacement curve. Figure 3.5 shows a typical force-displacement curve at resonance from which the equivalent viscous damping ratio is calculated as [10],

$$W / 2 \pi m \omega^2 a^2$$

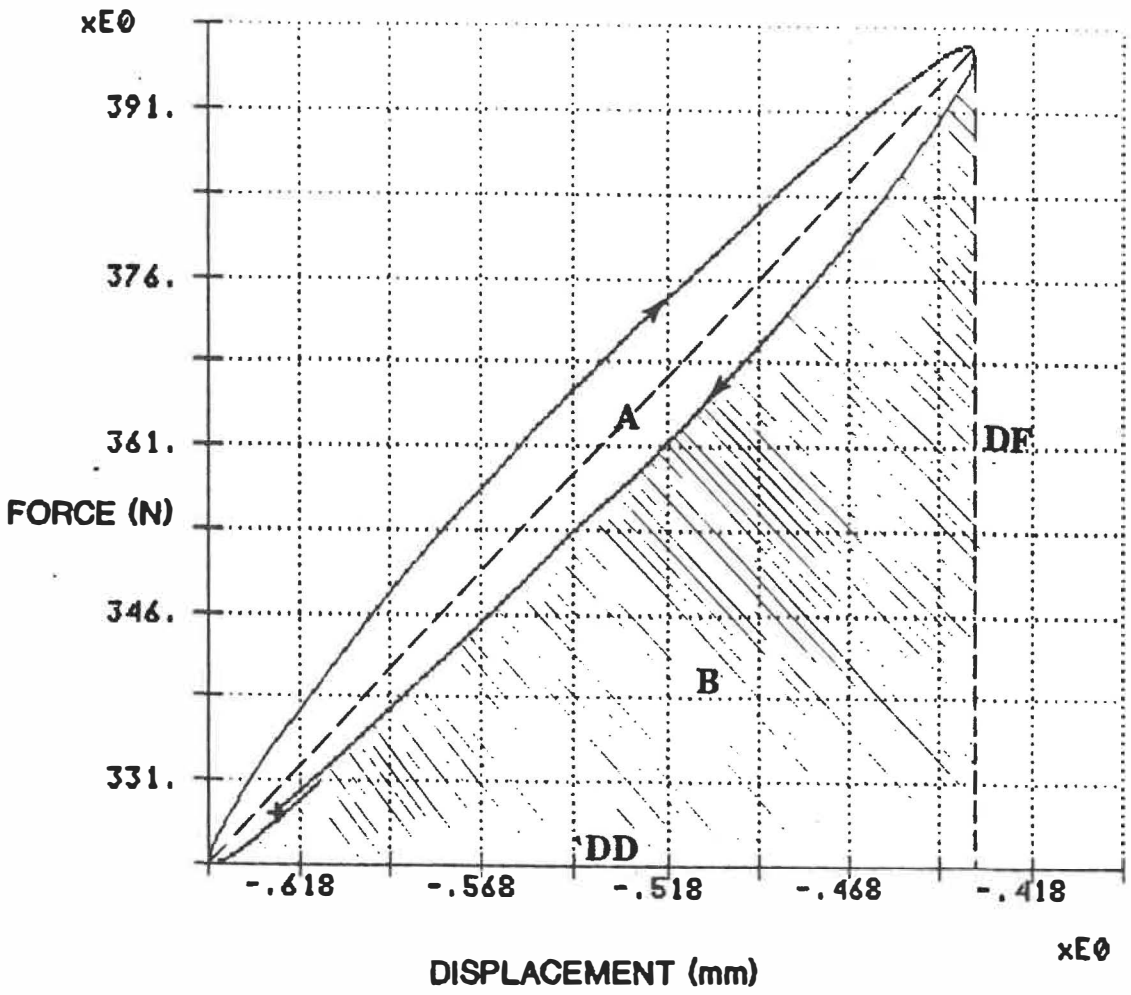

Fig. 3.4 A typical hysteresis loop at 1 Hz frequency.

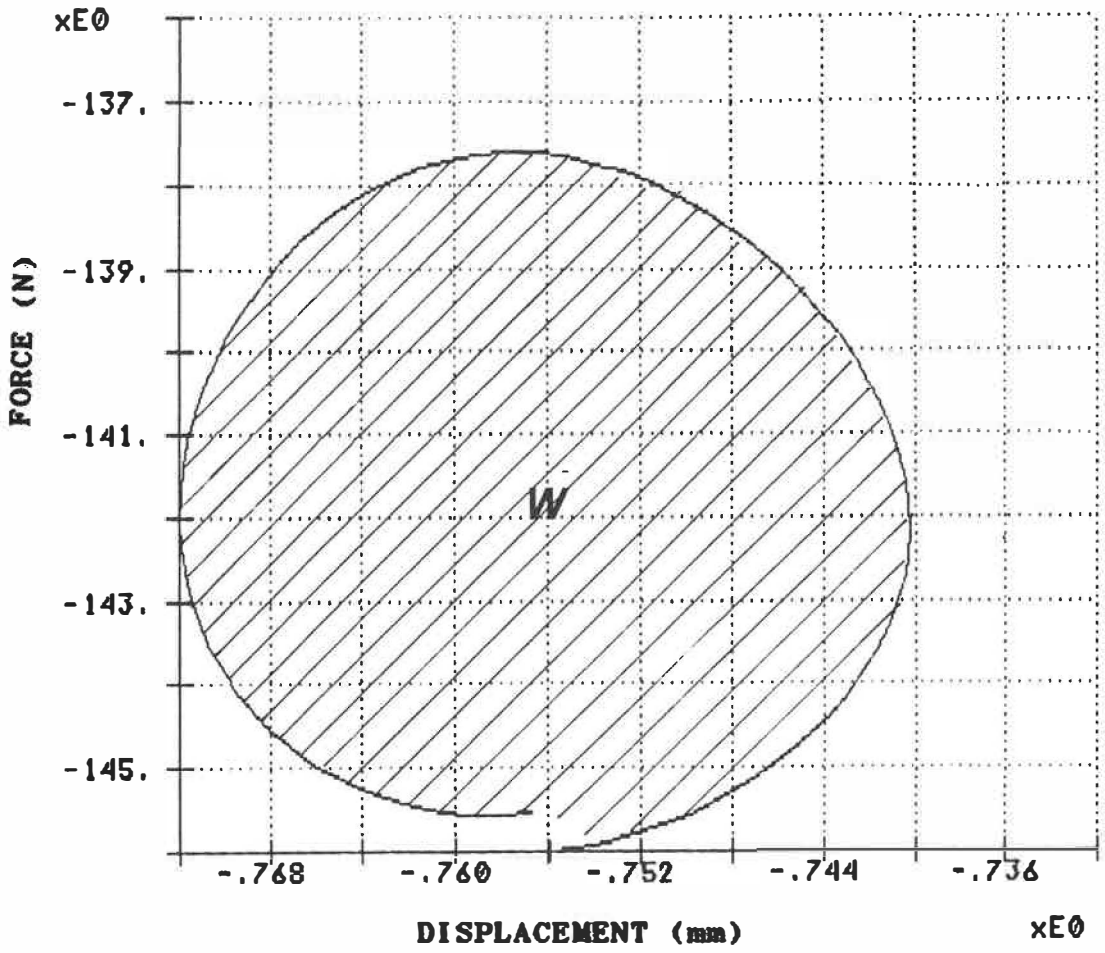

Fig. 3.5 A typical force-displacement curve at resonance.

where W = energy loss per cycle (the area enclosed by the force-displacement diagram), m = mass, ω = resonance frequency and a = maximum amplitude

3.3 FINITE ELEMENT MODELS

As was discussed earlier, a lumbar intervertebral joint is a complex structure consisting of various components with irregular geometries and different materials ranging from the soft matrix substance of the annulus to hard cortical shell of the vertebra. Stiffening effects of disc fibres (which carry the tensile forces only in the direction of their fibres), and state of nucleus incompressibility which changes as the age advances are the additional complicating features of the joint. Consideration of the above joint characteristics is essential in the developement of a realistic model which can be relied upon to predict the joint behaviour accurately.

The present chapter deals with the development of such a model for static and dynamic analyses of the joint by discussing the appropriate finite element formulations and models. Material properties of different components, finite element grid representation and loadings are discussed for each model (axisymmetric & 3-D). The geometry of the models is based on direct measurements of a L2-L3 specimen of a 29 year old female available in the literature

[87,89,91].

3.3.1 Finite Element Formulation

The finite element package program used in this analysis, " ADINA (Automatic Dynamic Incremental nonlinear Analysis) " [2], uses the standard displacement-based finite element formulation for analyses of solid structures. For an in-depth knowledge in this case, the reader should refer to the numerous reported specialized literature [1,118]. The program also employes two different formulations namely, displacement-based [63] and potential-based [64], for the analysis of compressible, inviscid fluids which experience only small displacements. Here only a brief discussion on the equilibrium equations governing the fluid region is presented.

In this study the nulceus pulposus is modelled by fluid elements in order to simulate its hydrostatic behaviour. Since the rest of the structure is modeled by solid elements, we have a "fluid-solid" dynamic interaction problem. According to the type of relative motion between the fluid phase and the solid phase, there are different types of formulations reported in the litrature [3,5,6,15,23,35, 50,54,63,64,113,117]. Considering the limited fluid displacement in this study, three types of fluid formulations namely displacement-based, potential-based and nearly

incompressible solid are investigated.

Figures 3.6 (a) and (b) show the general systems under consideration. In these figures region S represents the solid phase, region F contains the fluid and surface I defines the fluid-structure interface. On the boundary B all displacements and velocities are zero.

The equilibrium equations in the matrix form for the solid parts are

$$M_s \ddot{U} + C_s \dot{U} + K_s U + F_s^I + F_s^E = 0 \qquad (1)$$

where U is the vector of unknown nodal displacements. M_s, C_s and K_s are respectively mass, damping and stiffness matrices of the solid. F_s^I and F_s^E stand respectively for forces due to the interaction with the fluid regions and those due to external forces. Since in general the tangential forces exerted by the fluid are negligible, the vector F_s^I can be given in terms of pressure p along the common interface I as

$$F_s^I = \int_I n\, p\, ds \qquad (3)$$

where n is a unit normal outward into the fluid at the interface.

In the case of displacement-based formulation [63,117], displacements are the nodal variables in both the solid and fluid regions (Fig 3.6 (a)), and in an identical

manner to the solids, the governing equations for the fluid regions are given as (1), i.e.,

$$M_f \ddot{U} + C_f \dot{U} + K_f U + F_f^I + F_f^E = 0 \qquad (4)$$

The continuity of interface displacements, i.e. $U_f^I = U_s^I$, and the equilibrium of interface forces, i.e. $F_s^I + F_f^I = 0.$, are then used to assemble the overall structural equations from the foregoing regional equations.

In the above, the fluid is assumed to be elastic with a uniform hydrostatic pressure of

$$p = - B \, \mathrm{div}(u) \qquad (5)$$

where B is the bulk modulus and the shear modulus G is taken as zero. This results in some spurious modes, and the number of these so called "circulation modes" increases as the mesh becomes finer [23]. These modes can be separated from the real modes by observation of the mode shapes. An alternative to this is to admit the inviscid nature of the fluid and its corollary which states that the motion (starting from rest) must remain irrotational in the absence of shear stresses and the irrotationality constraint can be imposed in a penalty manner. This, however, might result in an over stiffened structure.

Figure 3.6 (b) shows the system used in the potential-based formulation [64]. Considering the compressible, inviscid fluid which experiences only small displacements,

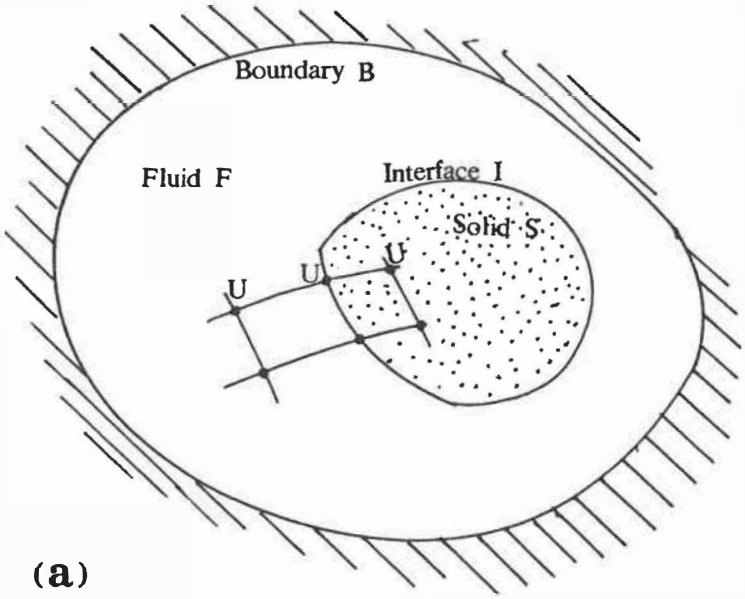

(a)

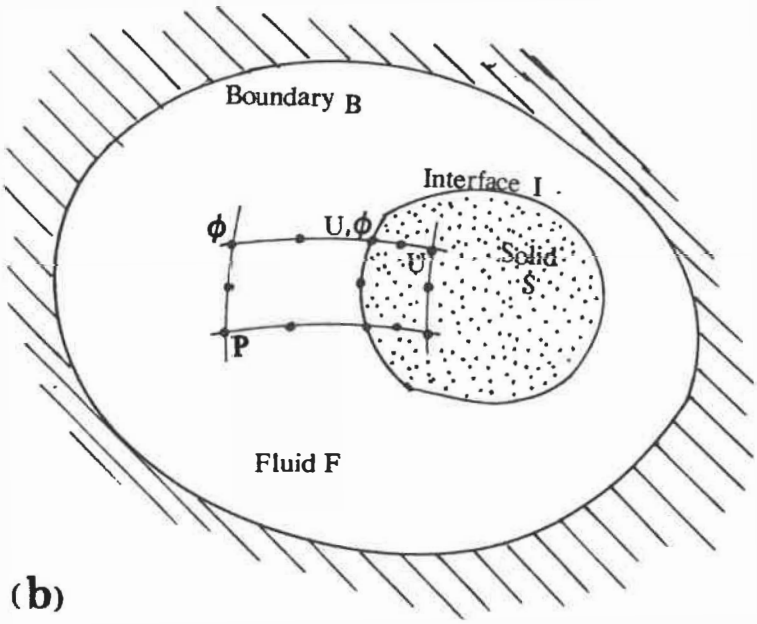

(b)

Fig. 3.6 Fluid-Structure problem geometry.
(a): Displacement Based (b): Potential Based

the finite element formulation is derived using Euler equations [42,64]. In this case, velocity potentials (ϕ) are used as the nodal variables in the fluid, and a hydrostatic pressure variable (P_0) is introduced at one node in each fluid region. Displacements (U) stay the nodal variables in the solid. The coupled system of equations becomes,

$$M \ddot{X} + D \dot{X} + K X = F^E \quad (6)$$

in which X is the vector of nodal variables i.e.,

$$X^T = [\ U\ ,\ \phi\ ,\ P_0\ ] \quad (7)$$

Matrix D couples the fluid to the solid and links the pressure to the velocity potential in the fluid region.

In the case of simulating nearly incompressible solid, the fluid region is modelled by standard solid elements with a Poisson's ratio ν with a magnitude very close to 0.5, making an almost incompressible elements with a hydrostatic state of stress. The modulus of elasticity E is computed from the following equation, by choosing the desired bulk modulus B. The values of E and the shear modulus G reach toward zero as the Poisson's ratio approaches 0.5.

$$B = E / 3(1 - 2\nu) \quad (8)$$

3.3.2 Axisymmetric Model

Figure 3.7 shows the axisymmetric finite element model of a vertebra-disc-vertebra unit of the L2-L3 lumbar segment. Symmetry about both the vertical axis Z and the

horizontal plane (Z=0) is utilized. The present experimental results (Fig. 4.3) as well as those of other studies [90,115] indicate that, under low levels of axial compression considered in this study, the load is primarily carried by the disc and not the facet joints. The posterior elements are therefore neglected. In this model, the structure is divided into five distinct regions, namely the annulus fibrosus, nucleus pulposus, cartilaginous endplate, cancellous bone and cortical bone. The annulus fibrosus is modelled as a homogeneous orthotropic mixture of fibres and matrix with direction dependent mechanical properties. Transverse isotropy is assumed in the plane normal to the direction of the fibres. Geometric data and orthotropic material properties are based on the nonhomogeneous composite models of the disc reported in the litrature [87]. Figure 3.8 shows a typical fibre reinforced layer. To preserve the axisymmetric nature of the analysis, the adjacent fibres in both $+\alpha$ and $-\alpha$ directions are combined in a single equivalent layer [4,87,97].

The annulus region is simulated by seven layers, using 28 six node isoparametric solid elements. The evaluated material properties for the innermost and outermost layers are listed in Table 3.2. The properties for the remaining layers vary in between those of forgoing boundary layers. The other material properties which are in common

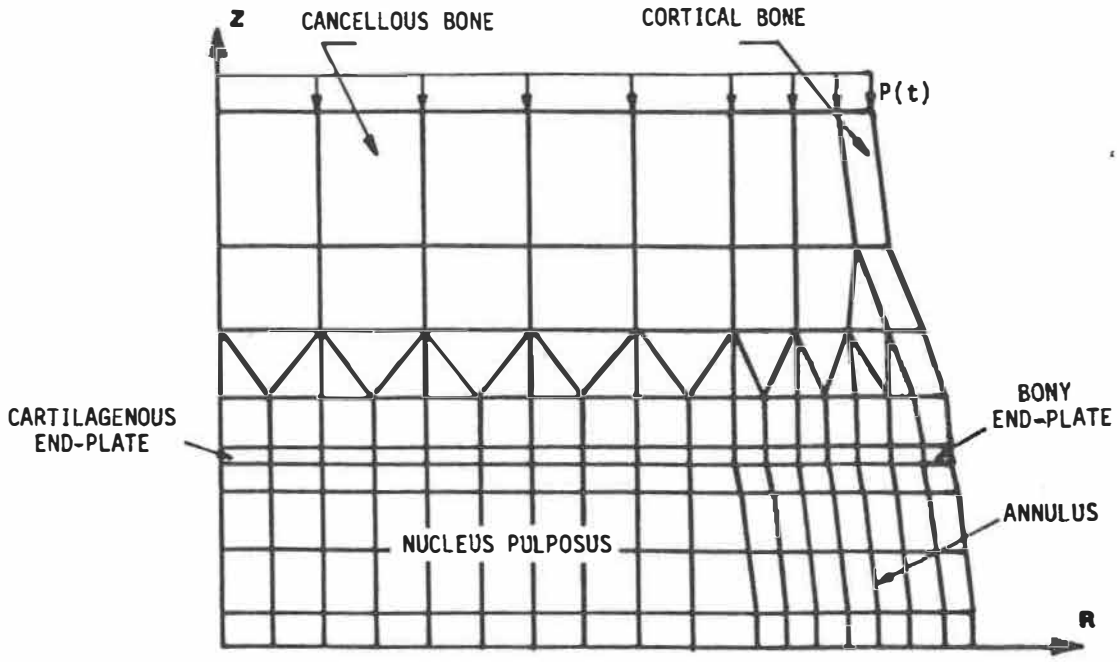

Fig. 3.7 Axisymmetric model of the disc-vertebra unit.

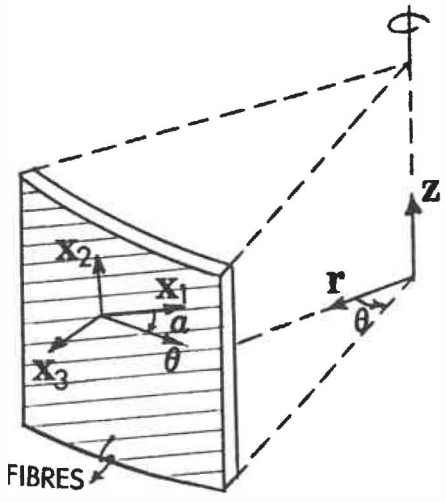

Fig. 3.8 A typical fibre reinforced layer of the annulus.

with the three-dimensional model are listed in Table 3.3.

The nucleus pulposus is considered as an invisid fluid with the bulk modulus of 2200 MPa (i.e. equal to that of the water) and is modelled by 40 six-node displacement-based [63] or potential-based [64] fluid elements. In this case, 2 x 2 reduced integration rule is used in order not to have too stiff elements [63]. By changing the bulk modulus of these fluid elements, the disc compressibility can be changed, making it possible to simulate loss of the disc fluid content. The rest of the structure is modelled by 76 three and four-node solid elements. In some analyses the upper body mass is modelled by concentrated nodal masses for the nodes on top of the upper vertebra. The axial load (static, sinusoidal and impact) are applied uniformly on top of the upper vertebra.

For verification purposes a static analysis is initially performed. In dynamic analysis of the models, first natural frequencies and corresponding mode shapes are computed. This is then followed by steady state analyses to find the response of the structure under sinusoidal axial compression in a frequency range from 1 to 50 Hz. The model is also subjected to a step load to simulate impact. In this case, the pressure variation in the nucleus region of the disc is investigated.

Table 3.2. Orthotropic material properties for the annulus layers in the axisymmetric model

	E1 (MPa)	E2=E3 (MPa)	G31 (MPa)	ν_{31}	ν_{32}*
Innermost layer	25.90	4.83	1.38	0.084	0.75
Outermost layer	66.23	4.94	1.38	0.034	0.79

* Orthogonal axes (1,2,3) represent the material principal directions with (1) being in the direction of fibres.

Table 3.3. Material properties

Material	Elastic Modulus MPa	Poisson's ratio	Density Kg/m^3
Cortical bone	12000.	0.3	418.
Cancellous bone	100.	0.2	418.
Cartilagenous end-plate	24.	0.4	1060.
Nucleous	-	-	1000.
Annulus	-	-	1060.
Ground Substance	4.2	0.45	1000.
Collagen Fibres	-	-	1200.

3.3.3 Three-Dimensional Model

Figure 3.9 shows the 3-D finite element grid used in the present study. It models the geometry of an L2-L3 motion segment which is based on in vitro measurements [91]. Assuming symmetry of the motion segment about its sagittal plane, for the loading considered, the deformations remain symmetrical about this plane and hence only half of the segment needs to be modelled. The representation of the annulus as a composite of collagenous fibres embedded in a matrix of ground substance is shown in Fig. 3.10. The fibres of the annulus are modelled by 240 axial elements and are arranged in eight layers in a criss-cross pattern, making an angle of, on an average, 29 degrees with the horizontal plane of the disc. The distribution of collagenous fibre properties among layers are listed in table 3.4 for the linear model and in table 3.5 for the nonlinear model. Figure 3.11 shows a typical stress-strain curve for the collageneous fibres considered in the analysis [89]. The ground substance is modelled by 90 twelve-node solid elements. The nucleus region is represented by 48 twelve-node displacement-based [63] and potential-based [64] fluid elements, and the rest of the structure is modelled by 276 eight-node solid elements. The model contains 741 nodal points. The remaining material properties listed in table 3.3 which are based on data reported in the literature [19,22,24,91,92].

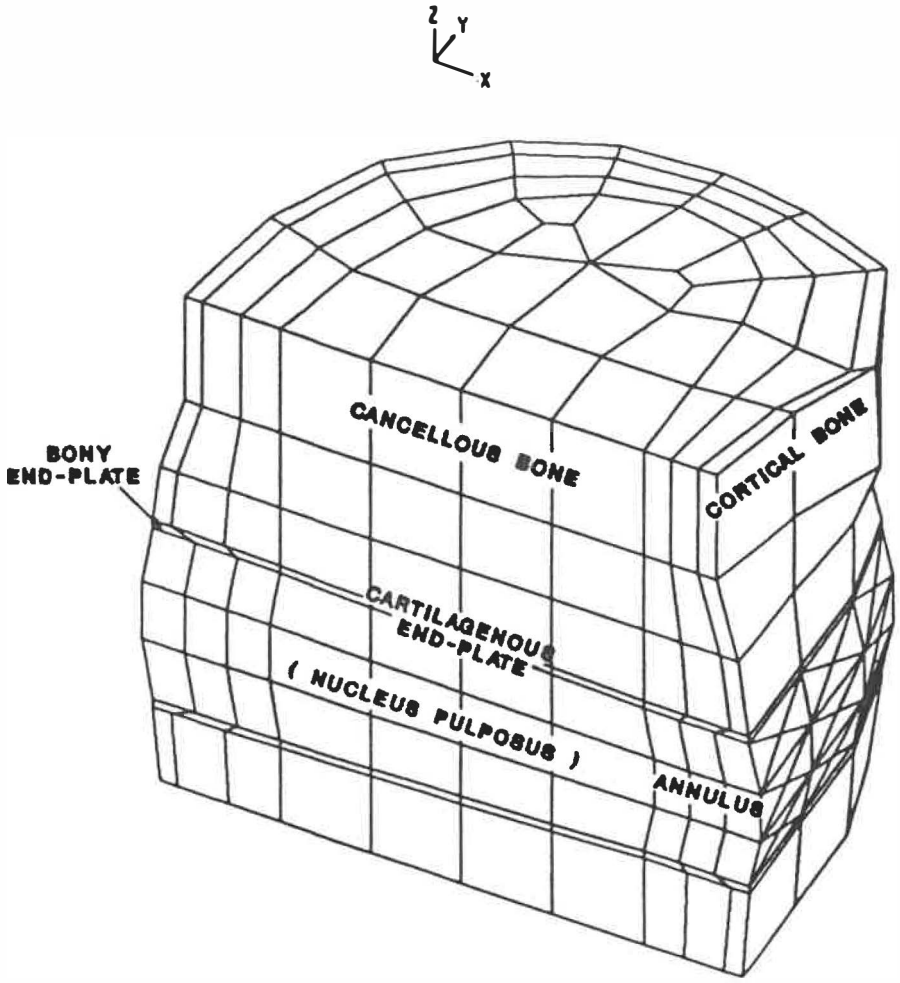

Fig. 3.9 Three dimensional model of a L2-L3 disc-vertebra unit.

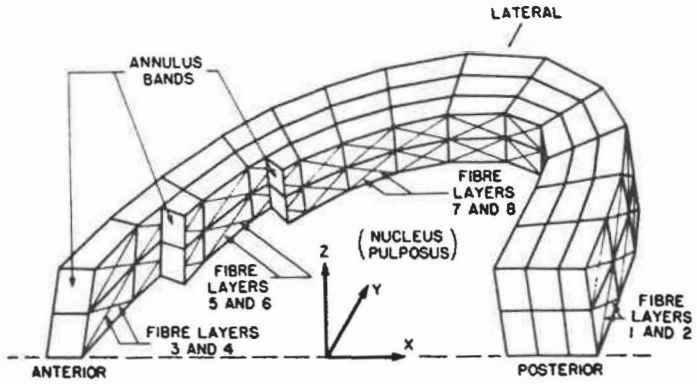

Fig. 3.10 Nonhomogeneous composite representation of the disc annulus [89].

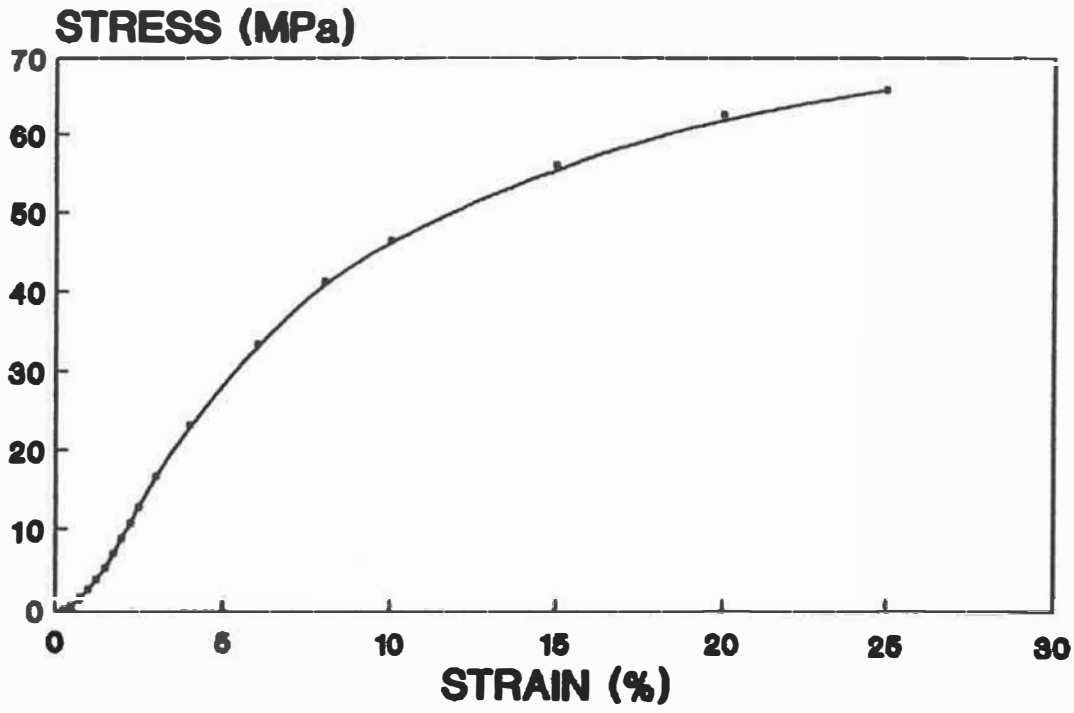

Fig. 3.11 Stress-Strain curve considered for the disc collagenous fibres [89].

In general, concentrated nodal masses for the top nodes on the upper vertebra are used to model the upper body mass, and the load is applied uniformly on top of the upper vertebra. In simulating the experimental analysis, the upper body mass is represented by 56 eight-node solid elements, the connecting assembly attaching the mass to the load cell is modelled by a beam element and the load is applied axially to the center of the upper mass through the connecting assembly.

Both linear and nonlinear analyses of the model are performed. As in the axisymmetric model, static, frequency and steady state, analyses are performed. The results of the linear model were compared with the axisymmetric model. In this case, the top surface of the upper vertebra is constrained to move only in the Z direction, and The bottom surface of the lower vertebra is fixed.

In order to accurately model experimental tests under various magnitudes of compression preload, 3-D nonlinear static analyses are performed a priori to set up the initial stress stiffness matrices required for the subsequent frequency analyses. Employing the computed mode shapes and the measured damping factor, the steady state compliance analysis of the model has also been performed under different compression preloads.

Table 3.4. Properties for the collagenous layers used in the linear 3-D model

	Layers 1,2 outermost	Layers 3,4	Layers 5,6	Layers 7,8 innermost
Cross-sectional area (mm^2)	0.8	1.14	0.79	0.27
Modulus of elasticity (MPa)	292	262	232	202

Table 3.5. Distribution of collagenous fibre properties among layers[92]

	Layers 1 & 2	Layers 3 & 4	Layers 5 & 6	Layers 7 & 8
Ratio of cross-sectional areas	1.0	0.78	0.62	0.47
Elasticity constant ratio	1.0	0.9	0.75	0.65

CHAPTER 4

RESULTS

4.1 INTRODUCTION

In this section, at first, the experimental results of the frequency and damping analyses are presented. These are then followed by the predictions of the linear and non-linear dynamic finite element model studies.

4.2 EXPERIMENTAL RESULTS

4.2.1 Static and Creep Response

The axial deflections of the specimens under 400 N compression force are measured to be 0.6(+/-.08) mm for intact specimens and 0.73(+/-.17) mm for the specimens with no posterior elements. These values are the average of the immediate static response (the response after 5 seconds) of the specimens +/- their standard deviation. The long-term creep response of the specimens under 400 N axial compression are shown in Figs. II.1-II.3 (Appendix II) for intact specimens and Figs. II.3-II.10 (Appendix II) after removing the posterior elements. The static response of each specimen can also be seen in these figures (the response after 5 seconds). The results are comparable with previous works reported in the literature [9,31] and they show that the intact specimens are stiffer than the specimens without the

posterior elements, but not significantly ($p<.2$).

4.2.2 Frequency Response Analyses

Figure 4.1 shows typical (not scaled) force and displacement responses at a frequency. In this figure displacement response and force response are superimposed to measure the phase angle. Figure 4.2 shows typical axial compliance response plots (specimen No. 2) carrying a mass of 40 Kg and different magnitudes of compression preload. In this figure, the compliance magnitude and its phase angle are shown as a function of frequency. It is noted that as the compression preload on the motion segment increases, the compliance magnitude decreases whereas the resonant frequency increases. These demonstrate the stiffening effect of the compression preload on the segmental response in the axial direction. In Fig. 4.2, for each curve, there are two peaks relating to two different natural modes of vibration. The first one corresponds to an axial mode while the second one is primarily a lateral mode with a secondary component in the axial direction. Although the experimental set-up was designed for axial motions only, the lateral flexibility of the loading system resulted in the second mode. This was verified by a finite element model of the whole specimen-loading system. Figures III.1-III.7 of Appendix III show the compliance magnitudes versus frequency for the specimens with and without the

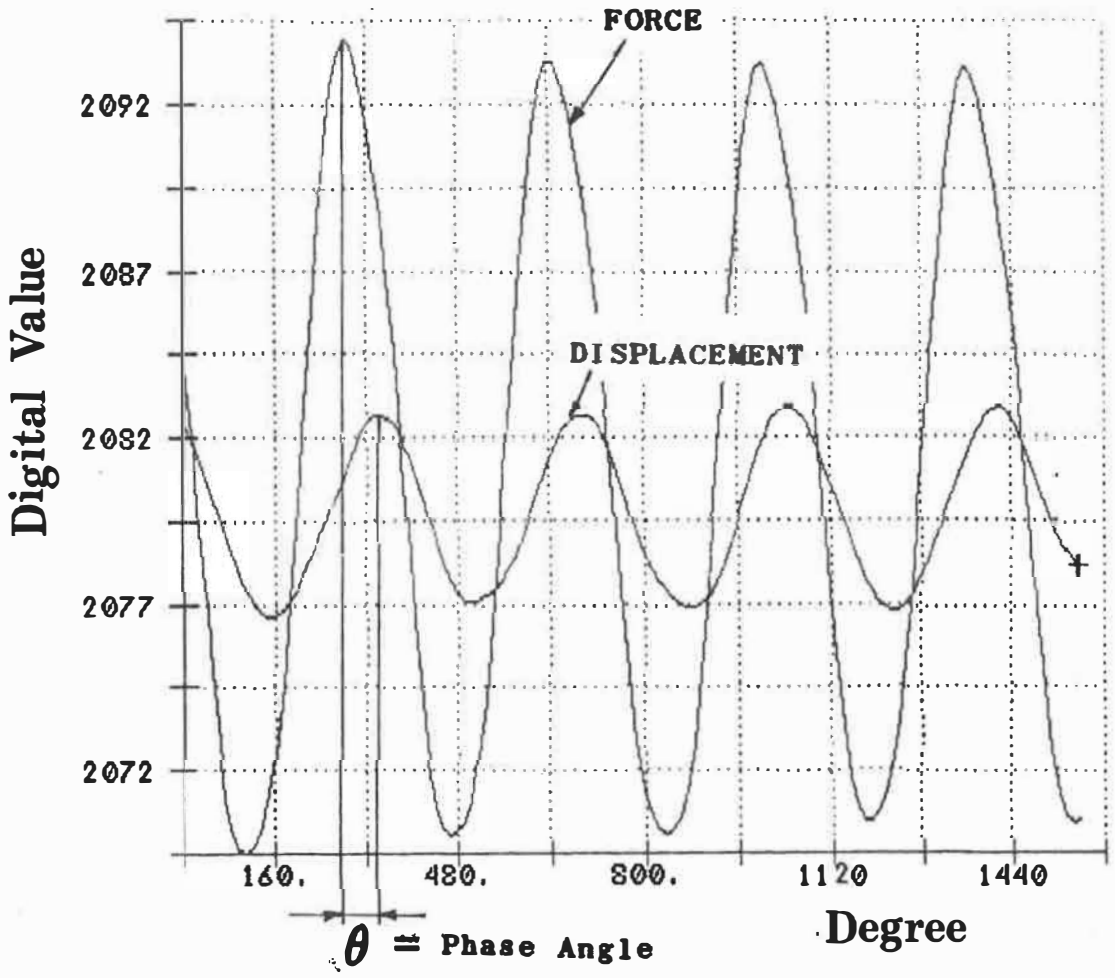

Fig. 4.1 Typical force and displacement responses at a certain frequency. Each digital value is equal to 1.2 N force, and 5.E-03 mm displacement.

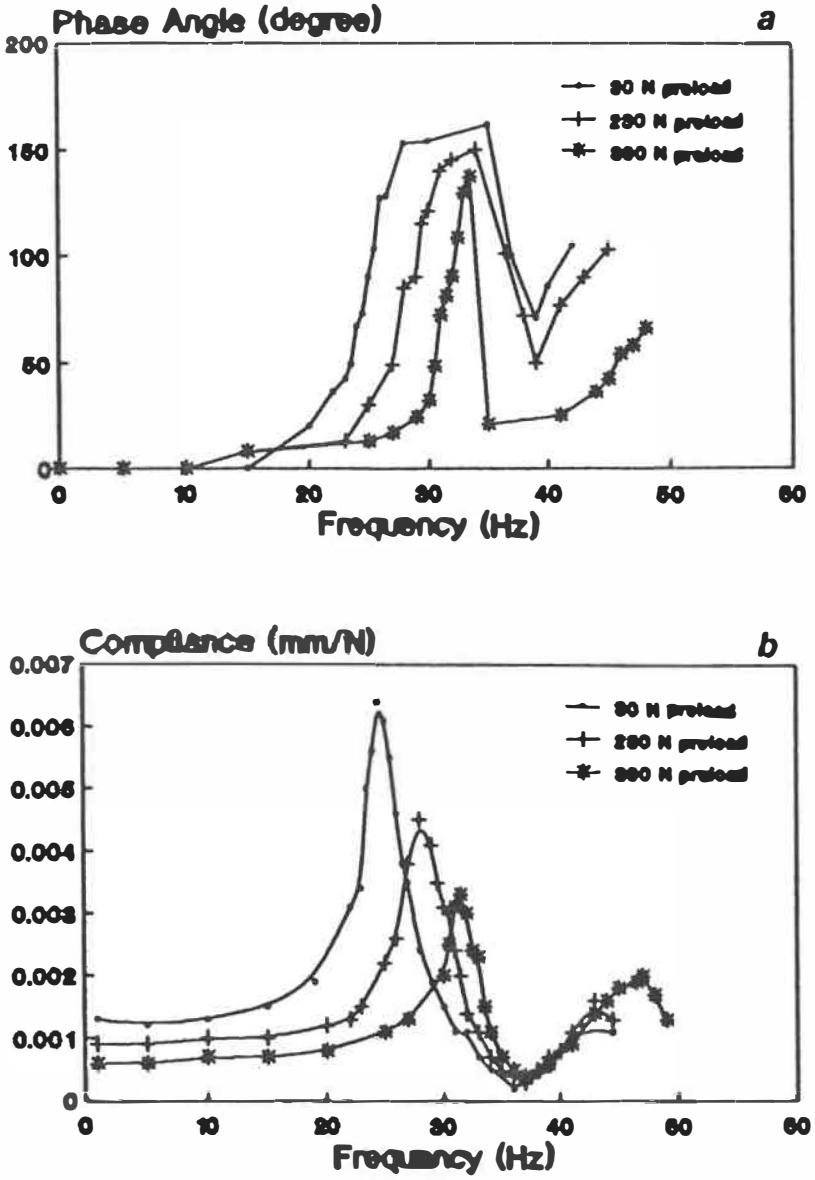

Fig. 4.2 A typical axial compliance response (intact specimen #2) with a mass of 40 Kg and different compression preloads. (a) Phase angle
(b) Compliance magnitude

posterior elements.

The measured variation of the resonant frequency with the compression preload in the presence of a 40 Kg mass is shown in Fig. 4.3 for the specimens with and without posterior elements. It is seen that an increase in the compression preload significantly increases the resonant frequency for both intact segments and segments with posterior elements removed ($p<.005$). On the other hand, in comparison with the intact segments, the removal of posterior elements tends to slightly decrease the resonant frequency irrespective of the magnitude of the compression preload considered ($p<.1$).

The variation of the mean compliance with the compression preload for the specimens with and without posterior elements are shown in Figs 4.4 and 4.5 under vibration at low frequencies (i.e. quasi-static conditions) and at resonant frequencies respectively.

It is worth noting that in the tests with the intact specimens, at a certain preload for some of the specimens, the rate of the frequency increment is much higher than that of its previous preloads. At this preload it seems that the facets are engaged, resulting in a relatively large increase in the specimen stiffness. This preload

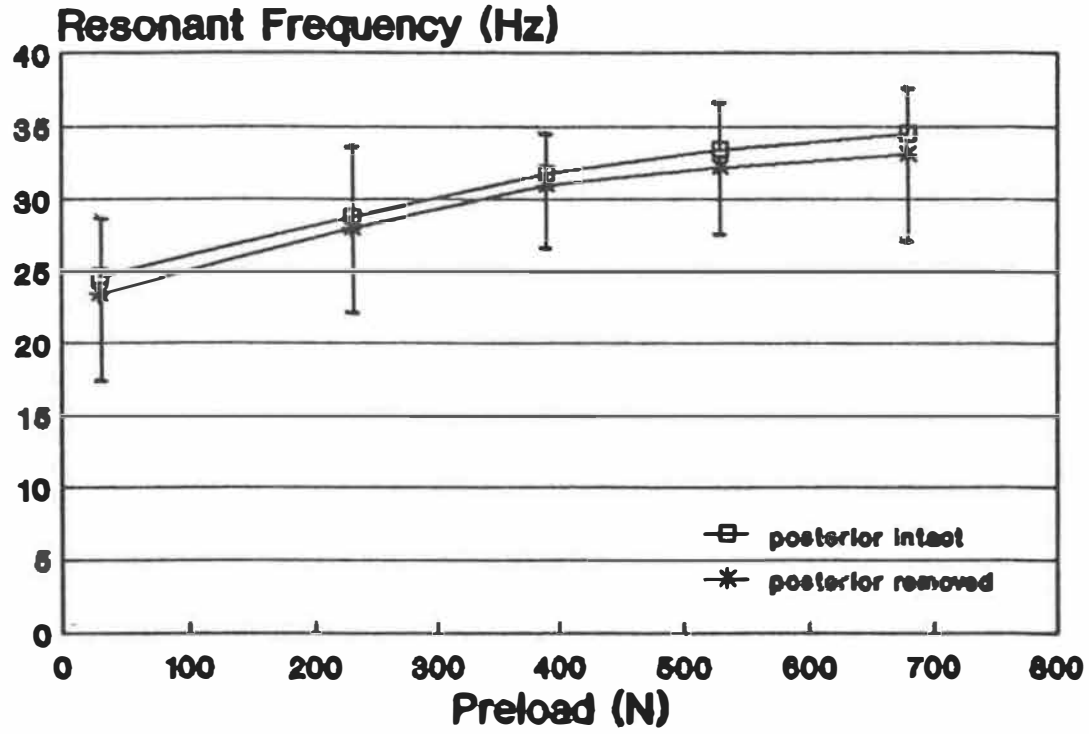

Fig. 4.3 Measured variation of the resonant frequency with the compression preload, for the segments with and without posterior elements. The bars denote one standard deviation above or below each mean value.

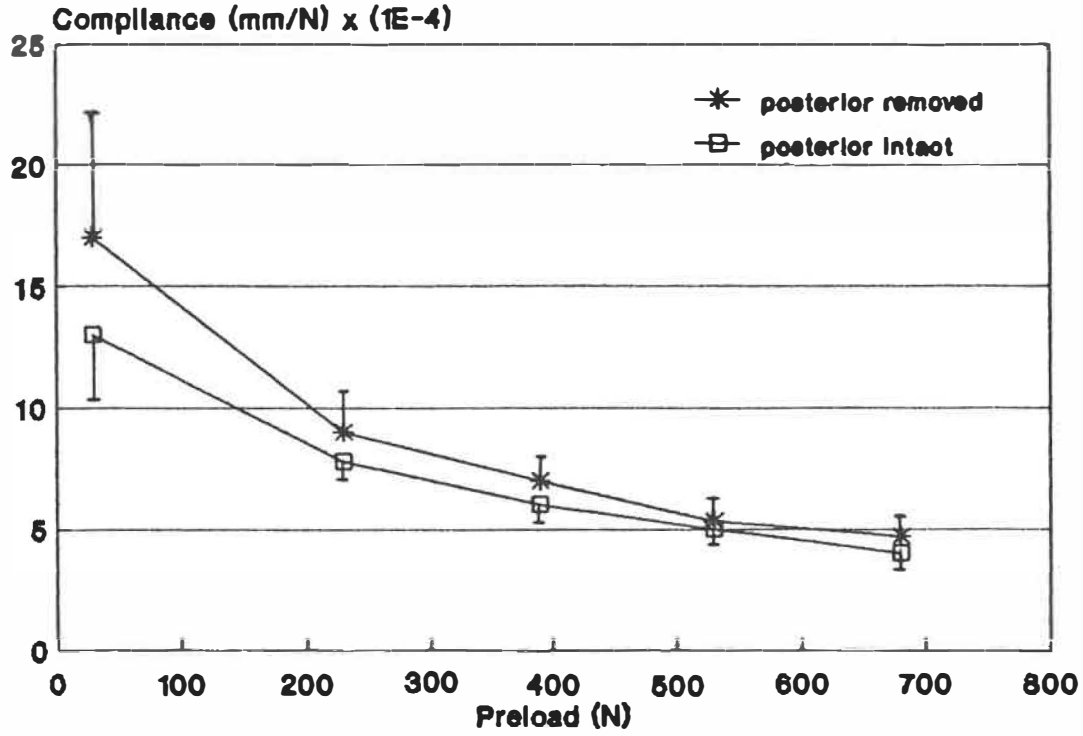

Fig. 4.4 Measured variation of the compliance at quasi-static frequencies (1 Hz) with the compression preload , for the segments with and without posterior elements. The bars denote standard deviation above or below the mean value.

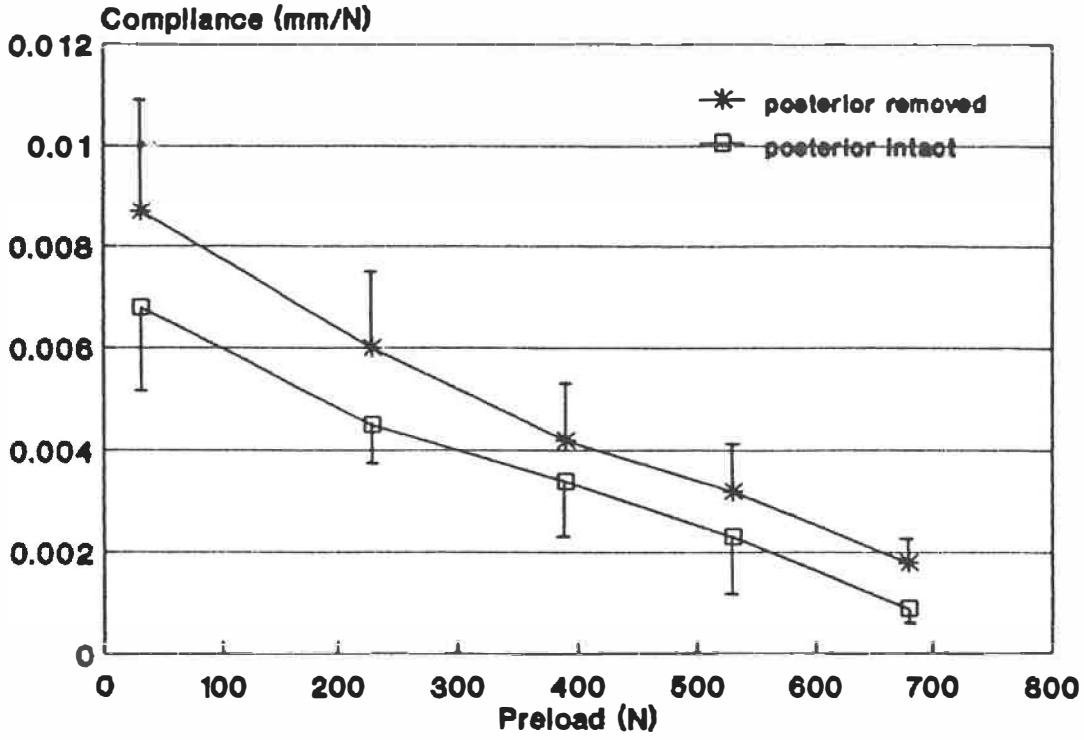

Fig 4.5 Measured variation of the compliance at resonant frequencies with the compression preload , for the segments with and without the posterior elements.

in these experiments is mostly between 530 N and 680 N. In these cases, the measured values are not cosidered in the statistical analysis.

4.2.3 Damping Measurements

Figures 4.6 and 4.7 show respectively the variations of hysteresis and dynamic stiffness values with the compression preload for the motion segments without posterior elements. It is seen that as the compression preload increases, the hysteresis decreases ($p<.005$) while the dynamic stiffness (at 1 Hz) increases ($p<.005$). The presence of posterior elements slightly increases the dynamic stiffness and decreases the hysteresis ($p<.1$). Typical axial load-displacement curves presenting hysteretic loops of a motion segment at three different compression preloads are shown in Fig. 4.8. In these tests the applied load has a frequency of 1 Hz and reaches a peak to peak value of about 100N. The dynamic components of force and displacements are only shown in this figure.

Table 4.1 lists magnitudes of the equivalent viscous damping factor measured at different compression preloads using three distinct methods of calculation, that is half-power (bandwidth), resonant amplification, and energy loss per cycle at resonance. Since the resonant response of the segments closely resembles that of a single degree-of-

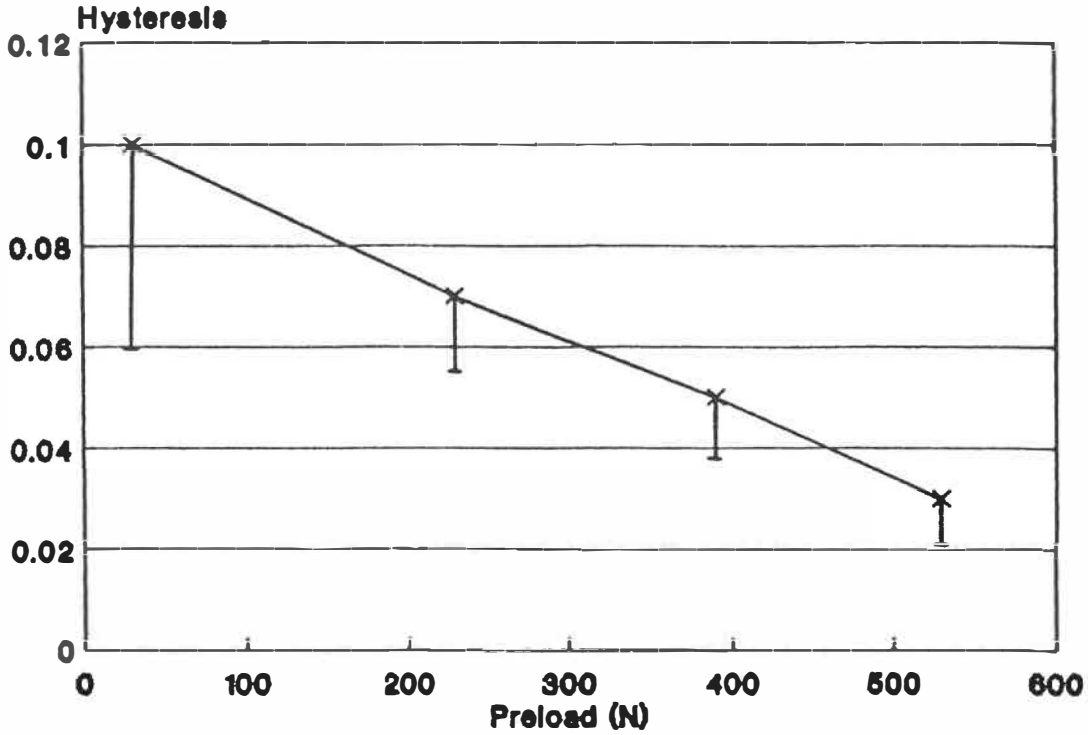

Fig. 4.6 Measured variation of hysteresis with the compression preload for the segments without posterior elements. The bars denote standard deviation below the mean value.

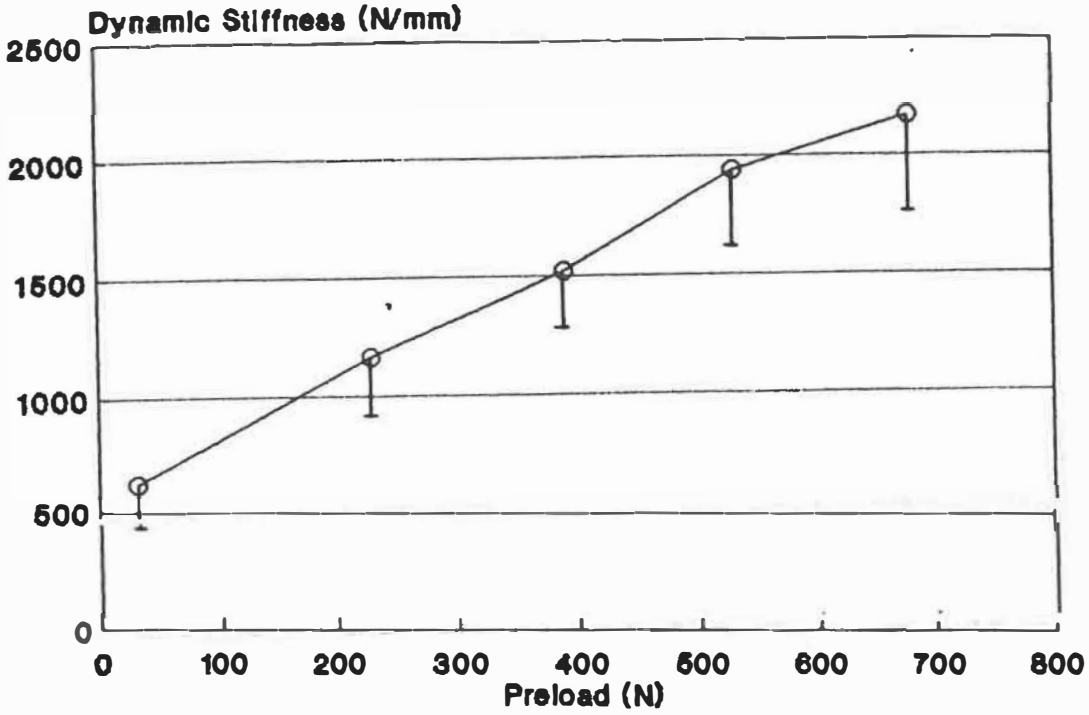

Fig. 4.7 Measured variation of dynamic stiffness at quasi-static frequencies (1 Hz) with the compression preload for the segments without posterior elements. The bars denote standard deviation below the mean value.

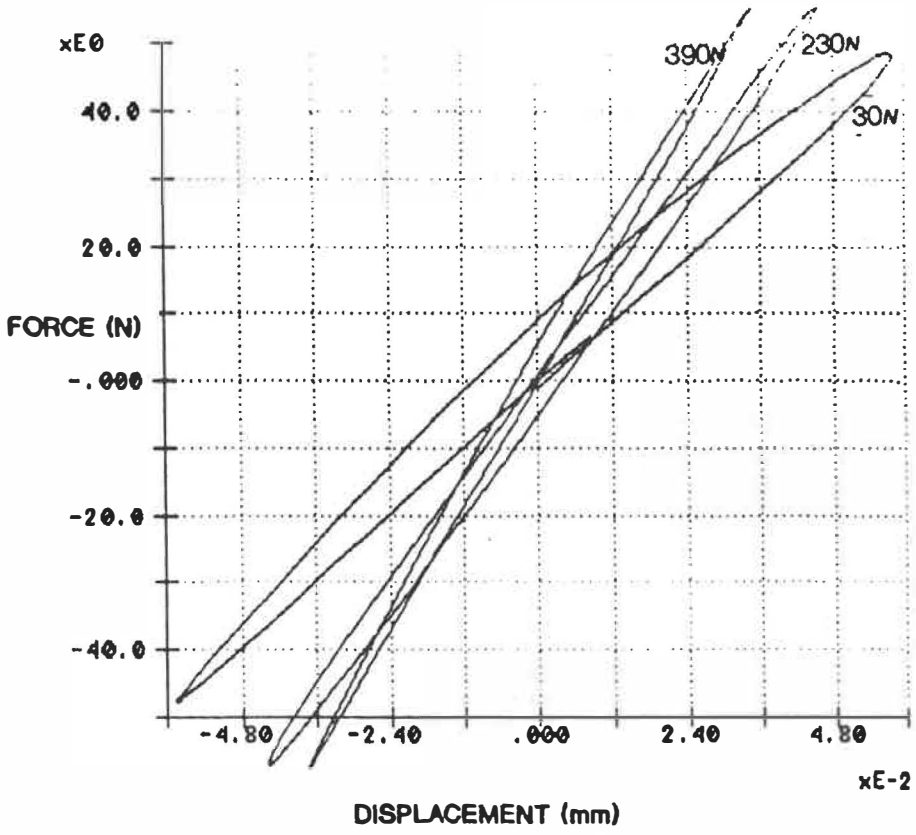

Fig. 4.8 Typical measured load-displacement curves at quasi-static frequencies (1 Hz) for different compression preloads.

freedom system, the measurement of viscous damping using the energy loss per cycle method is preferable, and it agrees very well with the damping ratios evaluated based on the resonance amplification procedure. Use of the half-power method yields lower damping ratios.

The normalized compliance magnitudes (dynamic magnification factor) at resonant frequencies for various compression preloads are shown in Fig. 4.9. This figure presents the dynamic magnification factor which is defined as the ratio of the response amplitude at resonant frequency to the low-frequency (quasi-static condition) response. Damping ratio is closely related to the dynamic magnification factor. A sudden decrease in the magnitude of the normalized compliance is noted to occur at the preload of 680 N ($p<.005$), while the differences are not significant for the remaining preloads ($p<.2$).

Table 4.1. Equivalent viscous damping using different methods

Preload	Energy Loss per cycle	Resonant amplification	Half-Power (band-width)
P=30 N	.08(.018)*	.08(.02)	.06(.02)
P=230 N	.07(.019)	.07(.012)	.06(.012)
P=390 N	.07(.016)	.08(.017)	.05(.016)
P=530 N	.07(.016)	.08(.013)	.05(.012)
P=680 N	.13(.04)	.13(.04)	.06(.00)

* Standard Deviation

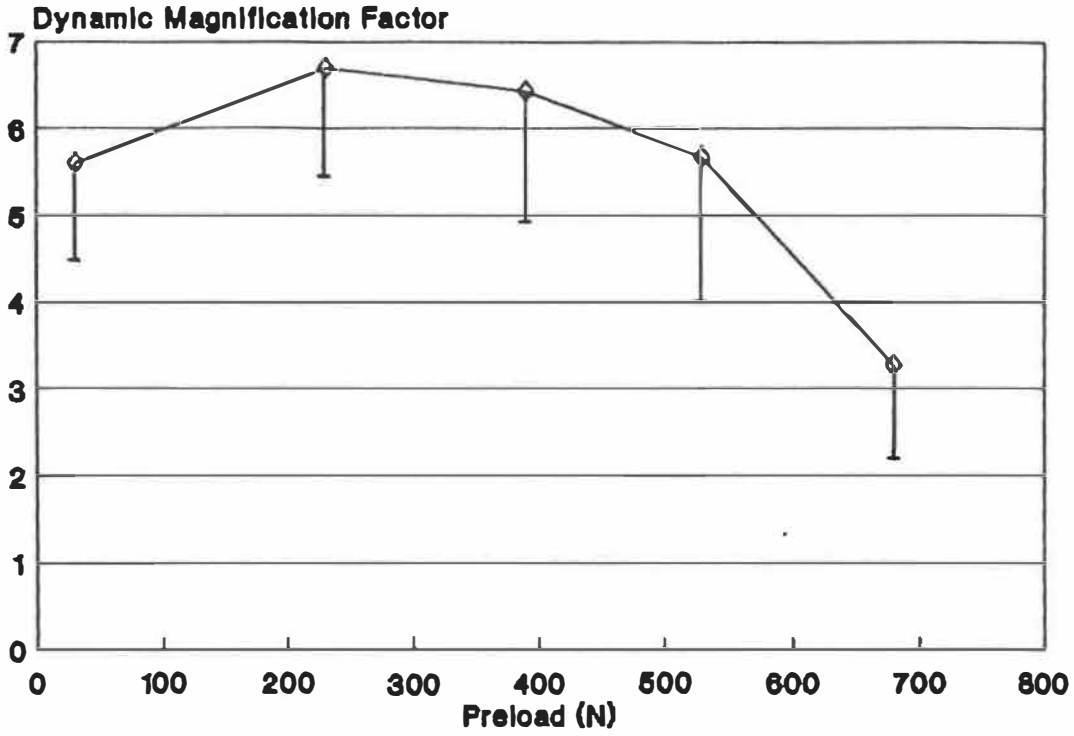

Fig. 4.9 Variation of dynamic magnification factors with the compression preload for the specimens without posterior elements. The bars denote standard deviation below the mean value.

4.3 FINITE ELEMENT RESULTS

4.3.1 Static Analyses

The axial displacement of disc-vertebra unit (under 400 N compression force) predicted by the axisymmetric model and the linear three-dimensional model are respectively 0.52 mm and 0.48 mm which are comparable with the experimental measurement of 0.73(+/- 0.17) mm. Table 4.2 lists some of the overall results of the models. These results are noticed to be in general agreement with other in-vitro measurements [7,45].

Table 4.2. Overal linear static response of the models

Models	Compressive Force (N)	Axial Displacement (mm)	Horizontal Disc Bulge (mm)	Intradiscal Pressure (MPa)
Axisymmetric	400.	.52	.53	.28
3-D	400.	.48	.50*	.25

* At the posterior region.

The predicted variation of the normal stresses and strains in the annulus matrix of the axisymmetric model along the radius at the disc mid-height horizontal section is shown in Figs. IV.1-IV.2 of Appendix IV which are in agreement with previous axisymmetric model studies [40,88].

The distribution of stresses and strains in the axisymmetric model are shown with the vector plots of principal stresses and strains (Figs. IV.3-IV.4 of Appendix IV). In these figures, the vectors are porportional to the stresses or the strains at the points they are representing and are normalized relative to their maximum value.

The predicted variation of axial displacement, horizontal disc bulge and intradiscal pressure with axial compression force for the nonlinear three-dimensional model is shown in Figs 4.10-4.12. These are found to be in agreement with the previous studies [91].

4.3.2 Free Vibration Analyses

The first five natural frequencies of the axisymmetric and top constraint three-dimensional models using various fluid elements, with and without the upper body mass of 40 Kg, are listed in Table 4.3. As was mentioned before, by using displacement-based fluid elements some circulation modes arise which their number increases as the mesh becomes finer [23]. These modes can be separated from the real modes by inspection of the mode shapes [15,23]. Figure 4.13 shows the first four mode-shapes of the axisymmetric model (without the added mass) using displacement-based fluid elements. The first mode in this figure is a typical circulation mode in which only the fluid region of

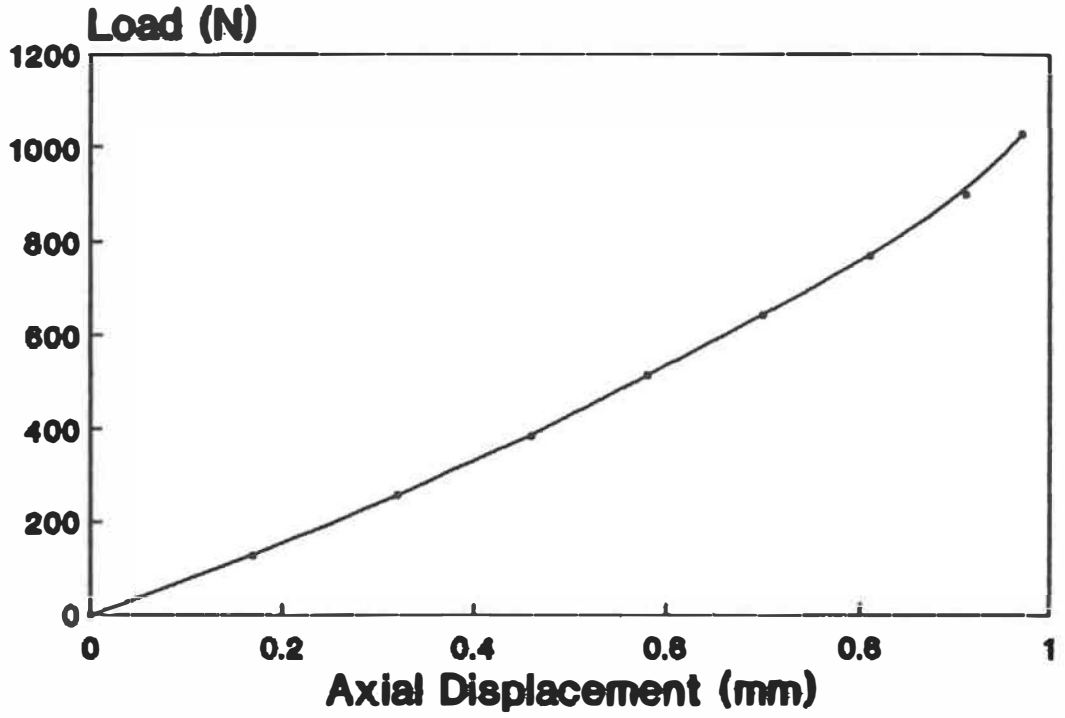

Fig. 4.10 Predicted variation of axial displacement versus static compressive force (nonlinear 3-D model).

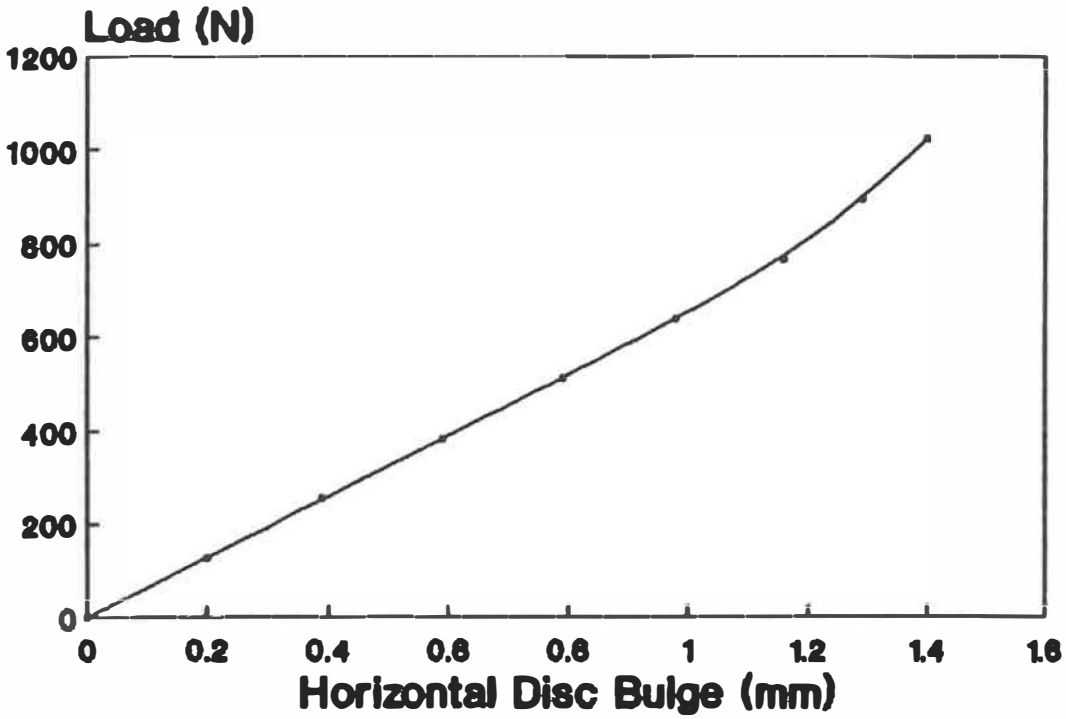

Fig. 4.11 Predicted variation of posterior horizontal disc bulge at its mid-hight section with axial compressive force (nonlinear 3-D model).

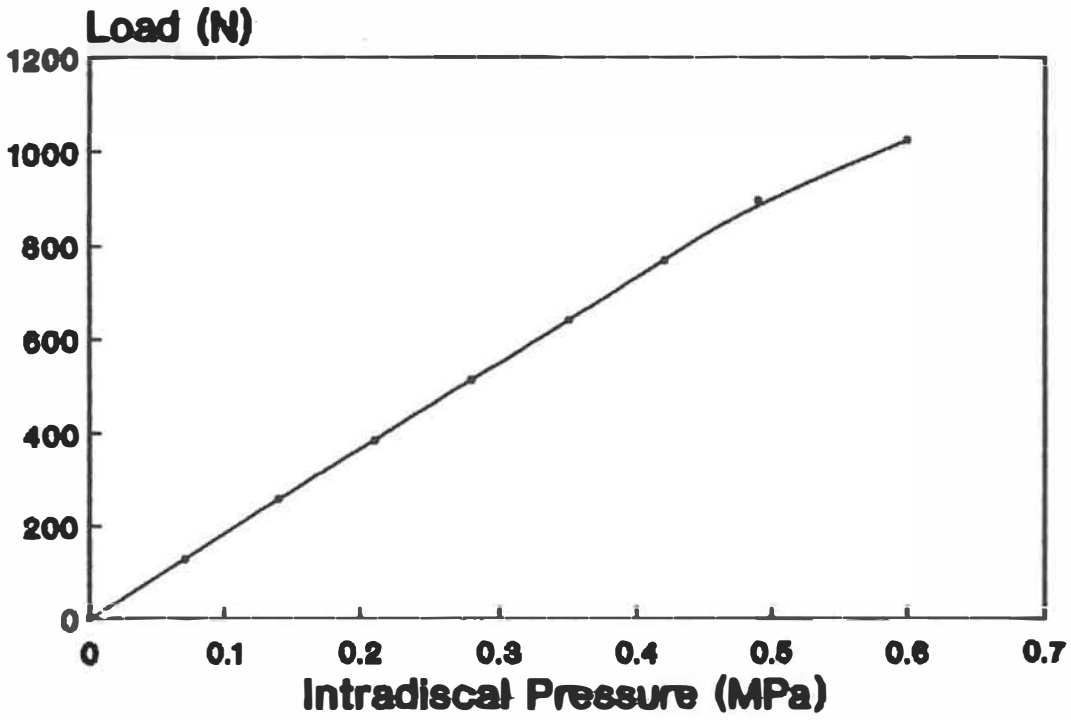

Fig. 4.12 Predicted variation of the intradiscal pressure versus axial compressive force (nonlinear 3-D model).

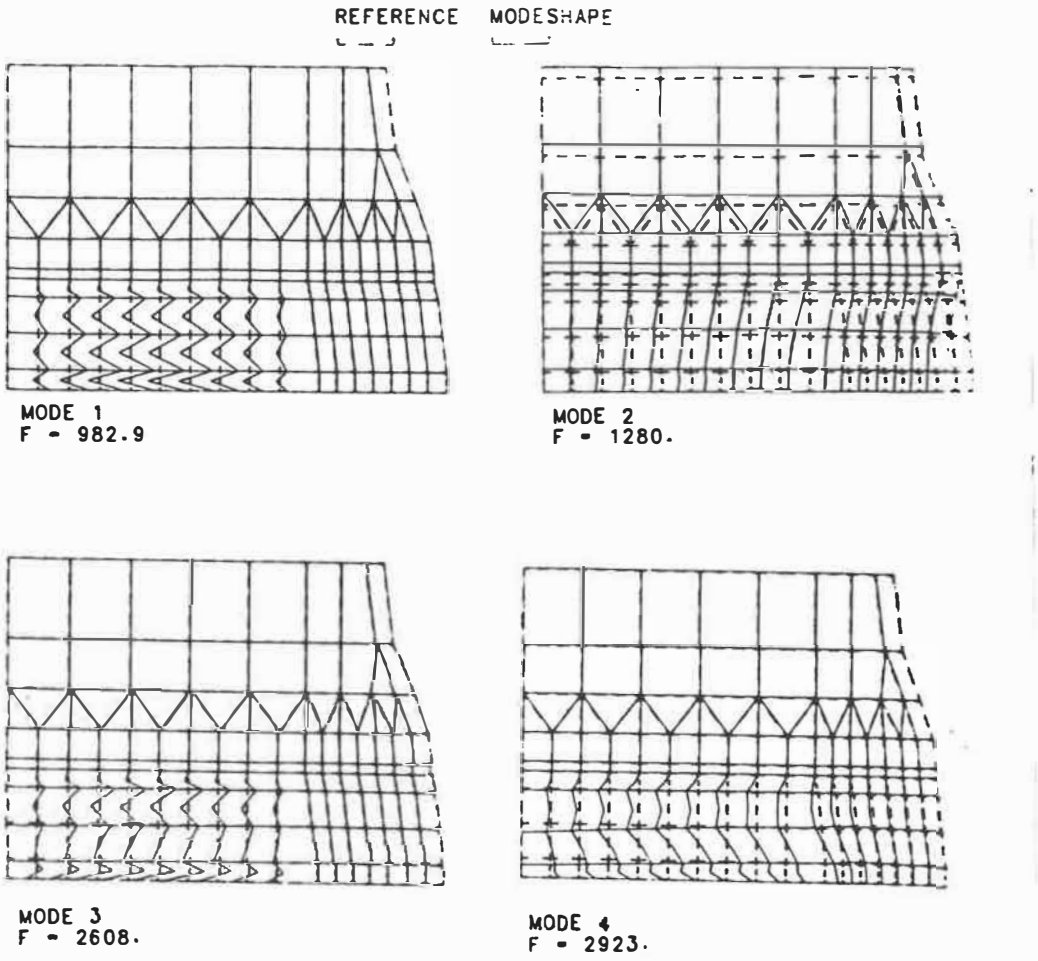

Fig. 4.13 The first four mode shapes of the displacement-based axisymmetric model without the added mass.

the nucleus is disturbed and the solid regions do not displace. Therefore, since the load is applied on the solid part of the structure, the effect of these circulation modes in total response of the structure is negligible. In this case, the second mode of the model is the fundamental mode. The first four mode-shapes of the axisymmetric model (without the added mass) with potential-based fluid elements are shown in Fig. V.1 of Appendix V. In these figures, no displacement in the fluid region is observed because in the formulation there is no displacement degree of freedom for the fluid region. In the 3-D model with displacement-based fluid elements, there is no circulation mode, probably due to the coarse mesh used. The first 4 mode-shapes of the 3-D top-constrained model (without the added mass) are shown in Fig. V.2 of Appendix V. By adding the upper body mass the fundamental frequency of the compression mode of the models reduces dramatically. Figure V.3 of Appendix V shows the first 4 mode-shape of the axisymmetric model with the upper body mass on top and displacement-based fluid elements.

The natural frequencies for the unconstrained 3-D model with and without body mass are listed in Table 4.4. The mode shapes corresponding to these frequencies are shown in Fig. 4.14 for the model with the body mass and Fig V.4 (Appendix V) for the model without the upper body mass.

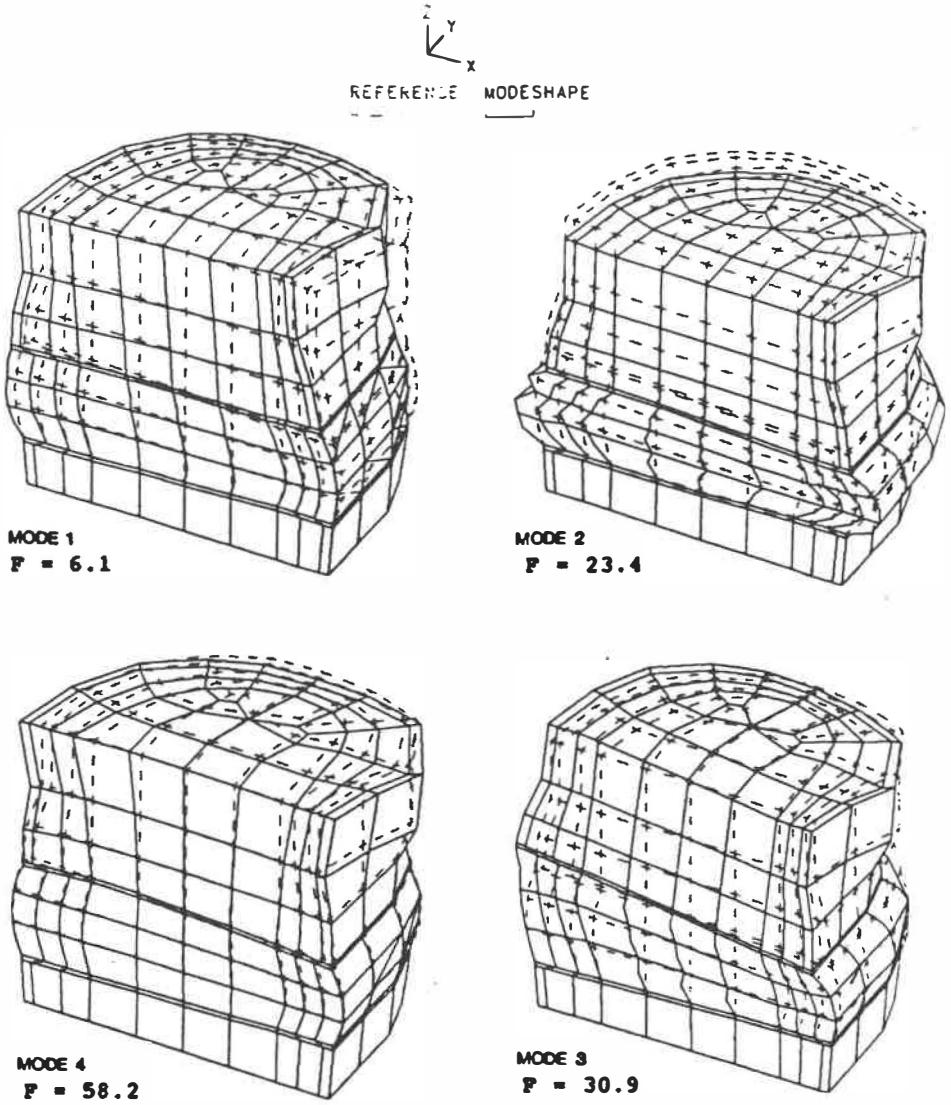

Fig. 4.14 The first four mode shapes of the unconstrained 3-D model with the upper body mass (no preload). (F = Frequency)

As is seen, the first frequencies in Table 4.4 are associated with rotation whereas the second frequencies correspond to the axial mode. The natural frequencies significantly decrease with the addition of the body mass.

Table 4.3. Natural frequencies of constrained models with no preloads (Hz)

		Mode #1	Mode #2	Mode #3	Mode #4	Mode #5
Axisymmetric displacement -based	m=0 Kg	983	1280*	2608	2923	3216
	m=40 Kg	32.2*	982.9	2602	2753	3213
Axisymmetric potential-based	m=0 Kg	1281*	3979	4364	5393	6766
	m=40 Kg	31.9*	3231	4556	5135	6544
Axisymmetric incompressible solid	m=0 Kg	1281*	2951	3508	3694	4251
3-D displacement -based	m=0 Kg	1158*	1256	1853	1902	1980

* Fundamental frequency of the structure

Table 4.4. Natural frequencies of unconstrained 3-D displacement-based model (Hz)

Mode No.	No preload m= 0 Kg	No preload m= 40 Kg
1	657.9	6.1
2	1163	23.4
3	1259	30.9
4	1723	58.2

Finally in order to directly compare the predictions with the measurements, the 3-D model is analysed under the body mass of 40 Kg and different compression preloads of 0 N and 680 N. In this case the top of the model is constrained to move only in the Z direction. The computed natural frequencies of the first four modes are listed in Table 4.5. The first four mode shapes of this case with no preload are shown in Fig. 4.15.

In order to show the possible effect of the disc degeneration on the dynamic response of the motion segment, the bulk modulus of the disc is reduced and frequency analyses are performed to find the natural frequencies. The natural frequencies of the 3-D model for different bulk moduli are listed in Table 4.6. From this table we can see that, reducing the nucleus bulk moduli (disc degeneration) markedly affects the axial mode frequency. Figure 4.16 shows the variation of the axial frequency of the model (with the added mass) with the bulk modulus. In this figure the model with no nucleus is considered as the model with zero bulk modulus.

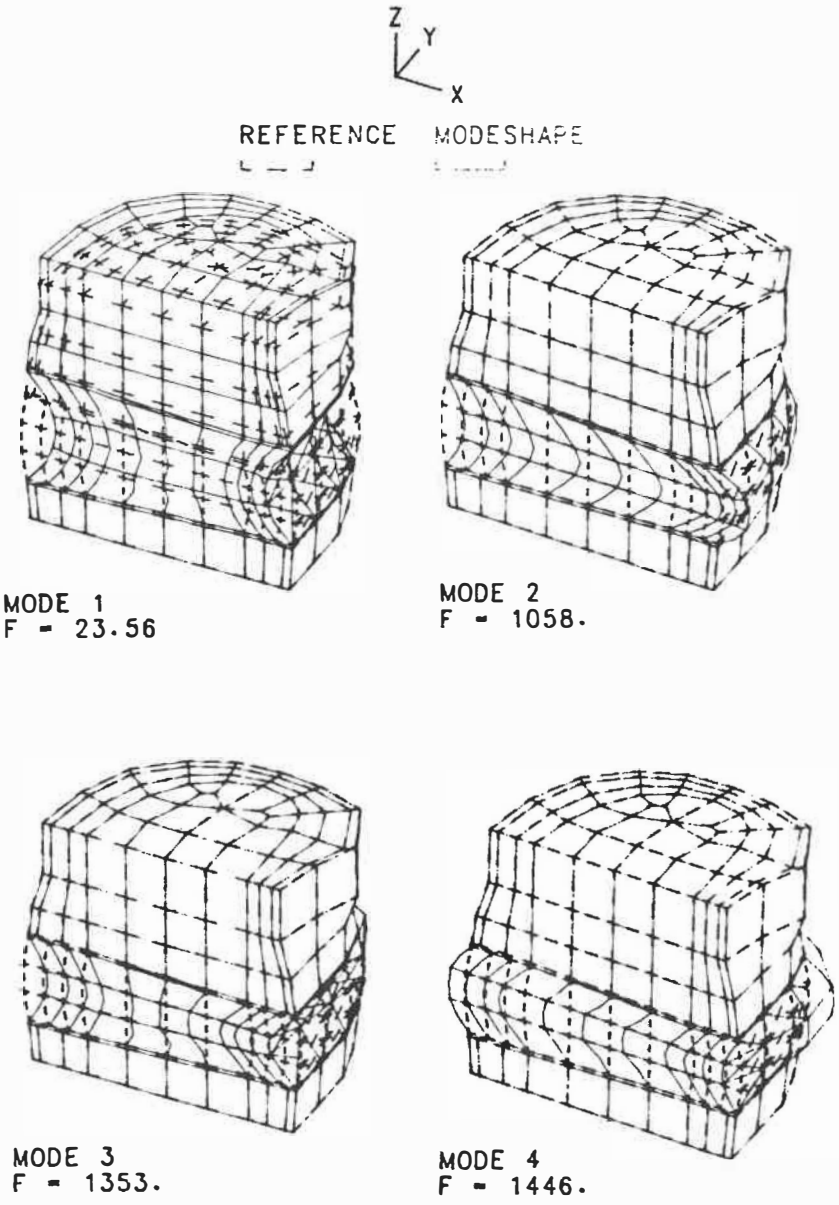

Fig. 4.15 The first four mode shapes of the top constrained 3-D model with the upper body mass (no preload). (F = Frequency)

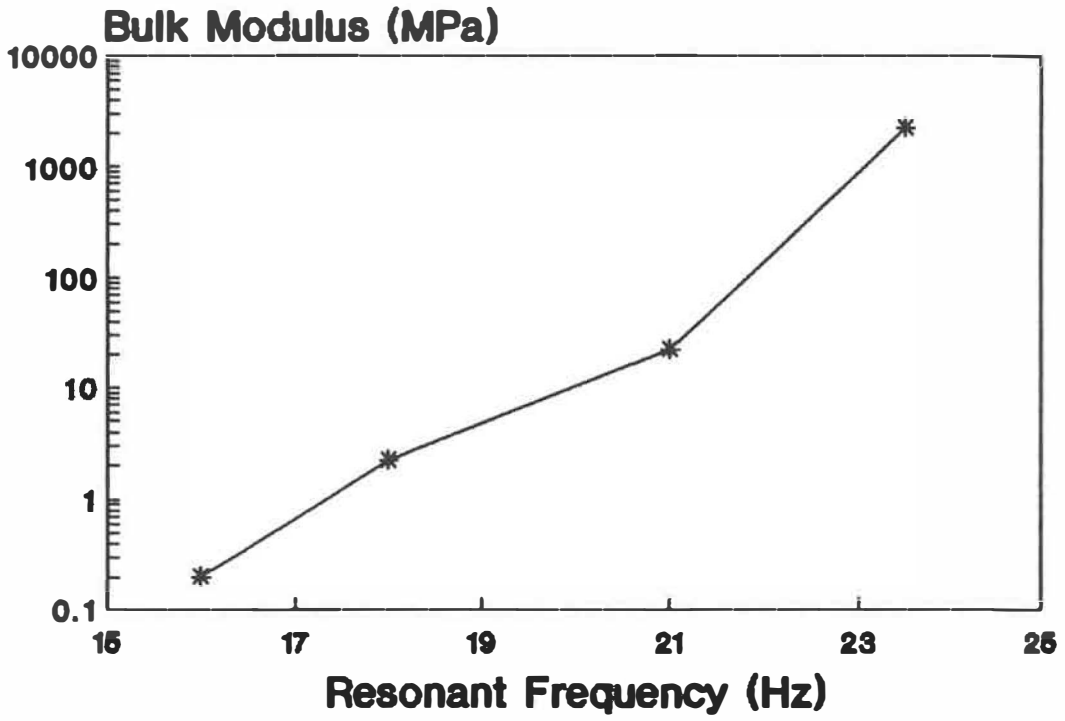

Fig. 4.16 Variarion of the resonant frequency (3-D model with the upper body mass) with the bulk modulus.

Table 4.5. Natural frequencies of the 3-D model simulating experiments with 40 Kg mass (Hz)

Mode No.	No preload	680 N preload
1	23.5	26.
2	1058.	1330.
3	1353.	1977.
4	1446.	2028.

Table 4.6. Natural frequencies (Hz) of the 3-D model for different bulk moduli (B) for the nucleus

Mode No	Disc with no nucleus	B=.22 (MPa)	B=2.2 (MPa)	B=22. (MPa)	B=2200. (MPa)
1	5.1	5.1	5.2	5.3	6.1
2*	15.8	16.1	18.0	21.4	23.4
3	25.3	25.2	25.6	26.0	30.9
4	58.1	58.1	58.2	58.2	58.2
5	77.3	77.1	77.4	77.4	77.9

* Axial mode

4.3.3 Forced Vibration Analyses

Initially the axisymmetric model without the body mass and compression preload is used to perform steady state response analyses. As expected, the model predicts quasi-static behaviour when the frequency of the applied harmonic load remains much lower than the fundamental frequency of the system. The effect of the presence of damping in such cases turns out to be negligible. In Fig. 4.17, the steady state impedance results of the model are compared

with the experimental data reported by Kazarian [30]. This figure shows mechanical impedance and phase angle versus frequency for different discs of the lumbar spine. The phase angle indicates the phase relation between the force and the velocity. As is shown in Fig. 4.17 the numerical results of the model which is related to the L2-L3 disc agree very well with the experimental results.

In order to excite as many modes as possible, a step load with a short rising time of 1.E-05 second and an amplitude of 400 N is applied and the linear transient response is computed. In this case the implicit time integration technic of Wilson-θ method with a time step of 1.E-05 second, and consistent mass matrix have been used. Figure 4.18 shows the pressure variation at three different points in the nucleus region under a step load of 400 N. The intradiscal pressure is found to vary both with location inside the nucleus and with time and reaches a maximum of 2.7 times that evaluated under equivalent static loading.

The band-plots of the pressure variation in the nucleus (Figs. IV.5 of Appendix IV) also show the gross pressure distribution in the nucleus at different time steps. In these figures different colors show different pressure intensities. As is shown, the pressure reaches its maximum first at the center of the nucleus along its ver-

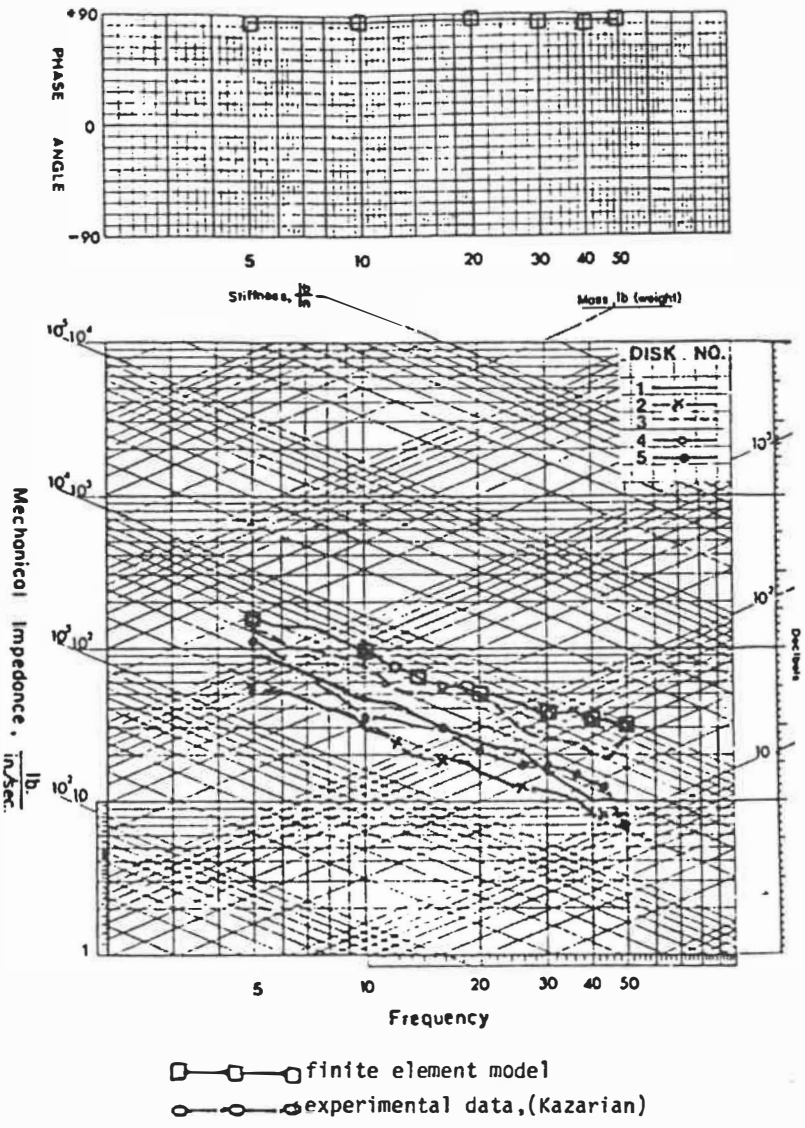

Fig. 4.17 Comparison of the steady state impedance results of the axiymmetric model with the experimental results reported by Kazarian [30].

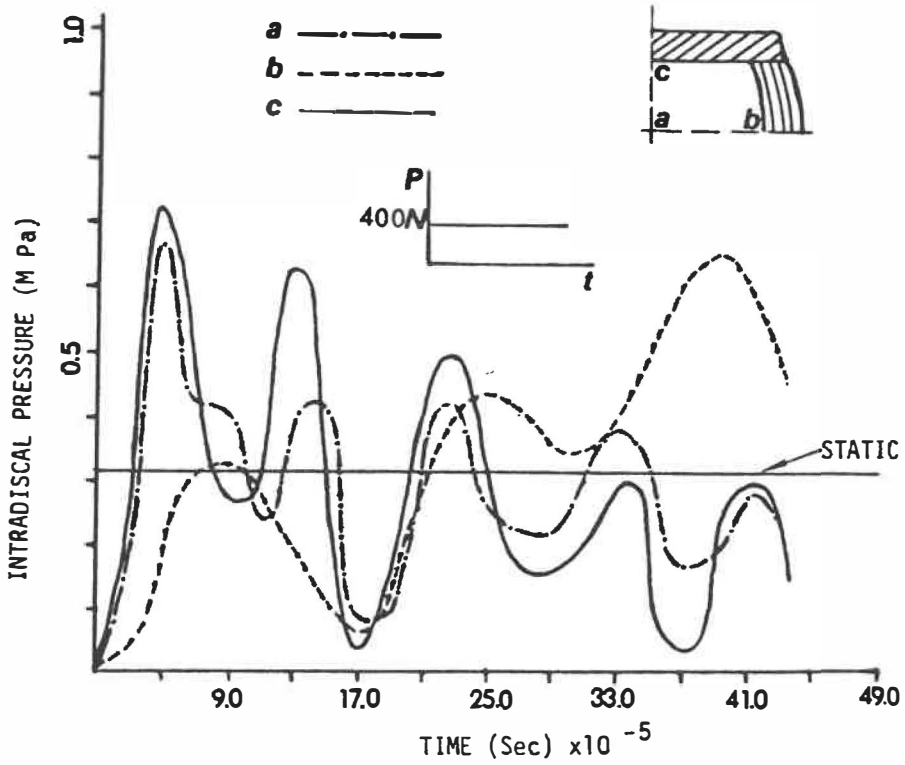

Fig. 4.18 Pressure variation in the nucleus with time and location, under 400 N step load (axisymmetric model without the upper body).

tical centerline and then as the time passes the maximum pressure shifts to the sides along the annulus-nucleus border. The maximum values of the axial displacement, horizontal disc bulge, and tensile hoop stress in the disc annulus are computed to be about twice larger than those in the equivalent static condition. When the body mass of 40 Kg is added on top of the model, a single degree-of-freedom behaviour is predicted under the step load. In this case, the nucleus pressure remains unchanged with the location and reaches a maximum of nearly twice the value of that in the equivalent static case.

The steady state compliance response of the 3-D model with the body mass is shown in Fig. 4.19 for different compression preloads. The results are computed using a measured equivalent damping ratio of .08. The compression preload is noted to have increasing effect on the resonant frequency and decreasing effect on the resonant amplitude.

The effect of disc nucleus material on the dynamic response of the motion segment is also shown in Fig. 4.20 by comparing the steady state compliance response of the 3-D model with and without the nucleus. The results for the remaining cases with the bulk modulus varying from zero (i.e. nucleutomy) to 2200 MPa (i.e. normal) are computed to be in between the cases shown in Fig. 4.20.

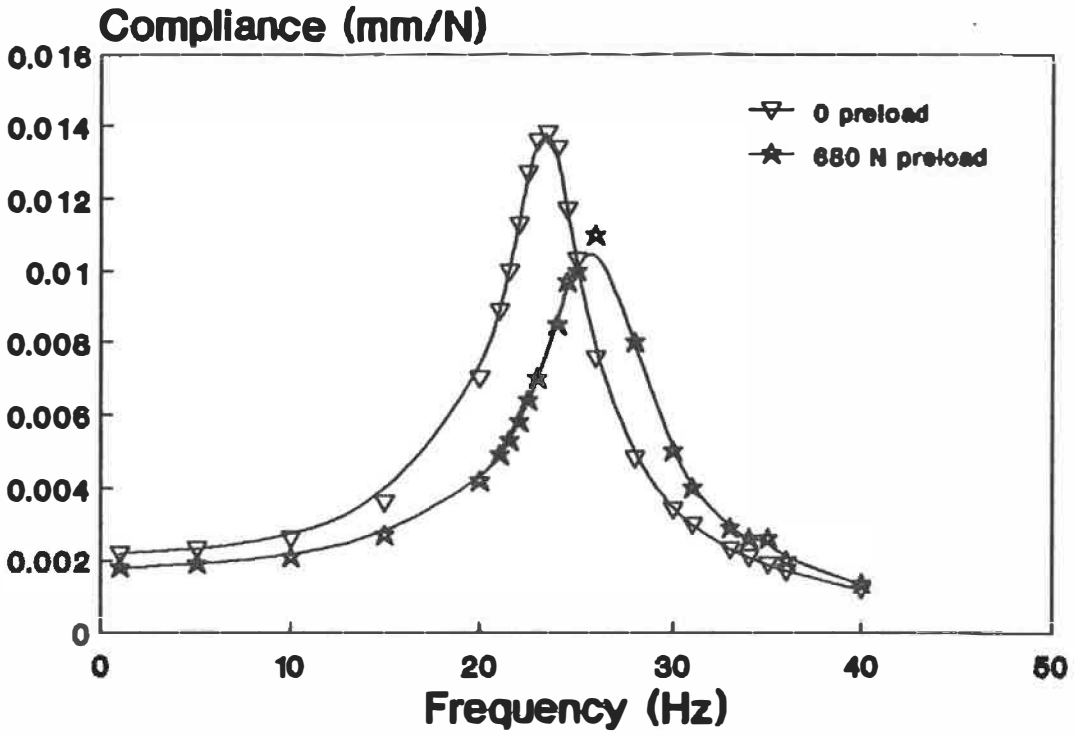

Fig. 4.19 Predicted steady state compliance response of the 3-D model with the upper body mass of 40 Kg and different compression preloads.

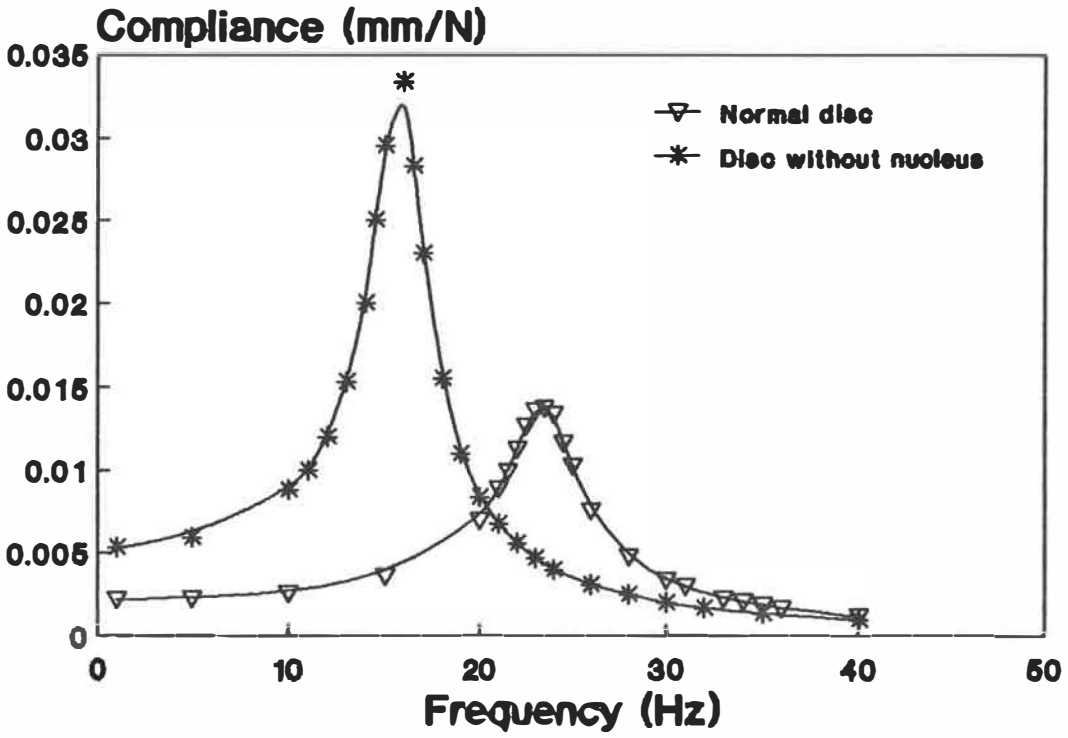

Fig. 4.20 Predicted steady state compliance response of the 3-D model with and without the nucleus, and with the upper body mass of 40 Kg.

CHAPTER 5

DISCUSSION

5.1 INTRODUCTION

This study has been performed to investigate the mechanical response of lumbar motion segments under dynamic loading situations such as those associated with impact and vibration. Although the frequencies of vibration are evaluated for both axial and nonaxial (i.e., lateral and rotation) modes, the response analyses are executed only under axial time-dependent loads. This is justified for the reasons that the axial mode of vibration inputs experienced by workers for example during the operation of motor vehicles is of prime importance. The effect of vibrations with nonaxial components on the flexed segments, however, needs to be studied separately.

Despite of the low number of specimens (7 motion segments), the power of the t-Tests [46] show that the sample size is adequate, specially for the comparison of the means at different preloads. In this case, since the samples related to different means are not independent, Matched Pairs t-Tests are used, and the computed powers are found to be 0.99 at a significant level of 0.5 percent. Considering a two-sided test, the powers for the tests (mean values of resonant frequency, compliance, etc.) are

about 0.95 with an allowance of 10 percent of the mean value at a significant level of 5 percent.

In contrast to the experimental part, the present finite element studies consider only the disc-vertebra unit with no posterior elements. The effect of the presence of facets on the state of stress and strain throughout the segment could also be the subject of another study which is planned for future investigations. Moreover, in the present study, only a single motion segment is considered. Accurate evaluation of the dynamic characteristics of the whole lumbar spine is however believed to be possible when based on the knowledge gained during the research on single motion segments.

5.2 FINITE ELEMENT MODELS

In this section some of the experiences using different fluid elements are presented. As mentioned before, displacement-based fluid formulation yields some spurious modes, which can be eliminated by either checking the mode shapes or using a penalty method for irrotationality of displacement in the fluid [15,23,63]. In both cases, to avoid over-stiffening behaviour, reduced integration order for the fluid elements is recommended [23,63]. In this study, using penalty on irrotationality or full integration order resulted in over-stiffened elements with nucleus

pressures larger than those reported in the experimental results (about 10 times). Considering no irrotationality constraint with reduced integration yielded satisfactory results in both mode superposition and time integration methods. In this case, under static loads, pressure values at the integration points in an element, are not uniform and pressure smoothing [27] are performed by averaging these values in each element [63]. It is also worth noting that refining the axisymmetric model by increasing the number of its fluid elements resulted in more circulation modes while in the three-dimentional model with a relatively coarse mesh, no circulation mode was observed. This agrees with the previous observations reported in the litrature [23].

As expected, no circulation mode is observed in the models with potential-based fluid elements. In this case the results obtained with the time integration method is satisfactory and preferable to the displacement-based method, since no pressure smoothing is required. But in the mode superposition technique, the displacement-based formulation is found to be more economical when the steady state displacement response of the structure is computed. In this case, the mode shapes are normalized relative to the mass [10], and they can be used directly to calculate the steady state displacement response by hand.

In modeling the fluid region with incompressible solid elements, although reasonable results are obtained in the static case, the computed stresses in dynamic analysis are less reliable than those based on displacement-based or potential-based methods. This is likely due to the possible numerical errors caused by choosing the value of the Poisson's ratio very close to 0.5.

5.3 FREQUENCY RESPONSE - COMPARISON OF RESULTS

The mean measured resonant frequencies (Fig. 4.3) for the case without facets are 23.5 Hz and 33. Hz for the compression preloads of 30 N and 680 N respectively. The fundamental frequencies in the axial vibration computed using the nonlinear 3-D model that simulates the experimental set up is listed in the first row in Table 4.5 for two different preloads. These frequencies are 23.5 Hz and 26. Hz under compression preloads of 0 N and 680 N respectively, and are found to compare with the foregoing measured frequencies. Both results indicate the stiffening effect of compression preload on the response. The computed and measured results for the 0 N compression preload compare very well, but for the 680 N preload the computed frequency (26 Hz) is less than the measured frequency (33 Hz). Therefore, by increasing the preload, the motion segment appears to become stiffer than its finite element model. This likely

suggests the existance of other stiffening effects besides the nonlinear material property of the collagenous fibres accounted in the nonlinear model. Apart from the frequencies, the measured and predicted steady state compliance data of Figs. 4.2 and 4.19 are also found to be in general agreement with each other.

Steady state measurements by Kazarian [30] indicate that the axial resonant frequency of motion segments (without any added mass) is well above the tested range of 5 to 50 Hz. Some of his L5-S1 multi-motion segments demonstrated resonant frequencies in the range of 30 to 40 Hz. Markolf [52] measured axial resonance of about 241 to 245 Hz for a L2-L3 disc with a mass simulating the head. Moreover, a fundamental axial frequency of 864 (Hz) was computed in a free vibration model study of a disc-vertebra unit [22]. The foregoing results qualitatively agree with those of the present study that, without a mass, the axial frequency is about 1200 Hz and that the presence of a mass on top of the model markedly decreases this frequency.

The in-vivo whole body axial vibration studies have indicated that the resonant frequency of the body is at about 4 to 6 Hz [44,70]. It is known that the axial frequency of a bar element is inversely proportional to its length. Simulating the whole spinal column as a uniform rod

[26], the evaluation of a resonant frequency of about 31.8 to 34.5 Hz (Fig. 4.3) for a single motion segment with a mass of 40 Kg and compression preloads of 390 N to 680 N respectively appears, therefore, to be in qualitative agreement with these in vivo tests.

The magnitude of magnification factor for the preloads up to 530 N is about 6 (Fig. 4.9) which is about three times larger than that of in-vivo whole-body vibration measurements [65,111]. This shows that in the linear range, the response of the system (displacements and strains) at resonance is about 6 times higher than its equivalent static case. The linear range in this analysis is considered when the applied force has a peak to peak value of less than 50 N.

Considering the nonlinear behaviour under high amplitude vibrations, the intervertebral joint is expected to act as a hard or soft spring. Therefore, under relatively large applied loads causing a nonlinear response with a large amplitude, the natural frequency of the system will be different from that of the linear system, and it might vary with the amplitude of vibration [12]. In this case the dynamic magnification factor might not become as large as that in the linear system.

5.4 DAMPING CHARACTERISTICS AND MEASUREMENTS

Using the half-power (bandwidth) method, Markolf [52] evaluated an equivalent damping ratio of 0.04 to 0.08 which compares well with the values of 0.05 to 0.06 of the present work. On the other hand, hysteresis values of about 0.13 to 0.22 which varies with age [38] and 0.37 which decreases with time to less than 0.10, due to long-term loadings [94], have been reported by other investigators. These are noted to be larger than the value of 0.05 under compression preload of 390 N shown in Fig. 4.6. Such difference could be due primarily to the vibrating loads of 540 N and 250 N in the foregoing studies which are much larger than the load of about 50 N in the present study. This resulted in a higher magnitude of displacement response as well as the hysteresis value which is proportional to the displacement response. The hysteresis damping significantly reduces as the preload increases. However, the variation of equivalent viscous damping of the system (which is proportional to the inverse of magnification factor Fig. 4.9) with preload is not significant.

5.5 EFFECT OF THE POSTERIOR ELEMENTS

The effect of facet joints in increasing the stiffness of segments and hence their fundamental frequency is corroborated by a number of static and dynamic investigations on the biomechanics of motion segments [7,28,30,90

,115].

As mentioned in section 4.2.2 at certain preloads for some of the intact specimens (specimens #1 and #5) the stiffness increment considerably increases. The results at these preloads are not accounted for in the statistical analyses. This suggests that the effect of the facet joints is not significant up to a certain preload (between 530 N and 680 N in these experiments). The value of this preload seems to depend on the structure of the posterior elements, particularly the facet articular surfaces and the way the top of the specimen is constrained in the tests. This is also shown by Yang and King [115] who performed some tests on isolated facet joint and concluded that in extension or compression of the facets, the joint stiffens rapidly with deformation, reaching a stiffness of 1.3 KN/mm at a deformation of 2.2 mm. They stated this as an indication of bony interaction through a thin intervening layer of soft tissue. Thus, the mechanism of load transmission is due to the bottoming-out of the tip of the inferior facet on the pars interarticularis of the vertebra below.

5.5 EFFECT OF POSTURE, VIBRATION AMPLITUDE AND PRELOAD ON THE WHOLE BODY RESONANCE FREQUENCY

Previous studies [13,71,105] have shown that variations of muscle activities during different postures,

vibration amplitude of the applied force, and compression preload on the spine can change the whole-body resonance frequency.

Fairley and Griffin [13] used five postures of sitting position and found a maximum increase of 1.5 Hz in resonance frequency over what was an extreme range of postures. They also found that the mean resonance frequency decreased from 6 Hz to 4 Hz when the amplitude of the input vibration was increased by a factor of eight.

Vogt et al [105] investigated the linearity of the seated body by measuring the mechanical impedance under different preloads in the form of different magnitudes of zero-frequency longitudinal (Z-axis) acceleration in a centrifuge. The main resonance frequency increased from 5 to 8 Hz as the acceleration was changed from 1g to 3g. They concluded that the stiffness of the body in the spinal direction had increased and proposed a linear relationship between the stiffness of the body and the force acting on it. It was argued that any frequency change due to muscle contraction alone would be less noticeable. In Fig. 4.3, it is also seen that, the resonance frequency of the motion segment increases with increase in the preload, but its slope is not linear. In this figure, the rate of increment in resonance frequency with preload decreases as preload

increases.

5.7 CLINICAL IMPLICATIONS

Previous static studies have demonstrated that under pure axial compression the most vulnerable elements of a normal disc-vertebra unit are the cancellous bone and the subchondral end-plate adjacent to the nucleus space and not the disc annulus [68,78,86,89,103]. The present finite element study predicts that the disc pressure and adjacent cancellous compressive stress may increase by as much as 2.7 times of that in static situation depending on the nature of the applied load (Figs. IV.5 of Appendix IV). This predicts the possible vulnerability of the end-plate and adjacent cancellous bone to fracture.

In axial impact experiments on single motion segments, localized end-plate fractures and compression fracture of the vertebral body occurred in about 34% of specimens tested [68]. Fracture of the bone adjacent to the nucleus space under axial vibration loads, occurring suddenly or cumulatively as in fatigue, results in the loss of disc confined fluid which could then initiate or accelerate the process of segmental degeneration [47,49,88,103].

It has been observed that the rate of creep increases with vibration [30.37,38]. The vibration, therefore,

may alter the disc properties such as permeability in order to facilitate the fluid flow. This likely mechanism appears to be advantageous in playing a positive role in the nutrition of the intervertebral discs [29]. In order to prevent injury, the vibration should, however, be limited to a safe range not to generate exessive stresses in the spinal elements.

Neuropharmacological effects of vibration on the dorsal root ganglion of rabbit have been studied to understand the possible relationship between vibration and the development of back pain [107]. A decrease in dorsal root ganglion substance P, a known pain mediator, and an increase in VIP, another pain modulator, were observed following low frequency vibration. These variations are compatible with those following peripheral nerve injury. The possible effect of vibration frequency and amplitude on the nerve injury, however, needs to be further clarified.

The present finite element studies predict that disc degeneration could cause a decrease in the resonance frequency (Table 4.6) and an increase in response amplitude (Fig. 4.20) of the motion segment. This suggests a deteriorating role of vibration in the degenerated discs. That is, in an already degenerated disc, the response under vibration markedly increases resulting in higher stresses

and strains and hence higher risk of further disc degeneration.

CHAPTER 6

CONCLUSIONS AND FUTURE WORK

6.1 CONCLUSIONS

Steady state response, resonant frequency, and damping of seven lumbar motion segments in axial direction are experimentally determined under an upper body mass of 40 Kg. The influence of facet joints and different compression preloads on the response is also measured. To supplement the measurements , axisymmetric and 3-D models of a L2-L3 disc-vertebra unit are developed and the response under impact and vibration is predicted. The effect of the presence of a mass of 40 Kg and a number of different compression preloads on the results are also computed. The salient conclusions of the present work are as follows:

1) There is a good agreement between the experimental and finite element results. The results are found to be comparable with those of the other studies.

2) The addition of the upper body mass of 40 Kg significantly decreases the segmental frequencies, irrespective of the magnitude of compression preload.

3) As the compression preload increases, the segmental frequencies markedly increase while the compliance

magnitudes decrease.

4) Up to a certain preload (mainly 530 N to 680 N in these experiments), removal of the facet joints slightly decreases the axial resonant frequency.

5) The viscous damping ratio of the segment is evaluated to be in the range of 0.05 to 0.13, using three different methods (half-power Bandwidth, Energy loss per cycle and Resonance amplification).

6) Vibration loadings with frequency close to the resonant frequency of the system and impact loading markedly increase the response and hence the state of stress and strain throughout the segment. The most vulnerable element is found to be the cancellous bone adjacent to the nucleus space.

7) A decrease in the value of the nucleus bulk modulus reduces the axial resonance frequency of the motion segment. Therefore, due to the degeneration, the disc becomes softer.

6.2 DIRECTION FOR FURTHER RESEARCH

The experimental part of the present research work can be continued by dynamic testing of different spinal

units consisting of a number of vertebrae and intervertebral discs in order to investigate the effect of other parameters such as spinal curvature and level on the resonance frequency and damping.

The dynamic load distribution between various components can be investigated by measuring the intradiscal pressure and bone strains. In this way the biomechanical role of different elements under vibration can be better understood.

The hardening or softening behaviour of the motion segment due to the high amplitude vibrations can also be investigated by applying high amplitude sinusoidal force or displacement and studying the nonlinear response of the structure.

The complementary finite element studies are suggested for the above experimental works. Also by modelling the facet joints, the effect of the facets contact at high preloads on the system resonance frequency can be investigated.

REFERENCES

1. Bathe KJ: "Finite element procedures in engineering analysis." New Jersey, Prentice Hall Inc, 1982

2. Bathe KJ: "Adina- A finite element program for automatic dynamic incremental nonlinear analysis." Rep. 82448-1, Dept Mech Eng, MIT, 1975

3. Bathe KJ, Hahn WF: "On transient analysis of fluid-structure systems." Computers & Structures 10:383-391, 1979

4. Belytschko T, Kulak RF, Schultz AB, Galante JO: "Finite element stress analysis of an intervertebral disc." J Biomech Eng 101:53-57, 1979

5. Belytschko T, Kulak RF: "A finite-element method for a solid enclosing an inviscid,incompressible fluid." J Appl Mech, 609-610, 1973

6. Belytchko TB, Kennedy JM: "A fluid-structure finite element method for the analysis of reactor safety problems." Nuclear Engineering and Design 38:71-78, 1976

7. Berkson MH, Nachemson A, Schultz AB: "Mechanical pro-

perties of human lumbar spine motion segments. II Response in compression and shear, influence of gross morphology." J Biomech Eng 101:53-57, 1979

8. Brown T, Hansen RJ, Yorra AJ: "Some mechanical tests on the lumbosacral spine with particular reference to the intervertebral discs." J Bone Joint Surg 39A:1135-1164,1957

9. Burns ML, Kaleps I, Kazarian LE: "Analysis of compressive creep behaviour of the vertebral unit subjected to a uniform axial loading using exact parametric solution equations of Kelvin-solid models-Part I. Human intervertebral joints." J Biomechanics 17:113-130, 1984

10. Clough RW, Penzien J: "Dynamics of structures." New York, McGraw-Hill 1975, pp 52-77

11. Edwards RG, Lafferty JF, Knapp CF: "Exprimental and analytical determinations of the mechanical impedance response of animals to vertical vibration." J Biomech 9:56-61, 1976

12. Ewins DJ: "Modal Testing: Theory and Practice." NewYork, John Wiley & Sons Inc. 1984

13. Fairley TE, Griffen MJ: "The apparent mass of the seated human body: Vertical vibration." J Biomech 22:81-94, 1989

14. Farfan HF: "Mechanical Disorders of the Low-Back." Lea & Febiger, Philadelphia, 1973

15. Feng GC, Kiefling L: "Fluid-structure finite element vibrational analysis." AIAA J, 14:199-203, 1976

16. Friberg S, Hirsch C: "Anatomical and clinical studies on lumbar disc degeneration." Acta Orthop Scand (suppl) 19, 1945

17. Frymoyer JW, Pope MH, Costanza MC, Rosen JC, Goggin JE, Wilder DG: "Epidemiologic studies of Low-Back pain." Spine 5:419-423, 1980

18. Frymoyer JW, Pope MH, Clements JH, Wilder DG, Macpherson B, Ashikaga T: "Risk factors in low-back pain." J Bone joint Surg 65A:213-218, 1983

19. Galante JO: "Tensile properties of the human lumbar annulus fibrosus." Acta Orthop Scand (Suppl) 100, 1967

20. Goel VK, Kim YE, Zhang F: "Biomechanical effects of vibration on the human spine." Abstract, International Society for the study of the lumbar spine, Miami, 1988, pp 67

21. Gruber GJ: "Relationships between wholebody vibration and morbidity patterns among interstate truck drivers." National Institute of Occupational Safety and Health, Cincinnati, 1976, pp77-167

22. Hakim NS, King AI: "A three dimensional finite element dynamic response analysis of a vertebra with experimental verification." J Biomech 12:277-292, 1979

23. Hamdi MA, Ousset Y: "A displacement method for the analysis of vibrations of coupled fluid-structure systems." International Journal for Numerical Methods in Engineering 13:139-150, 1978

24. Harkness RD: "Biological functions of collagen." Biol Rev 36:399-463, 1961

25. Heliovaara M: "Occupation and risk of herniated lumbar intervertebral disc leading to hospitalization." J Chronic Diseases 40:259-264, 1987

26. Hess JL, Lombard CF: "Theoretical investigations of dynamic response of man to high vertical accelerations." J Aviat Med 29:66-74, 1958

27. Hinton E, Campbell JS: "Local and global smoothing of discontinuous finite element functions using a least squares Method." International journal for Numerical Methods in Engineering 8:461-480, 1974

28. Hirsch C: "The reaction of intervertebral discs to compression forces." J Bone Joint Surg 37A:1188-1196, 1955

29. Holm S, Nachemson A: "Variations in the nutrition of the canine intervertebral disc induced by motion." Spine 8:866-874, 1983

30. Kazarian LE: "Dynamic response characteristics of the human vertebral column." Acta Orthop Scacd (suppl) 146, 1972

31. Kazarian LE: "Creep characteristics of the human spinal column." Orthopedic Clinics of North America 6:3-18, 1975

32. Kelsey JL, Hardy RJ: "Driving of motor vehicles as a

risk factor for acute herniated lumbar intervertebral disc." Am J Epidemiol 102:63-73 1975

33. Kelsey JL: "An epidemiological study of acute herniated lumbar intervertebral discs." Rheum Rehab 14:144-159, 1975

34. Kelsey JL, White III AA: "Epidemiology and impact of low-back pain." Spine 5:133-142, 1980

35. Kennedy JM, Belytschko TB: "A survey of computational methods for fluid-structure analysis of reactor safety." Nuclear Engineering and Design 69:379-398, 1982

36. King AI: "Elastic deformation characteristics of the spine." Proceedings of Workshop on Bioengineering Approaches to Problems of the Spine, Bethessda, Md, 1970, pp 17-50

37. Klingenstierna U, Pope MH: "Body height changes from vibration." Spine 12:566-568, 1987

38. Koeller W, Muehlhaus S, Meier W, Hartmann F: "Biomechanical properties of human intervertebral discs subjected to axial dynamic compression-Influence of age

and degeneration." J Biomech 19:807-816, 1986

39. Koogle TA, Swenson LW, Piziali RL: "A large displacement dynamic model of the lumbar spine with experimentally determined material properties." Abstract, ORS, Atlanta, 1980, pp 276

40. Kulak RF, Belytchko TB, Schultz AB: "Nonlinear behaviour of the human intervertebral disc under axial load." J Biomech 9:377-386, 1976

41. Kulak RF, Schultz AB, Belytschko T, Galante J: "Biomechanical Characteristics of vertebral motion segments and intervertebral Discs." Orthopaedic Clinics of North America 6:121-133, 1975

42. Lamb H: "Hydrodynamics." New York, 6th Edn Dover publications 1945

43. Lé Comité international pour la Recherche Institut National de Recherche et de Sécurité (INRS). "Les Vibrations aux Postes de Travail." France, 1986

44. Lé Comité international pour la Recherche Institut National de Recherche et de Sécurité (INRS): "Les Vibrations Industrielles." France

45. Lin HS, Liu YK, Ray G, Nikravesh P: "Systems idenfication for material properties of the intervertebral joint." J Biomech 11:1-14, 1978

46. Lincoln EM: "Think and explain with statistics." Ontario, Addison-Wesley Co, 1986

47. Lipson SJ, Muir H: "Proteoglycans in experimental intervertebral disc degeneration." Spine 6:194-210, 1981

48. Liu YK, Ray G: "Systems idenfication scheme for estimation of the linear viscoelastic properties of the intervertebral disc." Aviation, Space and Environmental Medicine, 1978, pp 175-177

49. Liu YK: "Distributed-parameter dynamic models of the spine." Proceedings of Workshop on Bioengineering Approaches to Problems of the Spine, Bethesda, Md, 1970, pp 53-85

50. Liu WK, Chang H: "On a numerical methods for liquid filled systems." Computers & Structures 23:671-677, 1986

51. Malinsky J: "The ontogenetic developement of nerve terminations in the intervertebral discs of man." Acta Anat, 38:96-113, 1959

52. Markolf K: "Stiffness and damping characteristics of the thoracolumbar spine." Proceedings of Workshop on Bioengineering Approaches to Problems of the Spine. Bethesda, Md, 1970, pp 87-143

53. Markolf KL, Morris JM: "The structural components of the intervertebral disc: A study of their contributions to the ability of the disc to withstand compressive forces." J Bone Joint Surg 56A:675-687, 1974

54. Muller WC: "Simplified analysis of linear fluid-structure interaction." International Journal for Numerical Methods in Engineering. 17:113-121, 1981

55. Nachemson A: "Lumbar intradiscal pressure." Acta Orthop Scand (Suppl) 43:1-104, 1960

56. Nachemson A: "Disc pressure measurements." Spine 6:93-97, 1981

57. Nachemson A, Morris JM: "In vivo measurements of intradiscal pressure." J Bone Joint Surg

46A:1077-1092, 1964

58. Nachemson A: "Towards a better understanding of low-back pain: A review of the mechanics of the lumbar disc." Rheum Rehabl 14:129-143, 1975

59. Nade S, Bell E, Wyke BD: "The innervation of the lumbar spinal joints and its significance." J Bone Joint Surg, 62B:255, 1980

60. Natali A, Meroi E: "Nonlinear analysis of intervertebral disc under dynamic load." J Biomech Eng 112:358-363, 1990

61. National Center for Health Statistics: "Limitation of activity due to chronic conditions." United States, 1969 and 1970. Series 10, Number 80, 1973

62. Naylor A, Happey F, Macrae T: "The collagenous changes in the intervertebral disc with age and their effect on its elasticity." Br Med J:570-573, 1954

63. Olson LG, Bathe KJ: "A study of displacement-based fluid finite elements for calculating frequencies of fluid and fluid-structure systems." Nuclear Engineering and Design 76:137-151, 1983

64. Olson LG, Bathe KJ: "Analysis of fluid-structure interactions. A direct symmetric coupled formulation based on the fluid velocity potential." Computers and structures 21:21-32, 1985

65. Panjabi M, Anderson GBJ, Jorneus L, Hult E, Mattson L: "In vivo measurements of spinal column vibrations." J Bone Joint Surg 68A:695-702, 1986

66. Panjabi M, Brown M, Lindahl S, Irstam L, Hermens M: "Intrinsic disc pressure as a measure of integrity of the lumbar spine." Spine 13:913-917, 1988

67. Panjabi MM, Krag MH, White III AA, Southwick WO: "Effects of preload on load displacement curves of the lumbar spine." Orthop Clin North Am 8:181-192, 1977

68. Perey O: "Fracture of the intervertebral end-plate in the lumbar spine." Acta Orthop Scand (Suppl) 25:1-101, 1957

69. Pope MH, Broman H, Hansson T: "Factors affecting the dynamic response of the seated subject." J Spinal Dis 3:135-142, 1990

70. Pope MH, Wilder DG, Jorneus L, Broman H, Svensson M, Anderson G: "The response of the seated human to sinusoidal vibration and impact." J Biomech Eng 109: 279-284, 1987

71. Pope MH, Benda M, Svensson M, Ottoson C, Hansson T: "The impact response of the seated subject." Journal of Orthopaedic Research, 9:150-154, 1991

72. Prasad P, King AI, Ewing CL: "The role of articular facets during $+G_z$ acceleration." J Applied Mech, 41:321-326, 1974

73. Prasad P, King AI: "An experimentally validated dynamic model of the spine." J applied Mech 41:546-550, 1974

74. Quandieu P, Pellieux L: "Study in situ et in vivo of the acceleration of lumbar vertebrae of a primate exposed to vibration in the z-axis." J biomech 15:985-1006, 1982

75. Reuber M, Schultz A, Denis F, Spencer D: "Bulging of lumbar intervertebral discs." J Biomech Eng 104:187-192, 1982

76. Rigby BJ, Hirai N, Spikes JD, Eyring H: "The mechanical properties of rat tail tendon." J Gen Phys 43:265-283, 1959

77. Ritchie JH, Fahrani WH: "Age changes in lumbar intervertebral discs." Can J Surg, 13:65-71, 1970

78. Roaf R: "A study of the mechanics of spinal injuries." J Bone Joint Surg 42B:810-823, 1960

79. Rolander SD, Blair WE: "Deformation and fracture of the lumbar vertebral end plate." Orthop Clin North Am 6:75-81, 1975

80. Rome ML: "Low back pain in industry." A position paper. J occup Med II: 161-169, 1969

81. Sandover J: "Dynamic loading as a possible source of low-back disorders." Spine 8:652-658, 1983

82. Sanjeevi R, Somanathan N, Ramaswamy D: "A viscoelastic model for collagen fibres." J Biomech, 15:181-183, 1982

83. Sedowofia KA, Tomlinson IW, Weiss JB, Hilton RC, Jayson MIV: "Collagenolytic enzyme systems in human

intervertebral disc." Spine, 7:213-221, 1982

84. Seidel H, Bluethner R, Hinz B: Effects of sinusoidal whole-body vibration on the lumbar spine: "the stress-strain relationship." Int Archs Occup Envir Health 57:207-223, 1986

85. Seroussi RE, Wilder DG, Pope MH: "Trunk muscle electromyography and whole body vibration." J Biomech 22:219-229, 1989

86. Shirazi-Adl A: "Strain in fibres of a lumbar disc-Analysis of the role of lifting in producing disc prolapse." Spine 14:96-103, 1989

87. Shirazi-Adl A: "On the fibre composite material models of disc annulus-Comparison of predicted stresses." J Biomech 22:357-365, 1989

88. Shirazi-Adl A: "Simulation of change in the fluid content of human lumbar discs- Mechanical and clinical implications." Spine, in press, 1990

89. Shirazi-Adl A: "Three dimensional nonlinear finite element stress analysis of a lumbar intervertebral joint." PHD thesis, McGill University, 1984

90. Shirazi-Adl A, Drouin G: "Load bearing role of facets in a lumbard segment under sagittal plane loadings." J Biomech 20:601-613, 1987

91. Shirazi-Adl A, Ahmed AM, Shrivastava SC: "A finite element study of a lumbar motion segment subjected to pure sagittal plane moments." J Biomech 19:331-350, 1986

92. Simon BR, Wu JSS, Carlton M, Evans JH, Kazarian LE: "Structural models for human spinal motion segments based on a proelastic view of the intervertebral disc." J Biomech Eng 107:327-335, 1985

93. Simon BR, WU JSS, Carlton M, Kazarian LE, France EP, Evans JH, Zienkiewicz OC: "Poroelastic dynamic structural models of rhesus motion segments." Spine 10:494-507, 1985

94. Smeathers JE: "Some time dependent properties of the intervertebral joint when under compression." Engineering in Medicine 13:83-87, 1984

95. Spilker RL, Daugirda DM, Shultz AB: "Mechanical Response of a simple finite element model of the inter-

vertebral disc under complex loading." J Biomechanics 17:103-112, 1984

96. Spilker RL, Jakobs DM, Schultz AB: "Material constants for a finite element model of the intervertebral discs with a fiber composite annulus." J Biomech Eng 108:1-11, 1986

97. Spilker RL, Jakobs DM, Schultz AB: "Material constants for a finite element model of the intervertebral disk with a fibre composite annulus." J Biomech Eng 108:1-11,1986

98. Stevens RL, Ryvar R, Robertson WR, O Brien JP, Beard HK: "Biological changes in the annulus fibrosus in patients with low-back pain." Spine, 7:223-233, 1982

99. Svensson H, Andersson GBJ: "Low-back pain in 40- to 47-year-old men: Work history and work environment factors." Spine 8:272-276, 1983

100. Tencer AF, Ahmed AM, Burke DL: "Some static mechanical properties of the lumbar intervertebral joint. intact and injured." J Biomech Eng 104:193-201, 1982

101. Tortora GJ: "Principles of human anatomy." New York,

Harper & Row, 1983

102. Urban JPG, Mcmullin JF: "Swelling pressure of the lumbar intervertebral discs: Influence of age, spinal level, composition, and degeneration." Spine 13:179-186, 1988

103. Vernon-Roberts B, Pirie CJ: "Degenerative changes in the intervertebral discs of the lumbar spine and their sequelae." Rheum Rehaab 16:13-21, 1977

104. Virgin WJ: "Experimental investigations into the physical properties of the intervertebral disc." J Bone Joint Surg 33B:607-611, 1951

105. Vogt HL, Coermann RR, Fust HD: "Mechanical impedance of the sitting human under sustained acceleration." Aerospace Med, 39:675-679, 1968

106. Waters RL, Morris JM: "An in vitro study of normal and scoliotic interspinous ligaments." J Biomech, 6:343-348, 1973

107. Weinstein J, Pope M, Schmidt R, Seroussi R: "Neuropharmacologic effects of vibration on the dorsal root gangalion, An animal model." Spine 13:521-525, 1988

108. White III AA, Gordon SL: Synopsis: "Workshop on idiopathic low-back pain." Spine 7:141-149, 1982

109. White III AA, Panjabi MM: "Clinical Biomechanics of the spine." Philadelphia and Toronto, J B Lippincott, 1978

110. Wilder DG, Pope MH, Seroussi RE, Dimnet J: "Creep response of the statically and cyclically loaded lumbar motion segment." Absract, ORS, Sanfrancisco, 1987, p 367

111. Wilder DG, Woodworth BB, Frymoyer JW, Pope MH: "Vibration and the human spine." Spine 7:243-245, 1982

112. Williams JL, Belytschko TB: "A three-dimensional model of the human cervical spine for impact simulation." J Biomech Eng 105:321-331, 1983

113. Wilson EL, Khalvatti M: "Finite elements for the dynamic analysis of fluid-solid systems." International Journal for Numerical Methods in Engineering 19:1657-1668, 1983

114. Yahia H, Newman N: "A light and electron microscopic

study of spinal ligament innervation." Z. mikrosk.-anat. Forsch. Leipzig, 103:664-674, 1989

115. Yang KH, King AI: "Mechanism of facet load transmission as a hypothesis for low-back pain." Spine 9:557-565, 1984

116. Yoshizawa H, O Brien JP, Smith WT, Trumper M: "The neuropathology of intervertebral discs removed for low-back pain." J Pathology, 132:95-104, 1980

117. Zienkiewicz OC, Bettess P: "Fluid-structure dynamic interaction and wave forces. An introduction to numerical treatment." International Journal for Numerical Methods in Engineering 13:1-16, 1978

118. Zienkiewicz OC: "The finite element method." London, McGraw-Hill, 1977

APPENDIX I: The photographs of the gross appearance of the cut surfaces of the intervertebral discs used in the experiments. (Figs. I.1-I.7)

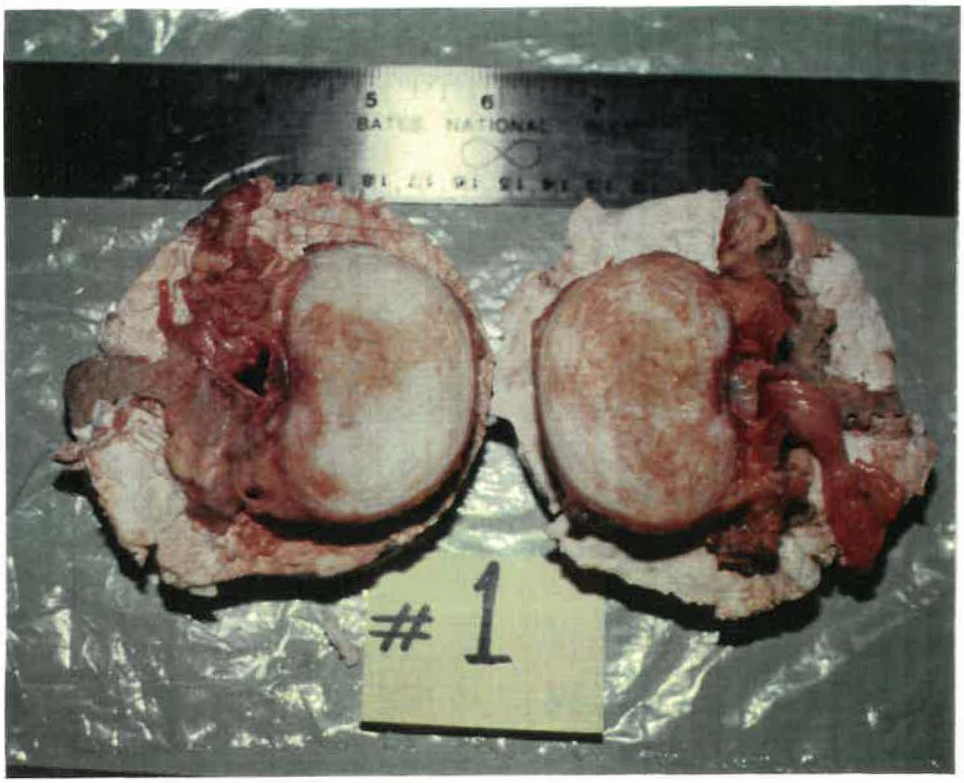

Fig I.1 The photograph of the gross appearance of the cut surfaces of the disc (specimen #1 , grade 0). In the above picture the red spots on the cut surfaces are blood, and they are not due to the disc degeneration.

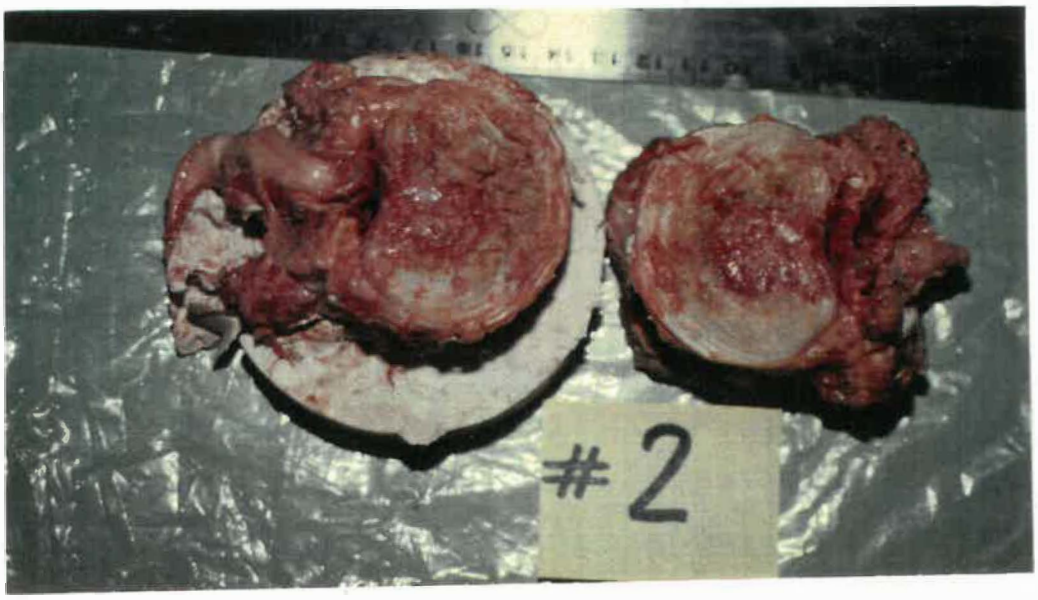

Fig I.2 The photograph of the gross appearance of the cut surfaces of the disc (specimen #2 , grade 2).

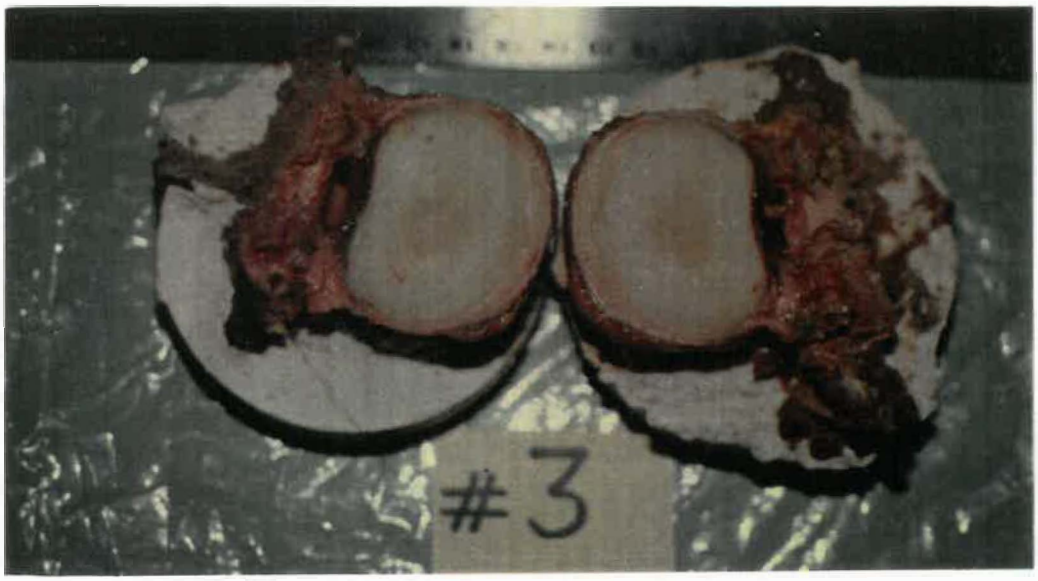

Fig I.3 The photograph of the gross appearance of the cut surfaces of the disc (specimen #3 , grade 1).

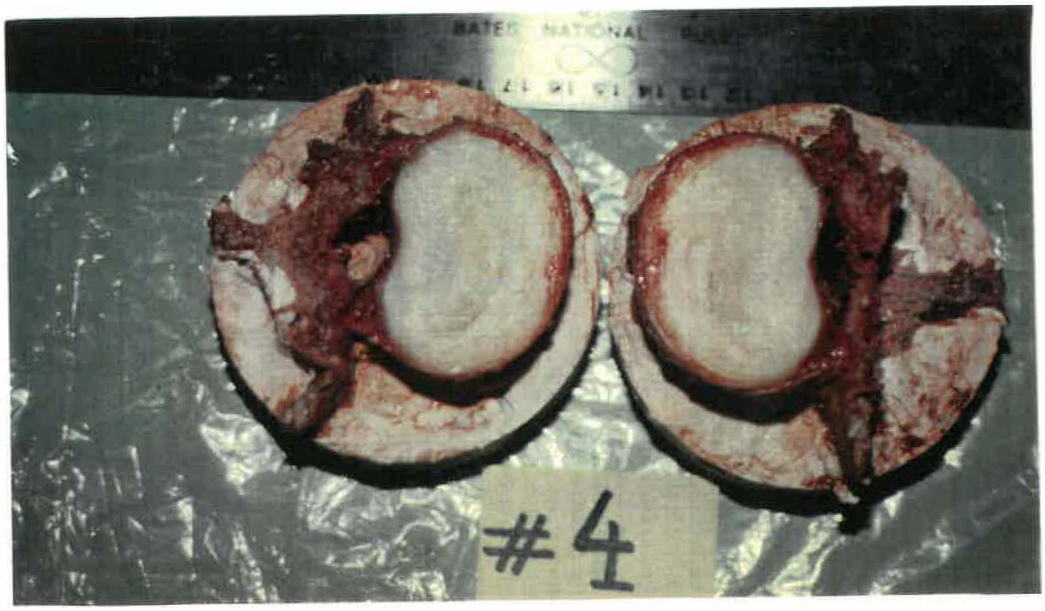

Fig I.4 The photograph of the gross appearance of the cut surfaces of the disc (specimen #4 , grade 0).

Fig I.5 The photograph of the gross appearance of the cut surfaces of the disc (specimen #5 , grade 2).

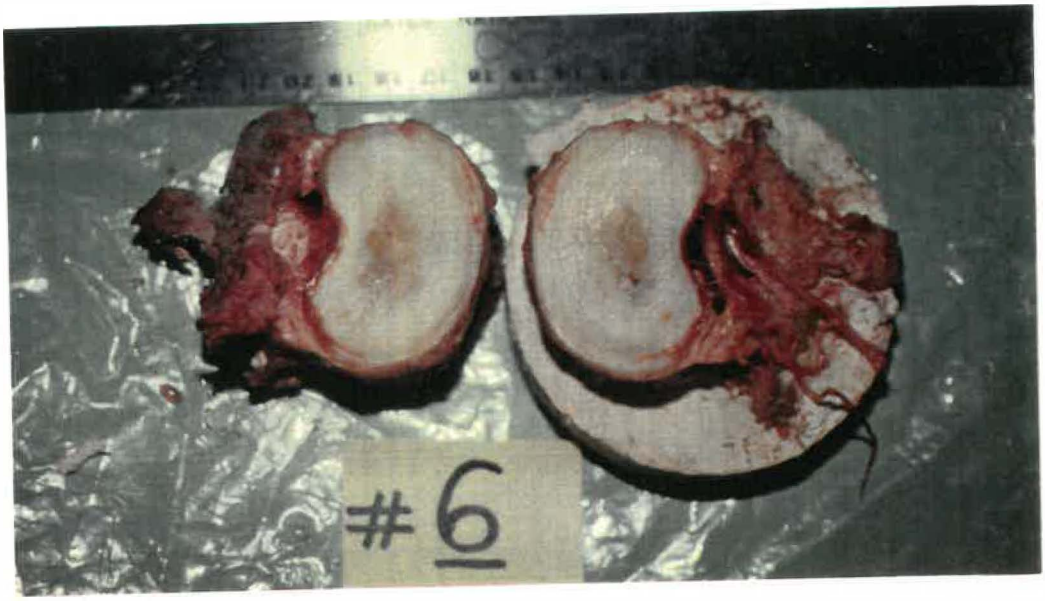

Fig I.6 The photograph of the gross appearance of the cut surfaces of the disc (specimen #6 , grade 1).

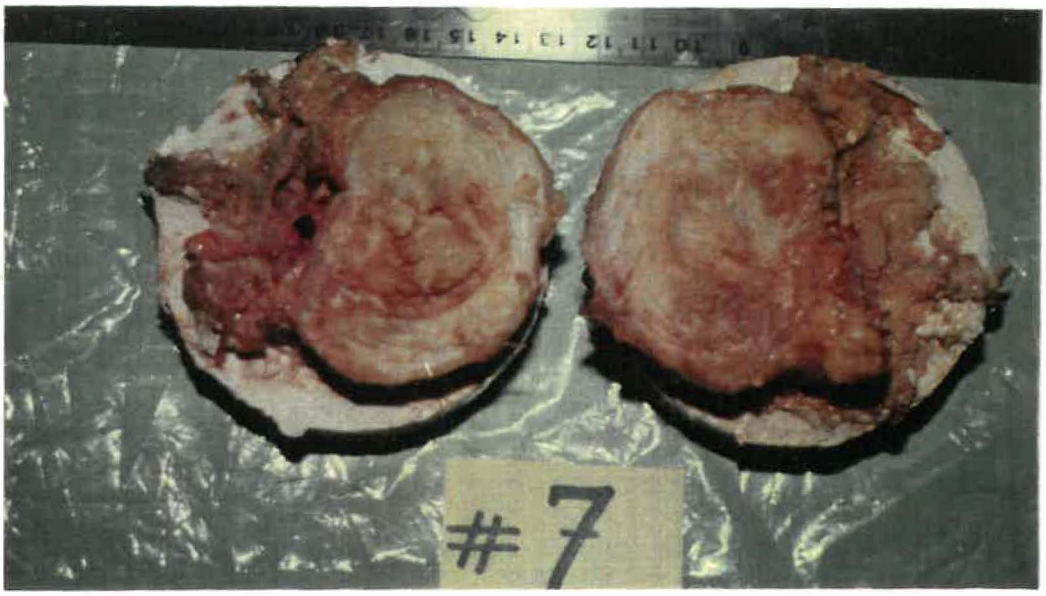

Fig I.7 The photograph of the gross appearance of the cut surfaces of the disc (specimen #7 , grade 2).

APPENDIX II: Creep responses of the specimens.

(Figs. II.1-II.10)

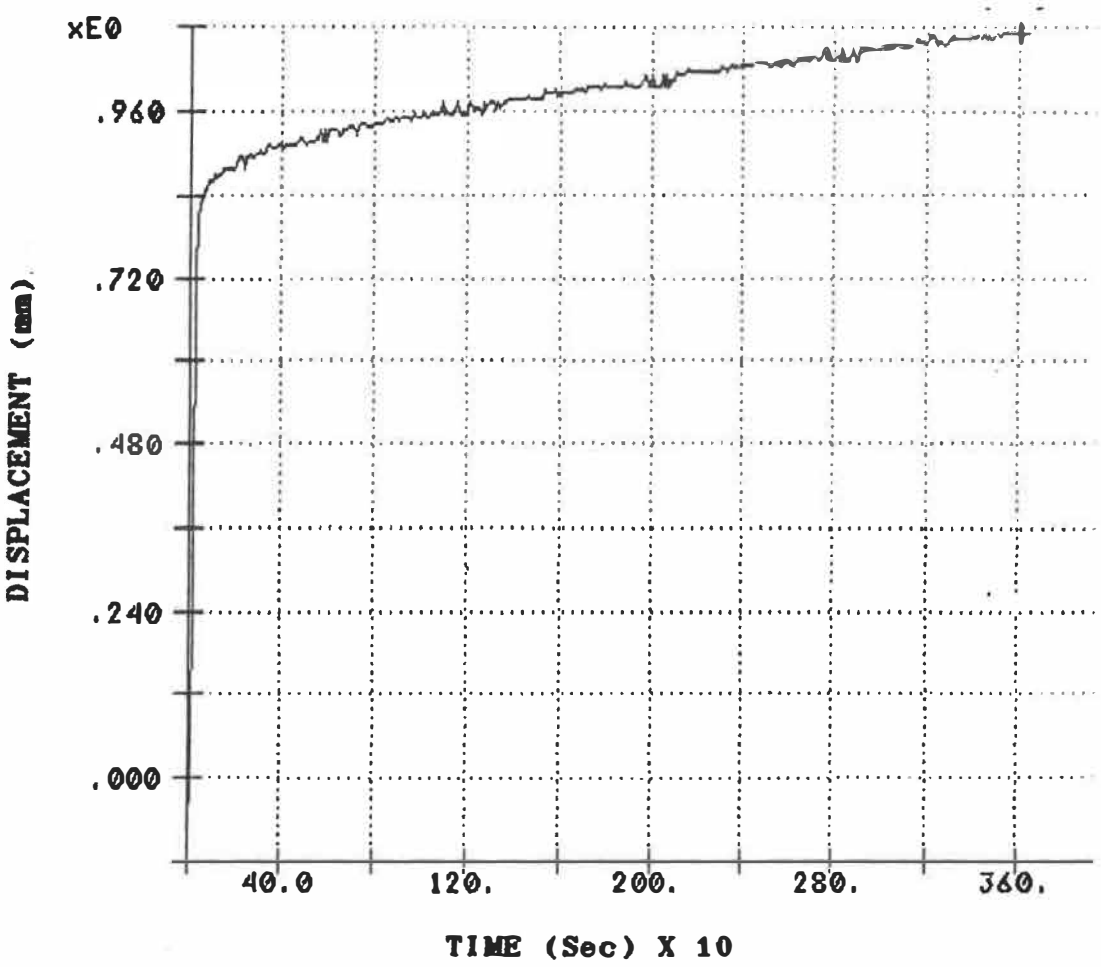

Fig. II.1 Creep response of the specimen #2 under 400 N axial compressive force (intact specimen).

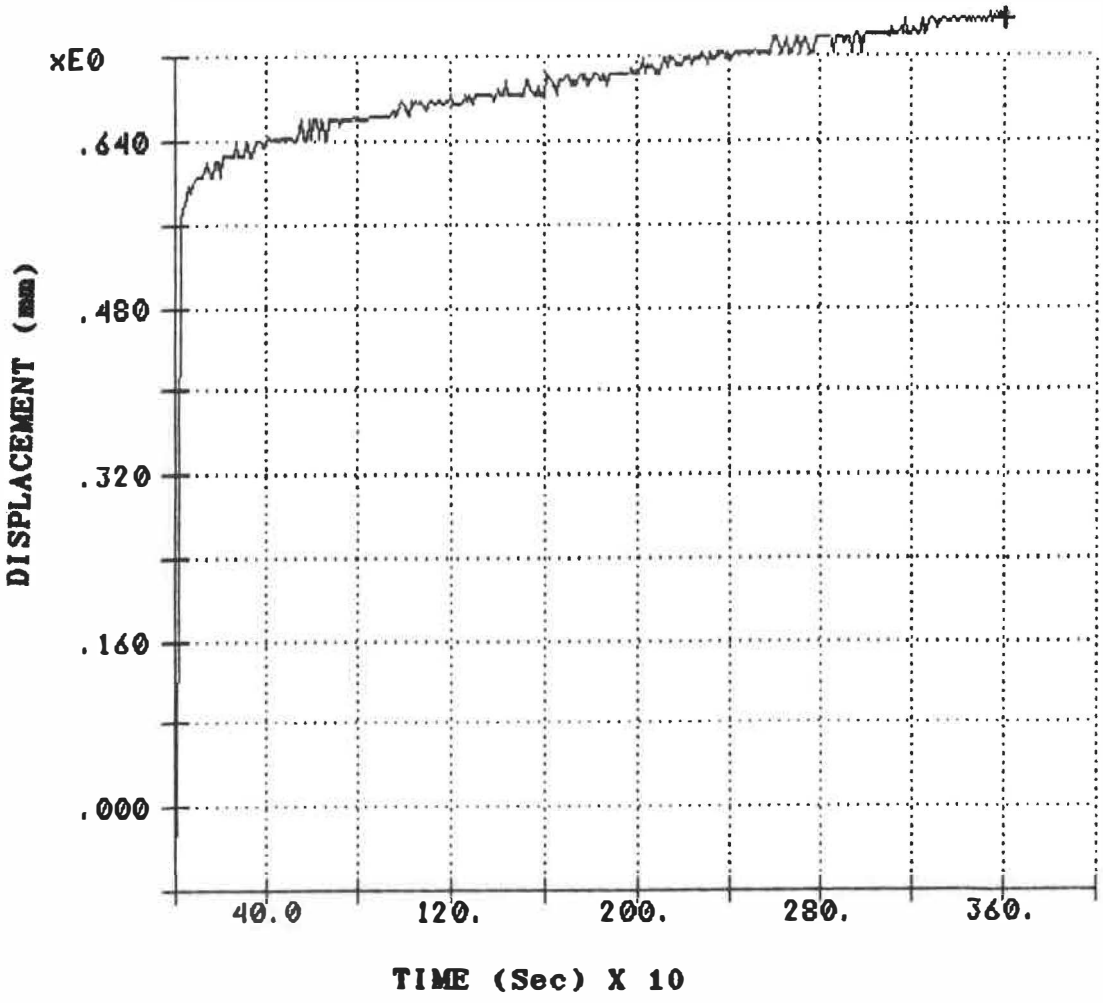

Fig. II.2 Creep response of the specimen #3 under 400 N axial compressive force (intact specimen).

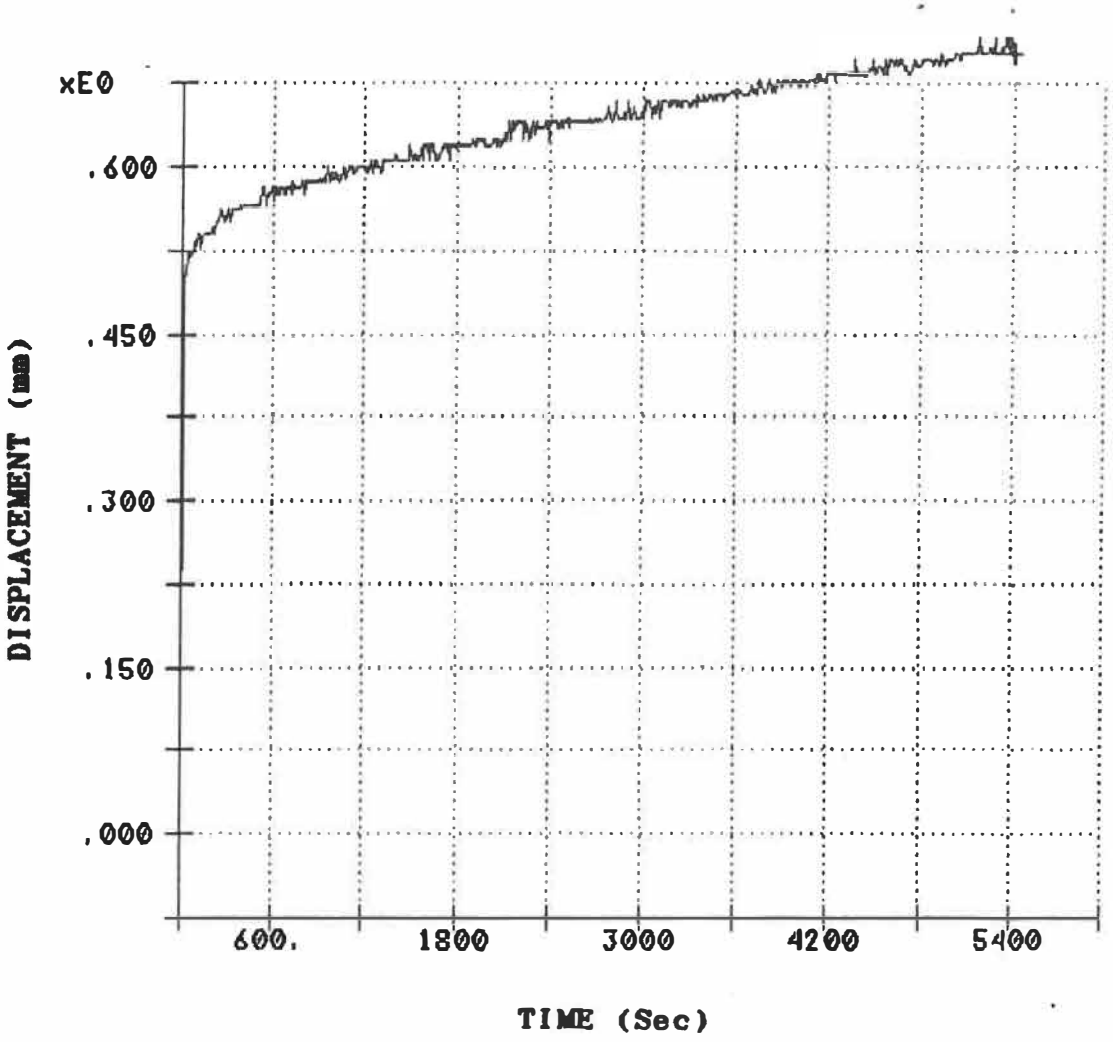

Fig. II.3 Creep response of the specimen #4 under 400 N axial compressive force (intact specimen).

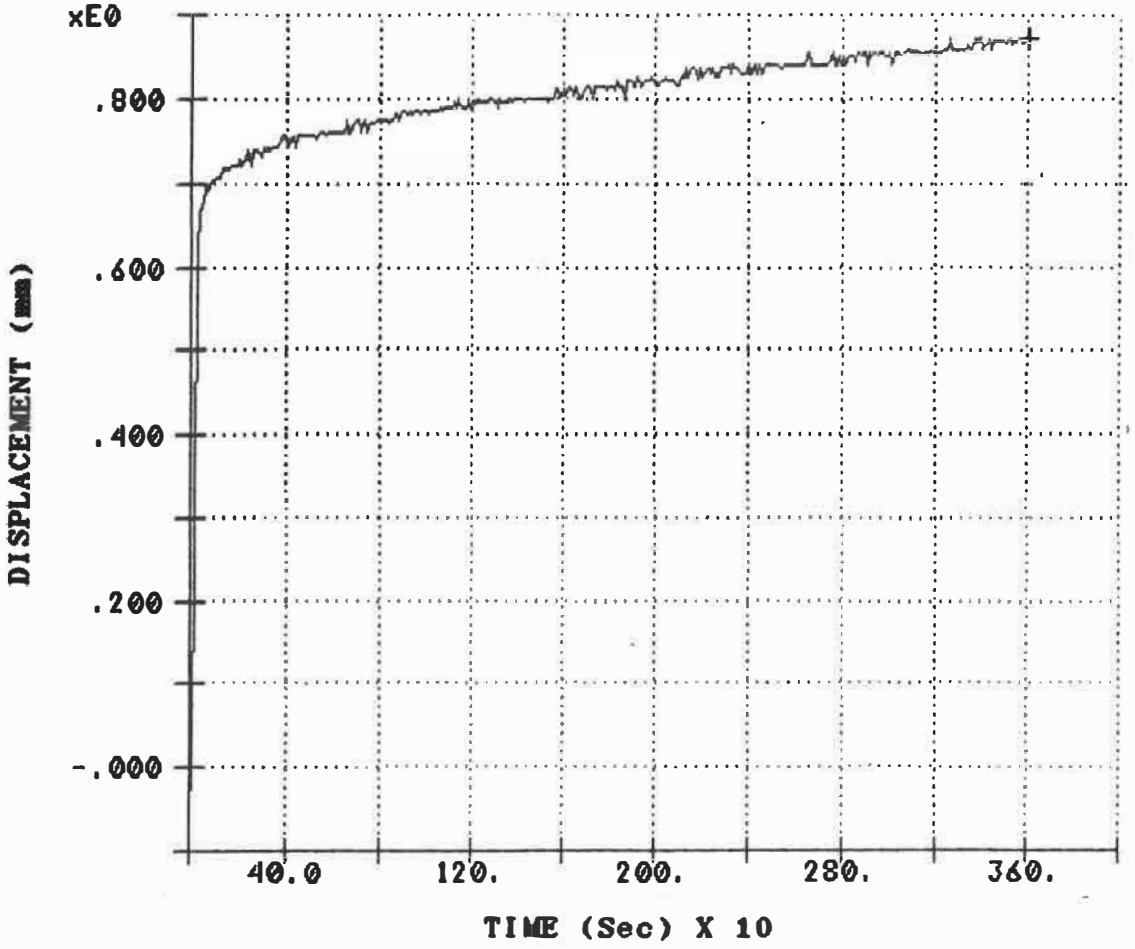

Fig. II.4 Creep response of the specimen #1 under 400 N axial compressive force (specimen without the posterior elements).

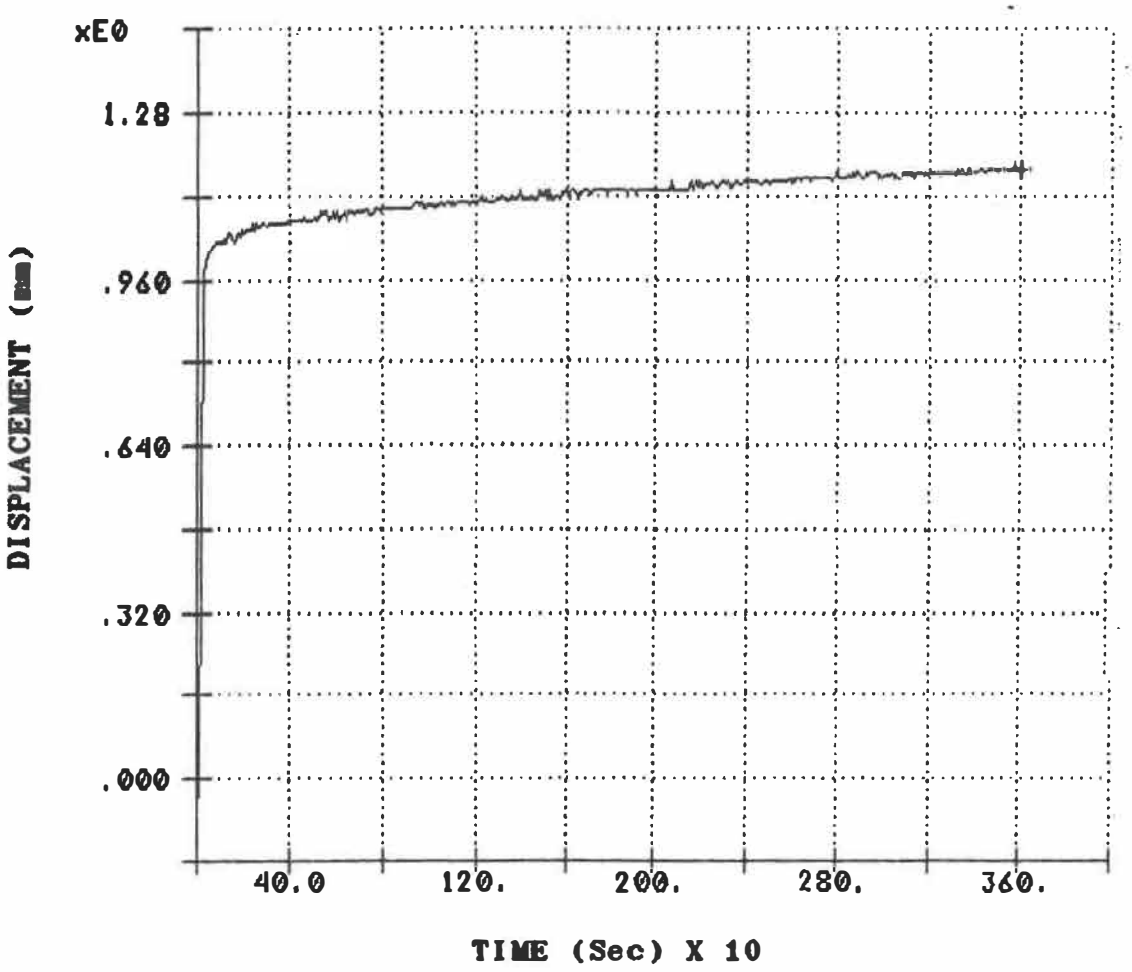

Fig. II.5 Creep response of the specimen #2 under 400 N axial compressive force (specimen without the posterior elements).

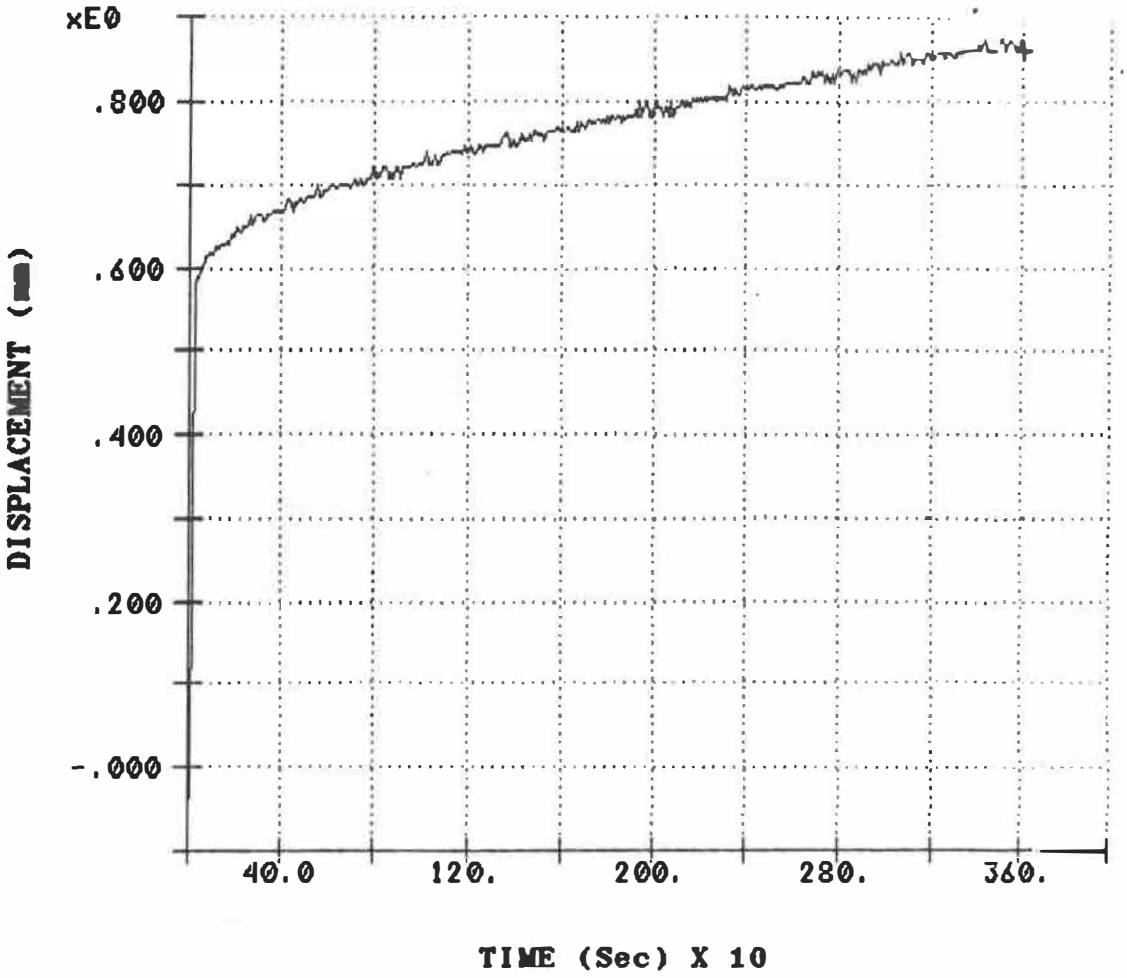

Fig. II.6 Creep response of the specimen #3 under 400 N axial compressive force (specimen without the posterior elements).

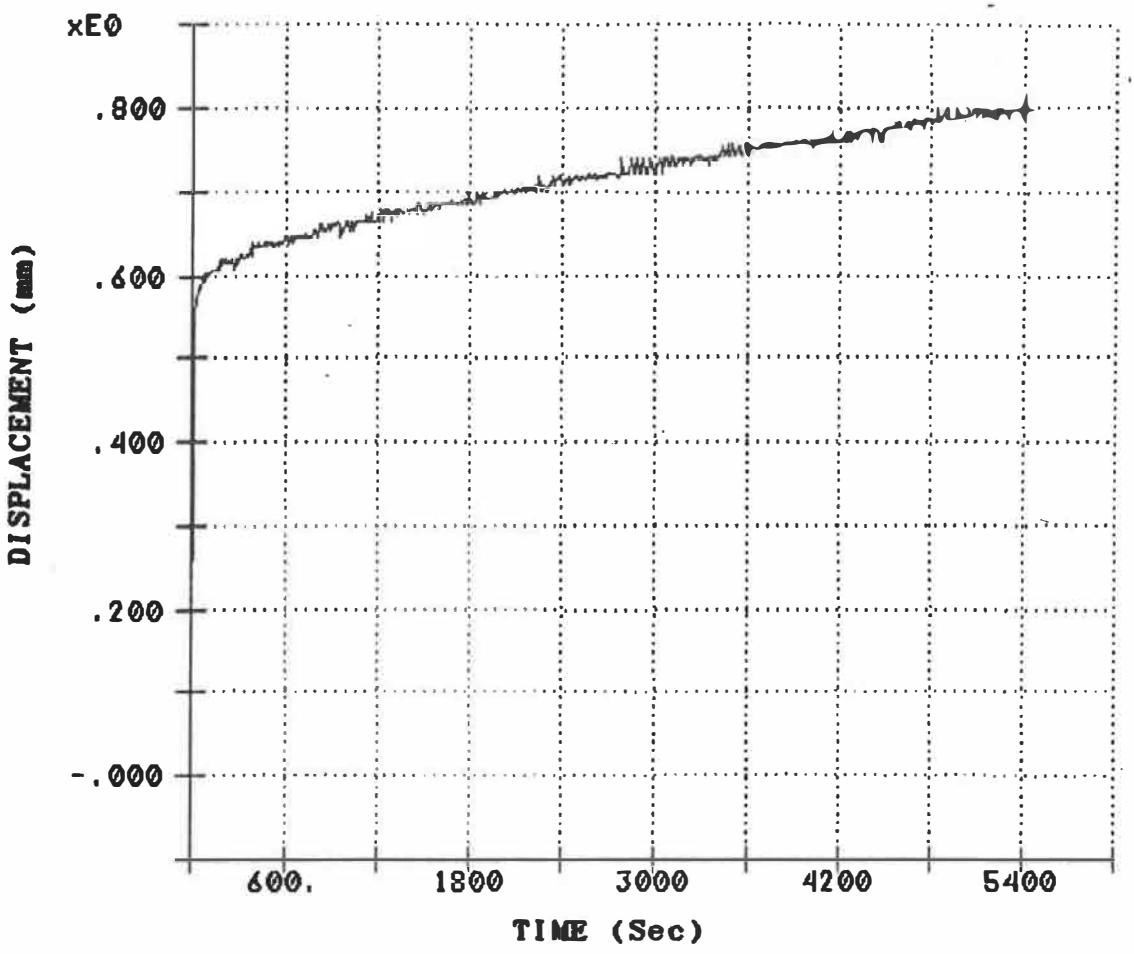

Fig. II.7 Creep response of the specimen #4 under 400 N axial compressive force (specimen without the posterior elements).

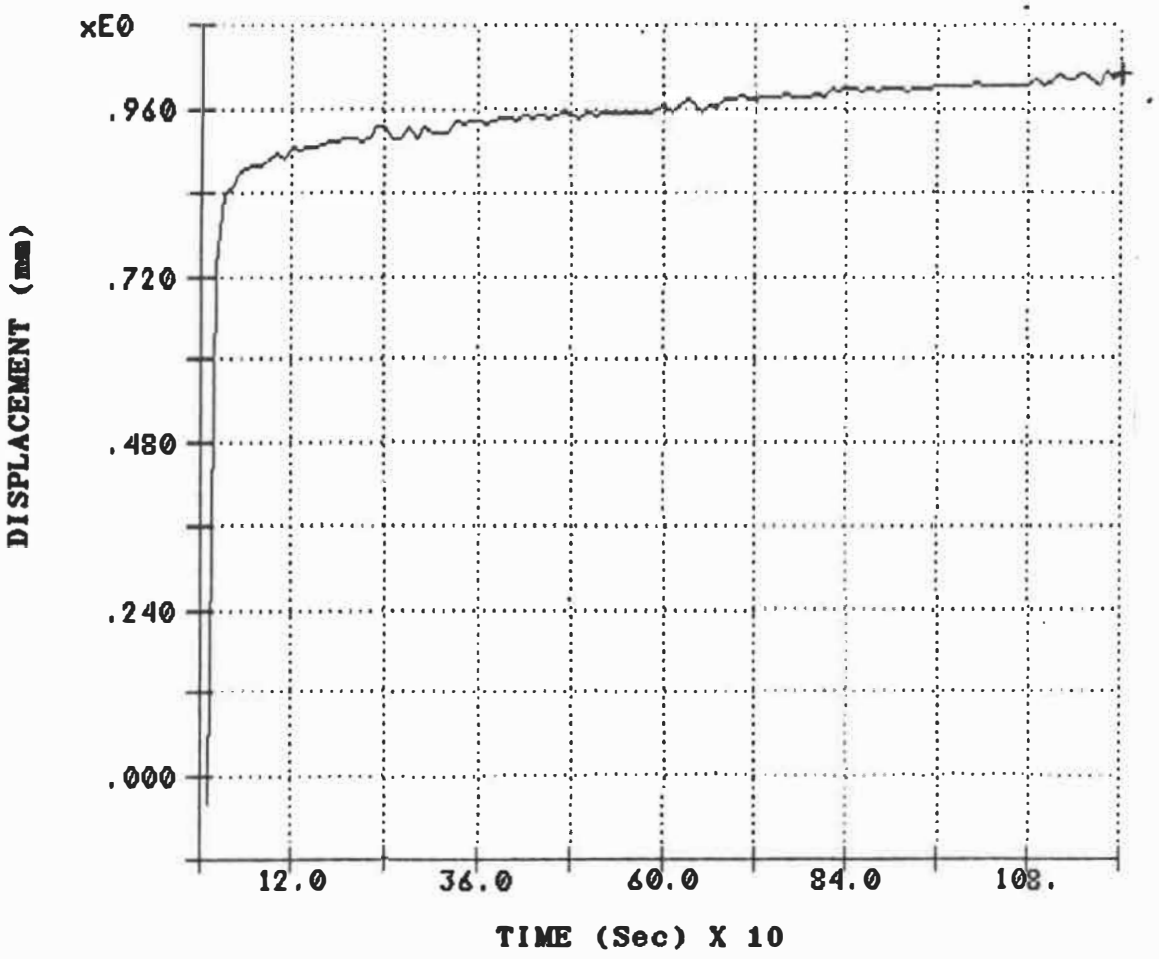

Fig. II.8 Creep response of the specimen #5 under 400 N axial compressive force (specimen without the posterior elements).

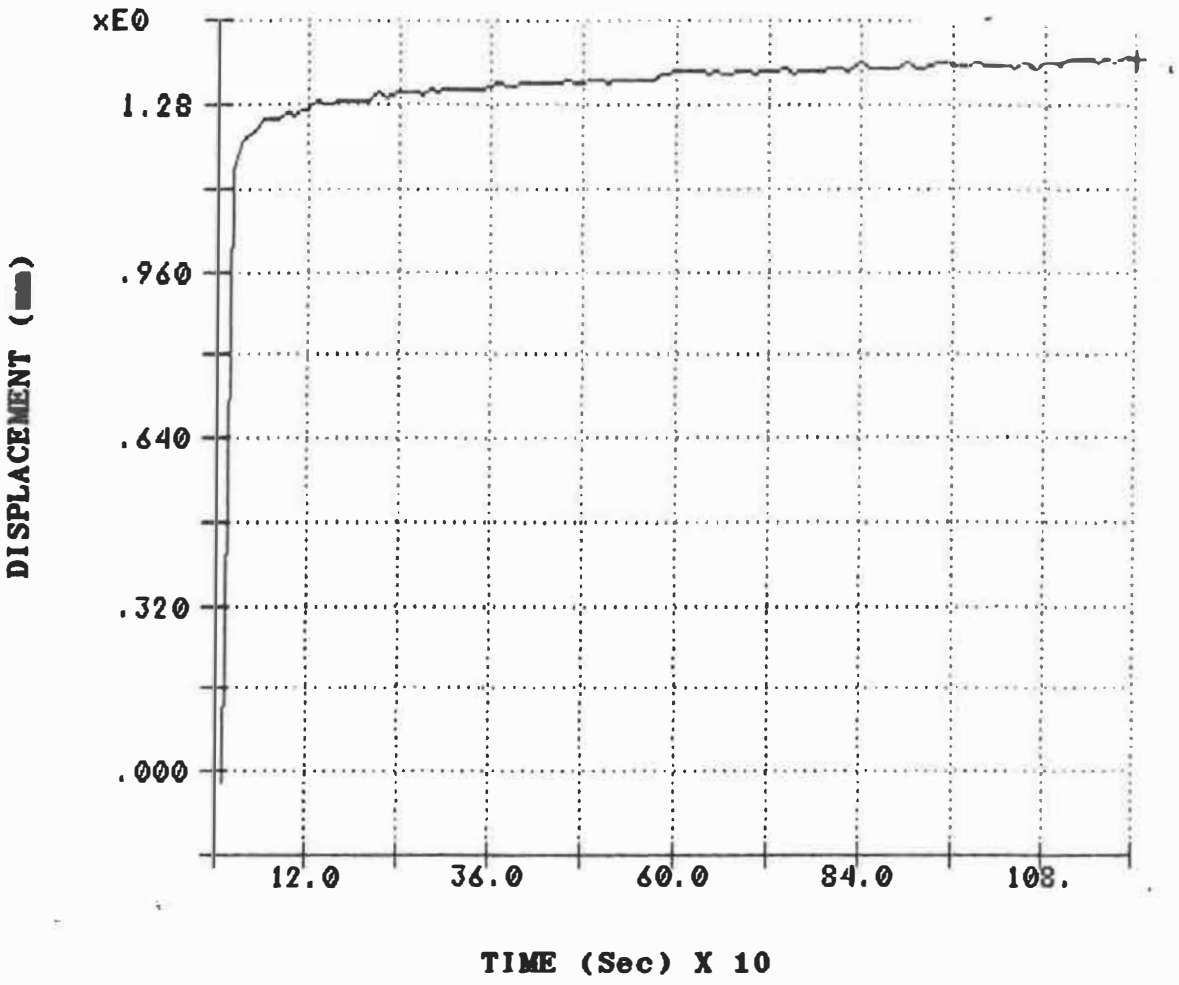

Fig. II.9 Creep response of the specimen #6 under 400 N axial compressive force (specimen without the posterior elements).

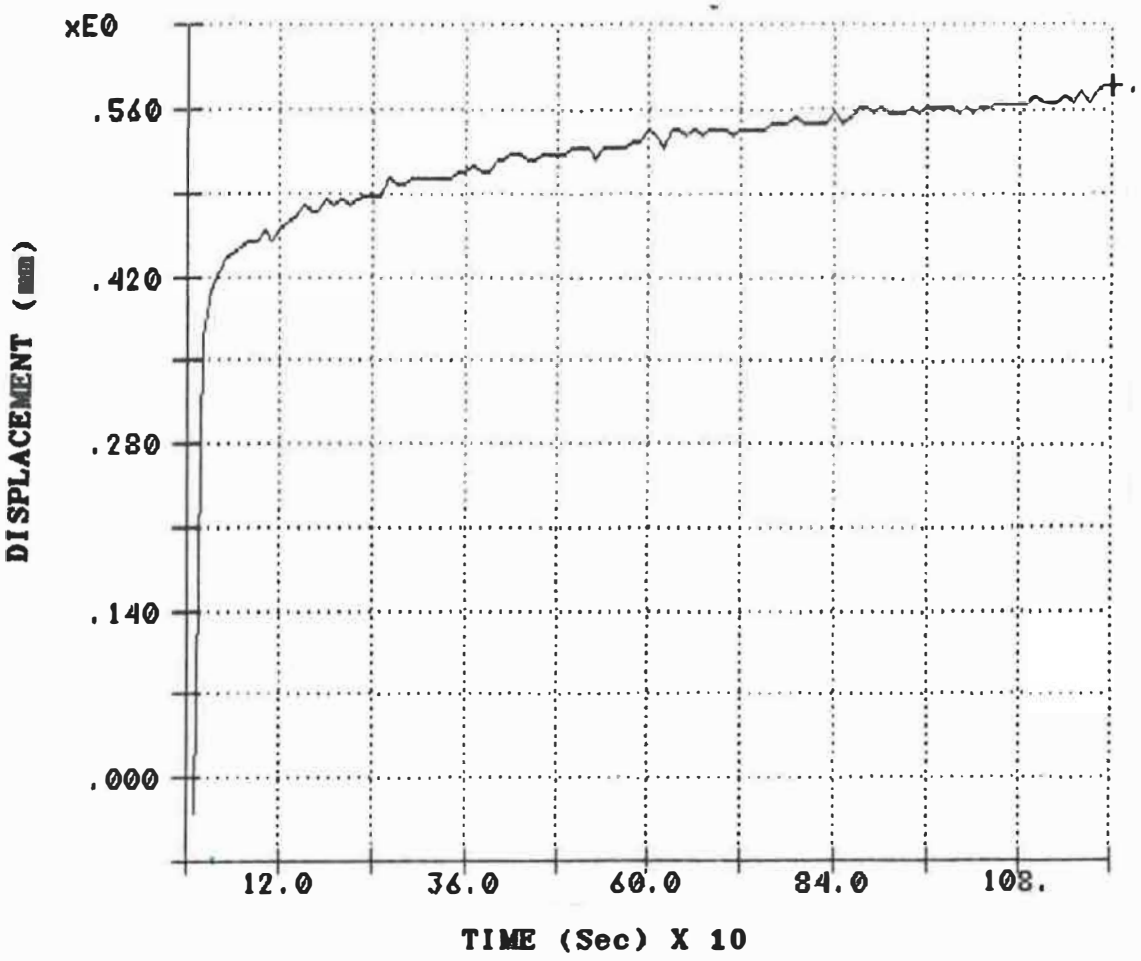

Fig. II.10 Creep response of the specimen #7 under 400 N axial compressive force (specimen without the posterior elements).

APPENDIX III: Compliance responses of the specimens.

(Fig. III.1-III.7)

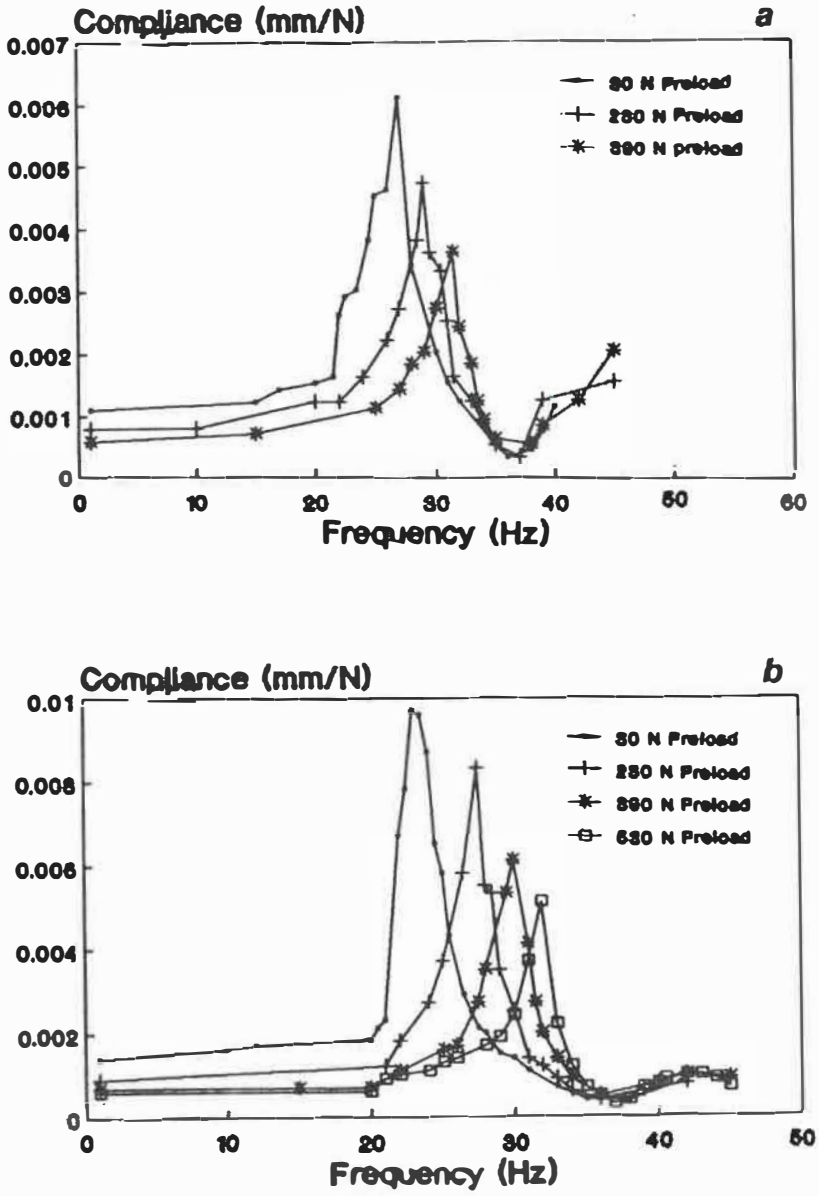

Fig. III.1 Compliance magnitude versus frequency for the specimen #1. a: intact specimen b: specimen without the posterior elements.

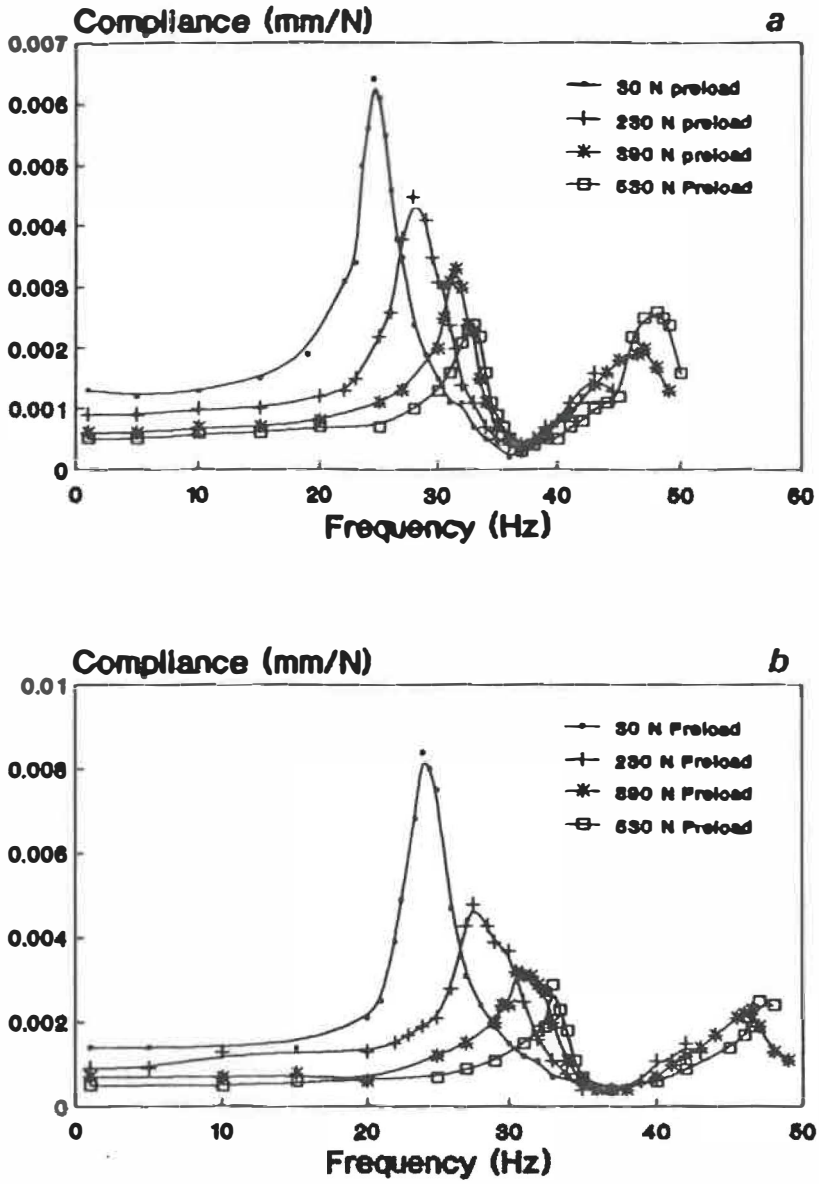

Fig. III.2 Compliance magnitude versus frequency for the specimen #2. a: intact specimen b: specimen without the posterior elements.

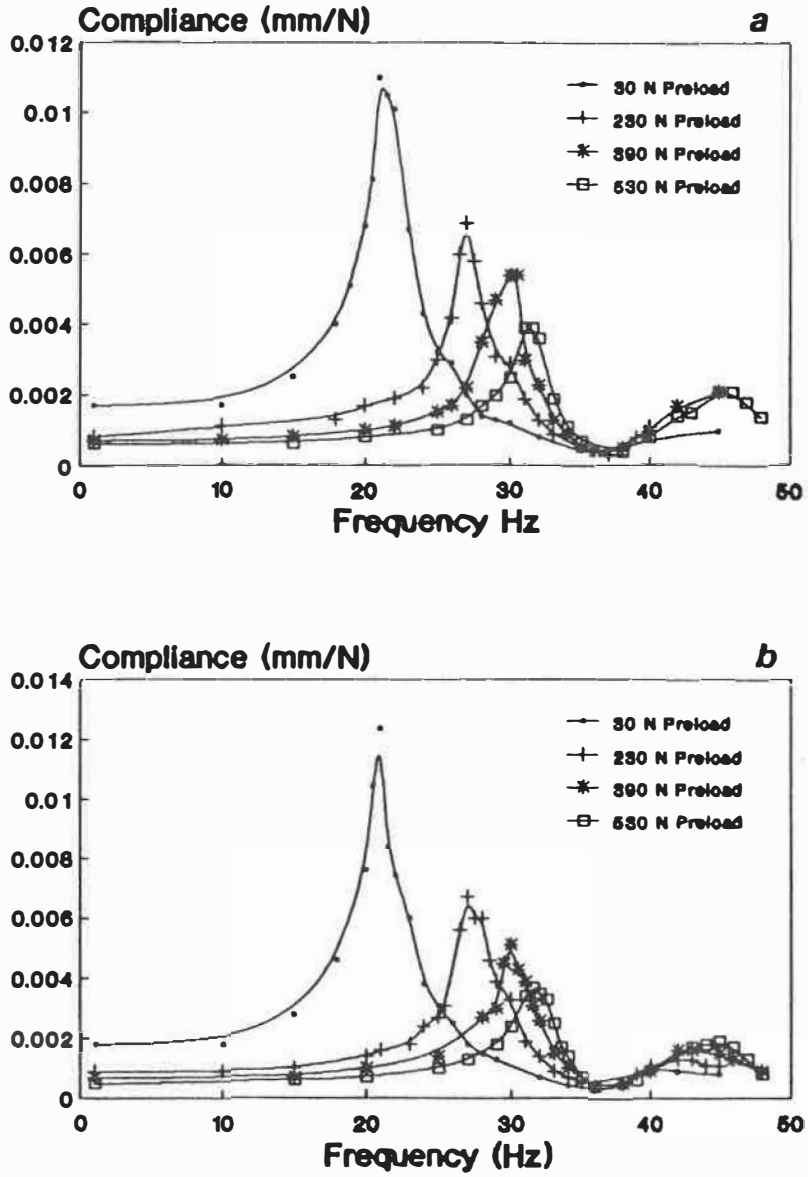

Fig. III.3 Compliance magnitude versus frequency for the specimen #3. a: intact specimen b: specimen without the posterior elements.

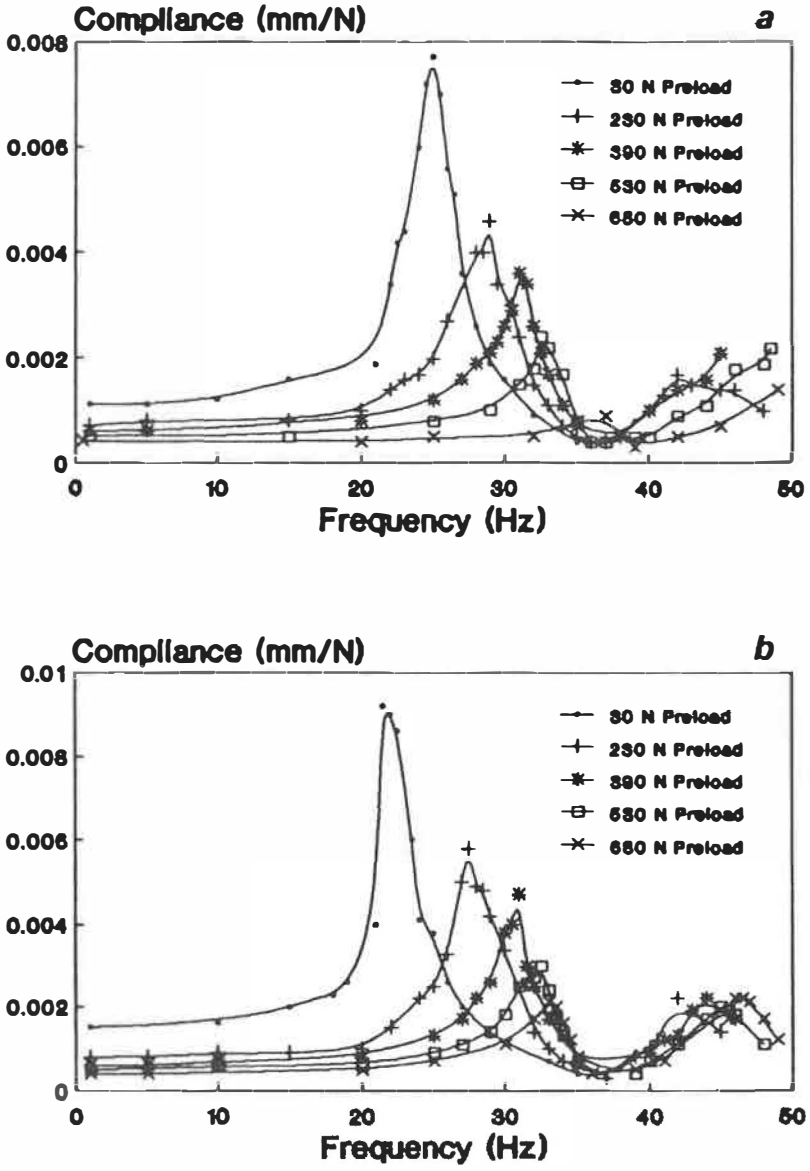

Fig. III.4 Compliance magnitude versus frequency for the specimen #4. a: intact specimen b: specimen without the posterior elements.

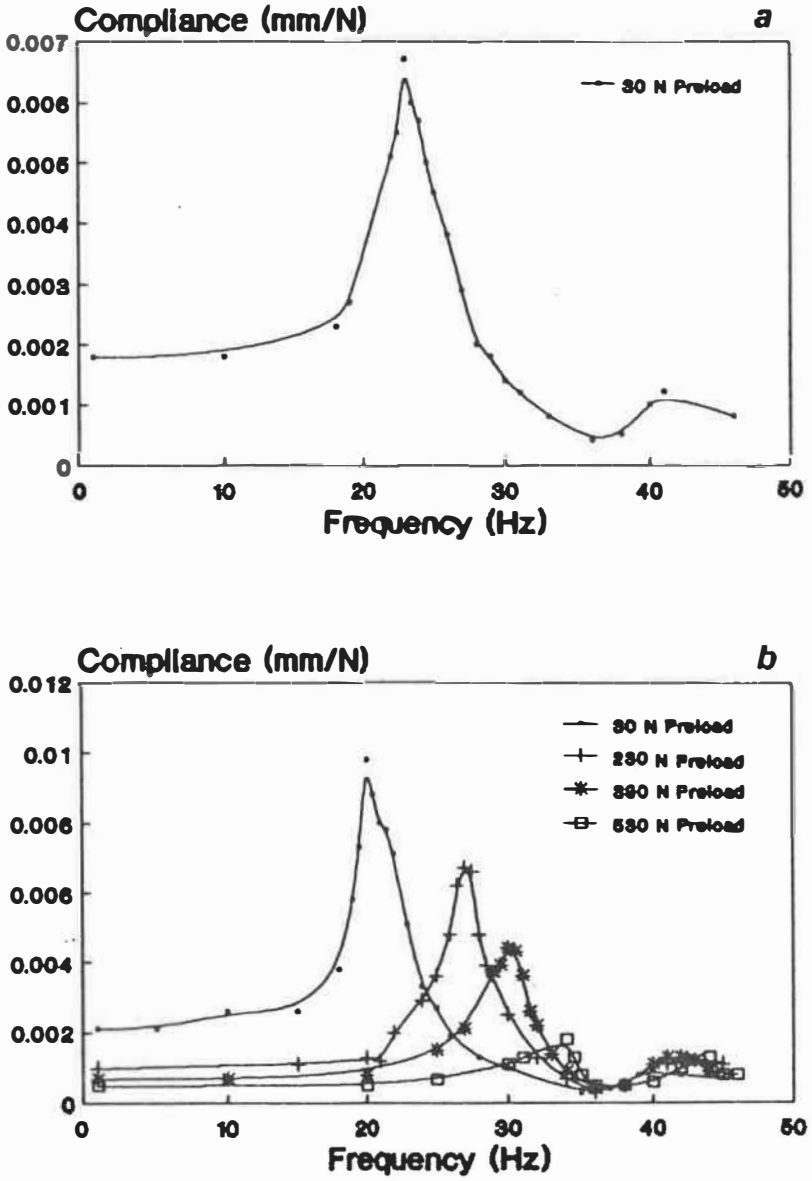

Fig. III.5 Compliance magnitude versus frequency for the specimen #5. a: intact specimen b: specimen without the posterior elements.

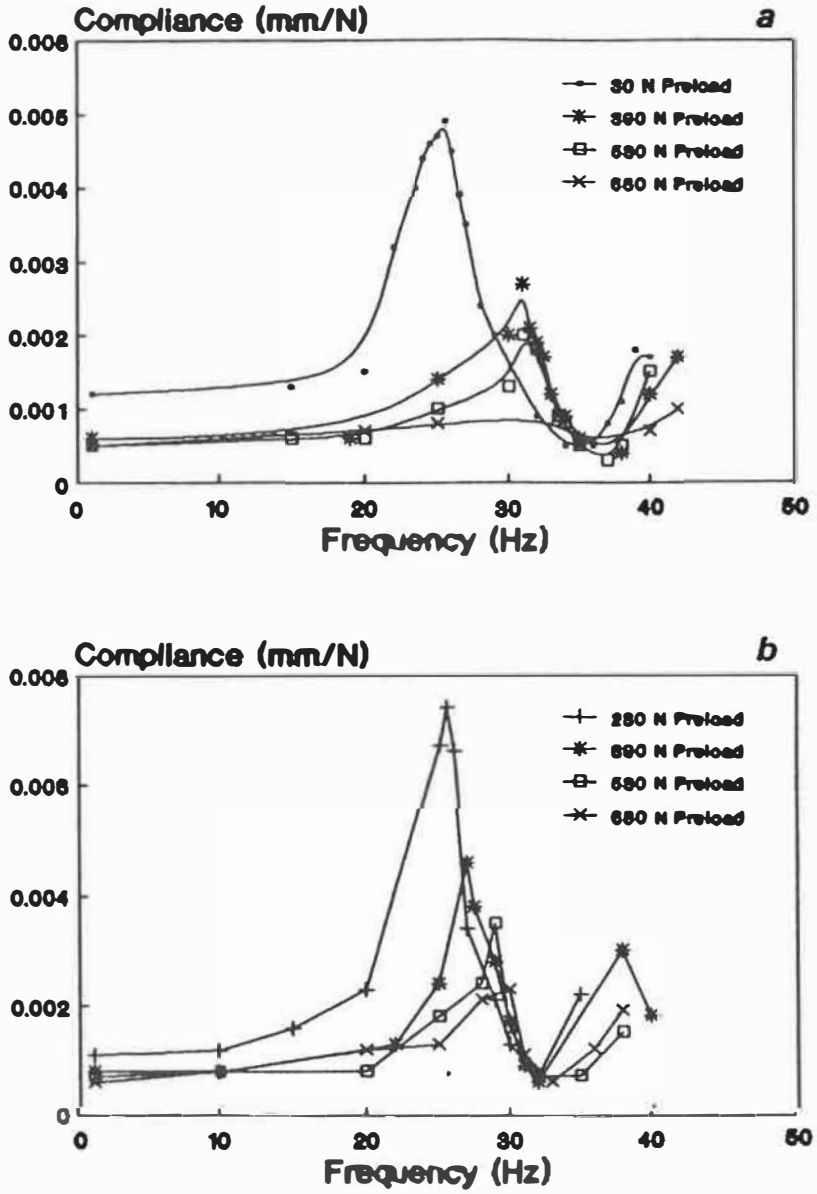

Fig. III.6 Compliance magnitude versus frequency for the specimen #6. a: intact specimen b: specimen without the posterior elements.

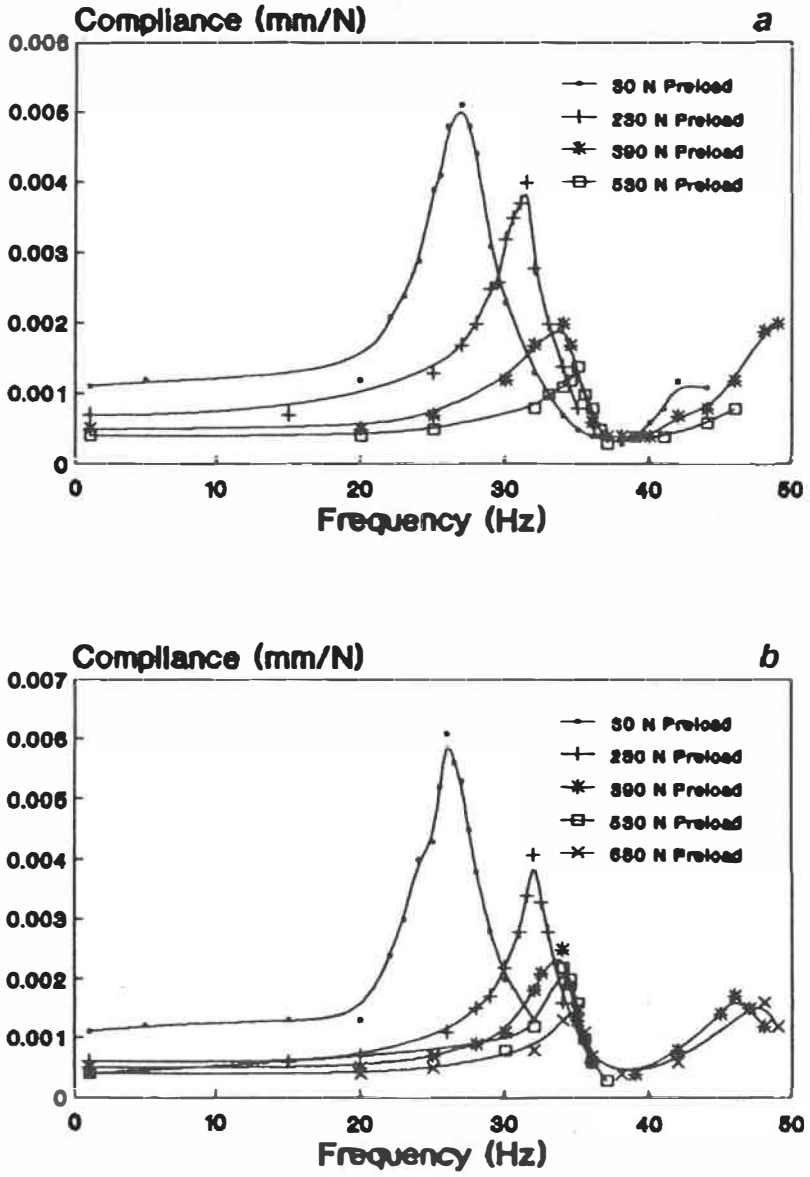

Fig. III.7 Compliance magnitude versus frequency for the specimen #7. a: intact specimen b: specimen without the posterior elements.

APPENDIX IV: Some of the results related to the axisymmetric model.

(Figs. IV.1-IV.5)

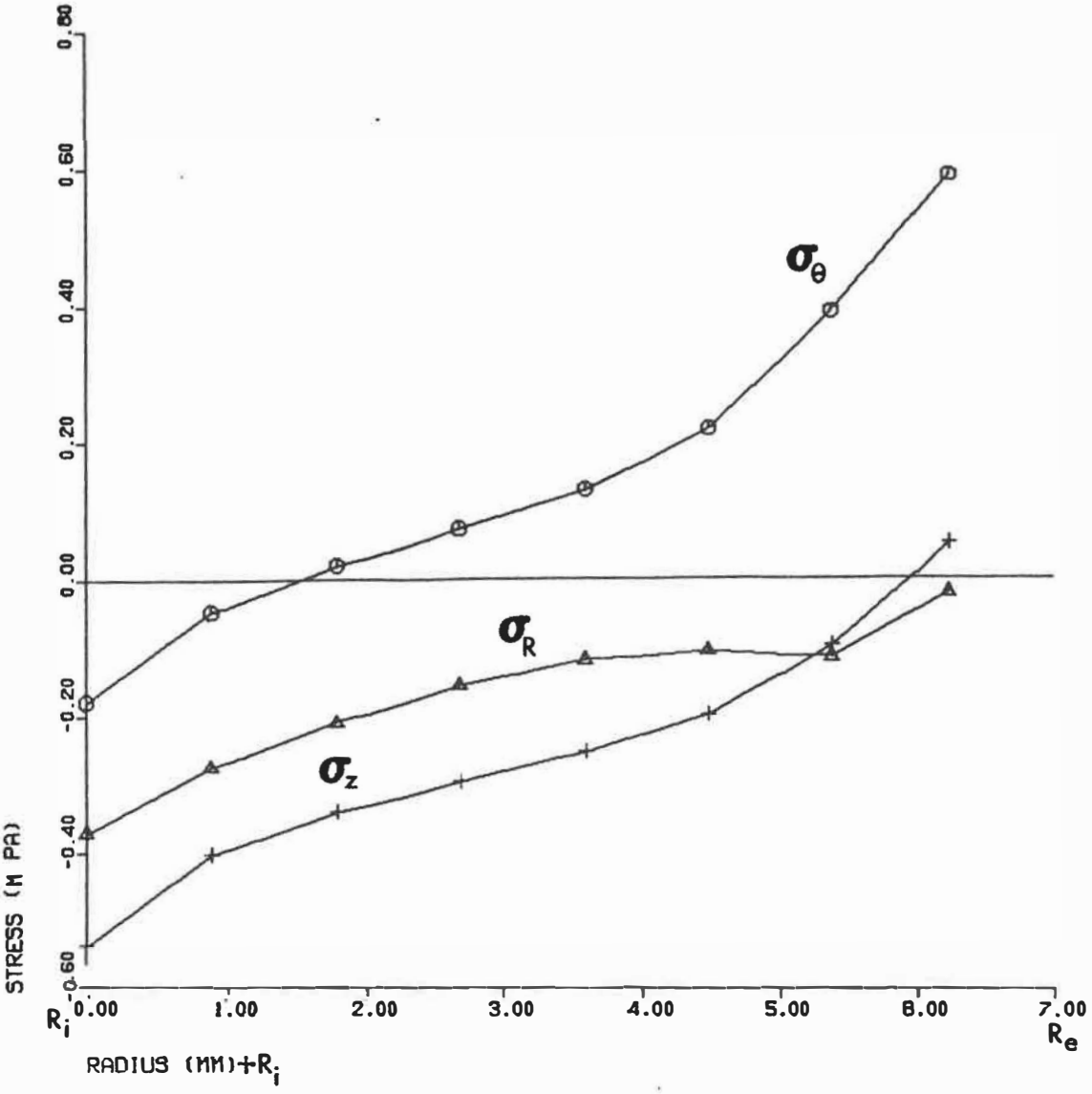

Fig. IV.1 The predicted variation of the normal stresses σ in the annulus matrix of the axisymmetric model along the radius at the disc mid-height horizontal section.

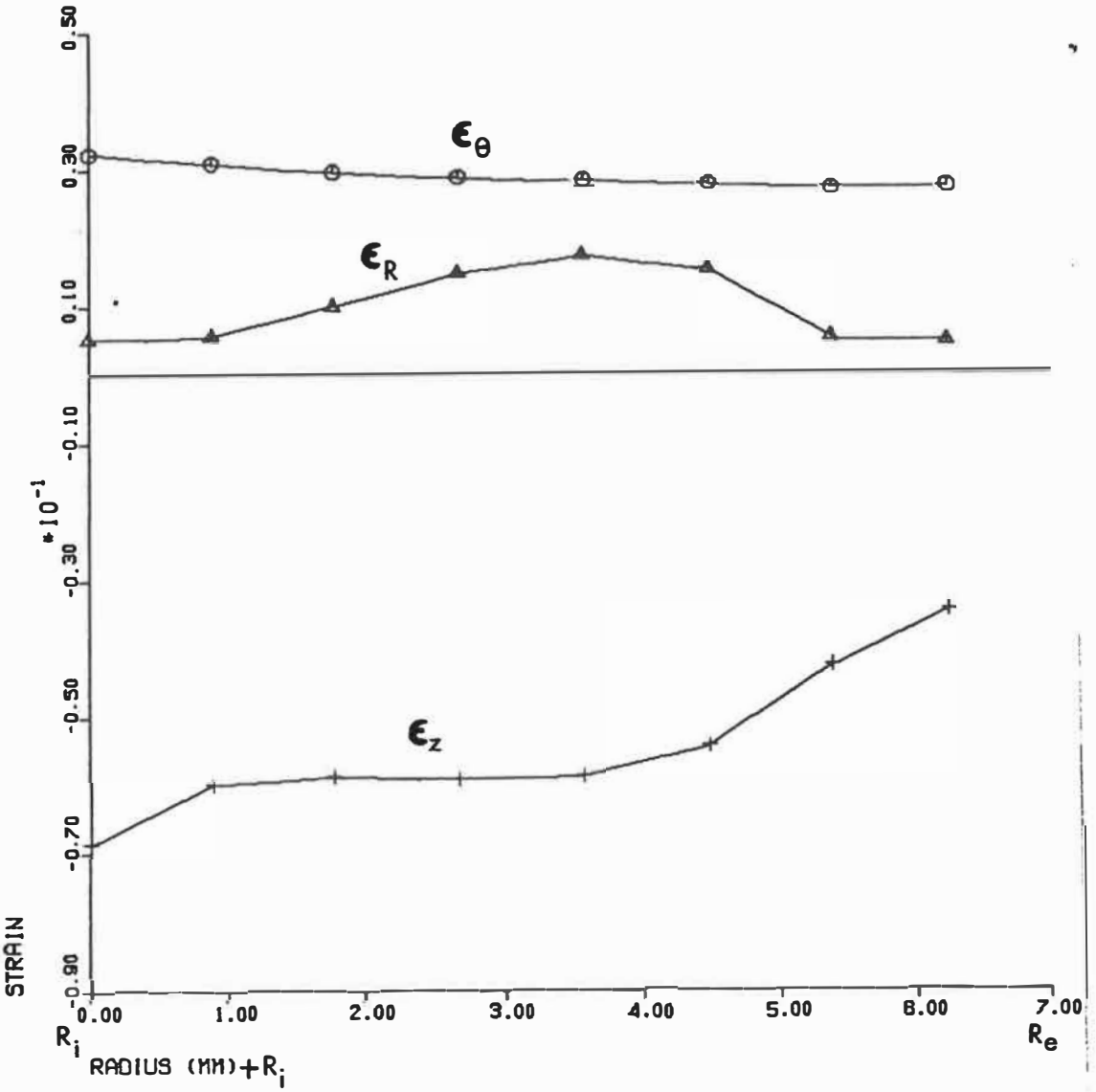

Fig. IV.2 The predicted variation of the normal strains ϵ in the annulus matrix of the axisymmetric model along the radius at the disc mid-height horizontal section.

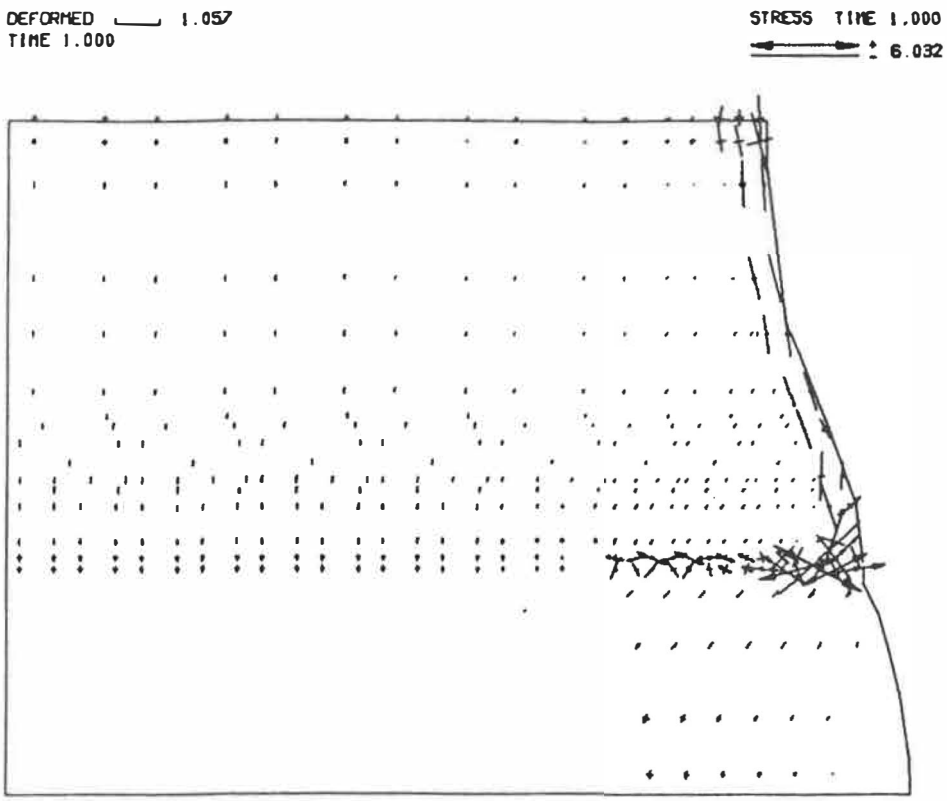

Fig. IV.3 Vector plots of principal stresses at different parts of the structure (stresses are normalized relative to their maximum value).

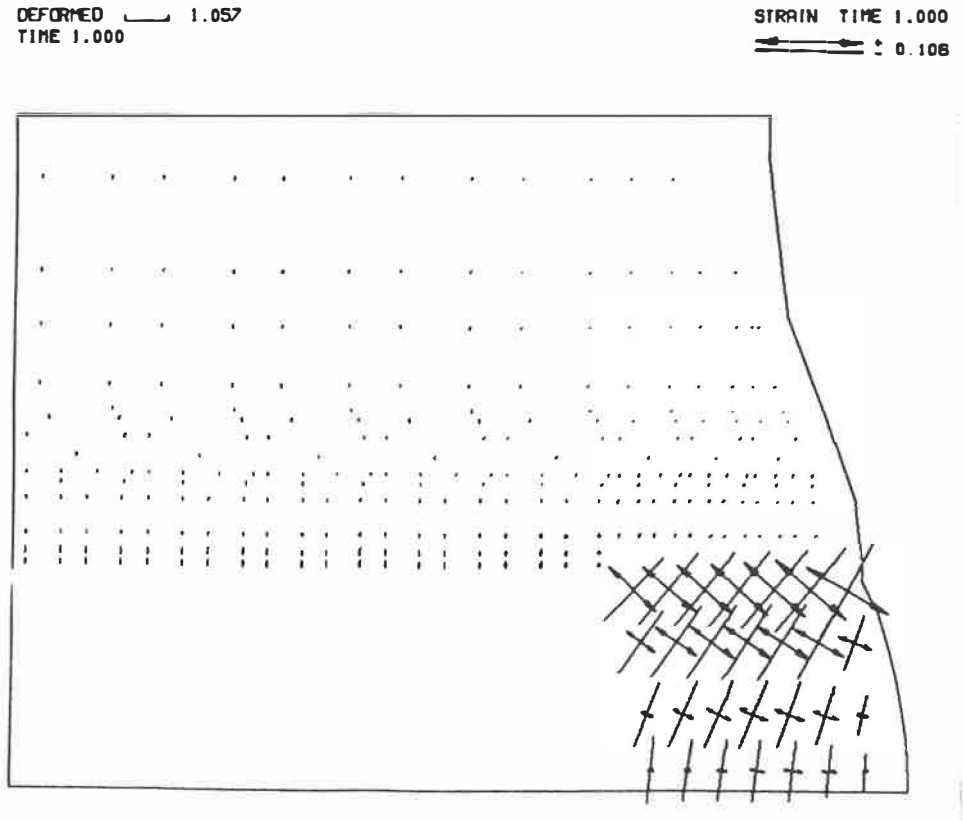

Fig. IV.4 Vector plots of principal strains at different parts of the structure (strains are normalized relative to their maximum value).

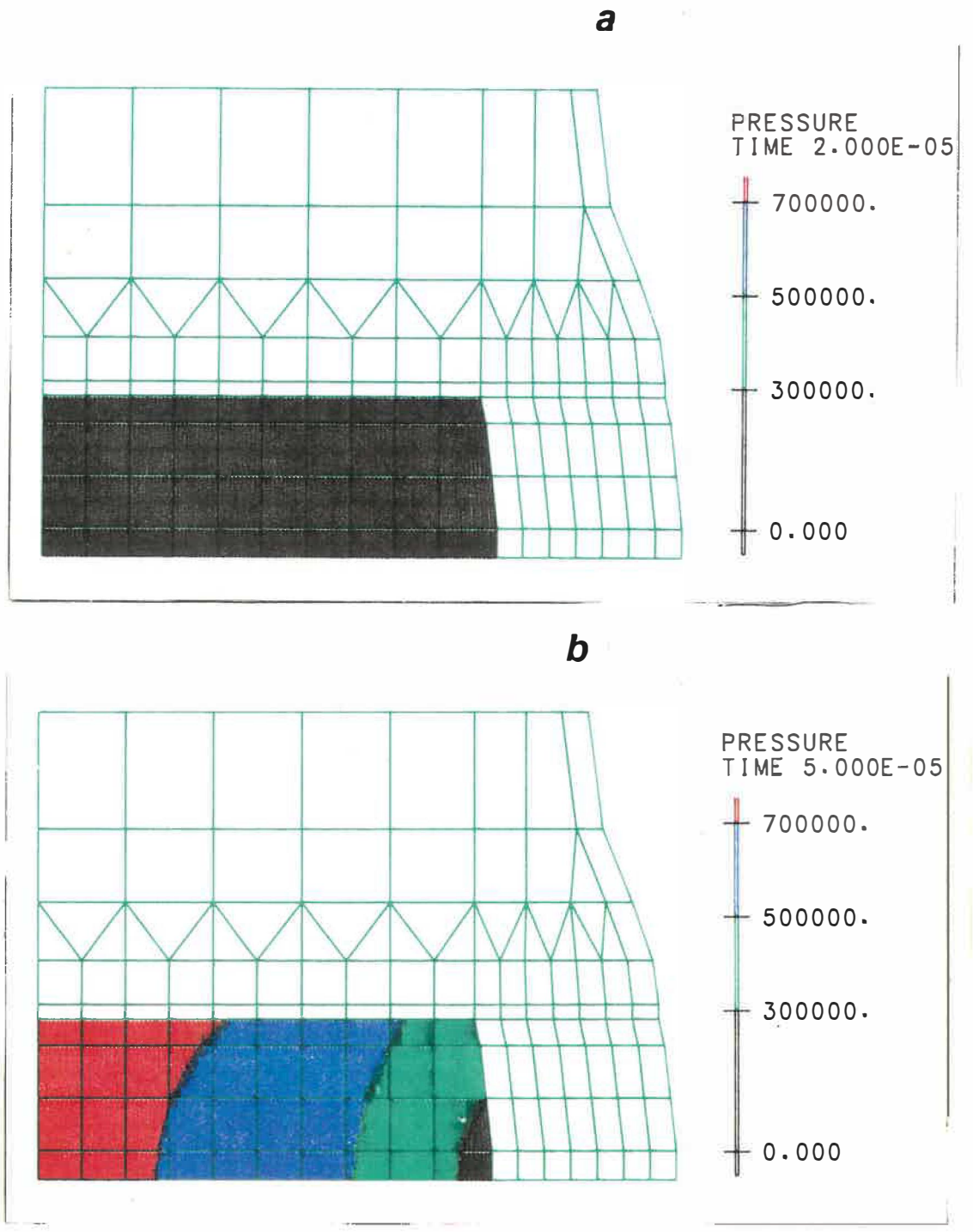

Fig. IV.5 Band plots of the pressure (Pa) distribution in the nucleus of the axisymmetric model, under a step load of 400 N with a rising time of 1.E-05 Sec. (a-h) for different time steps (Sec).

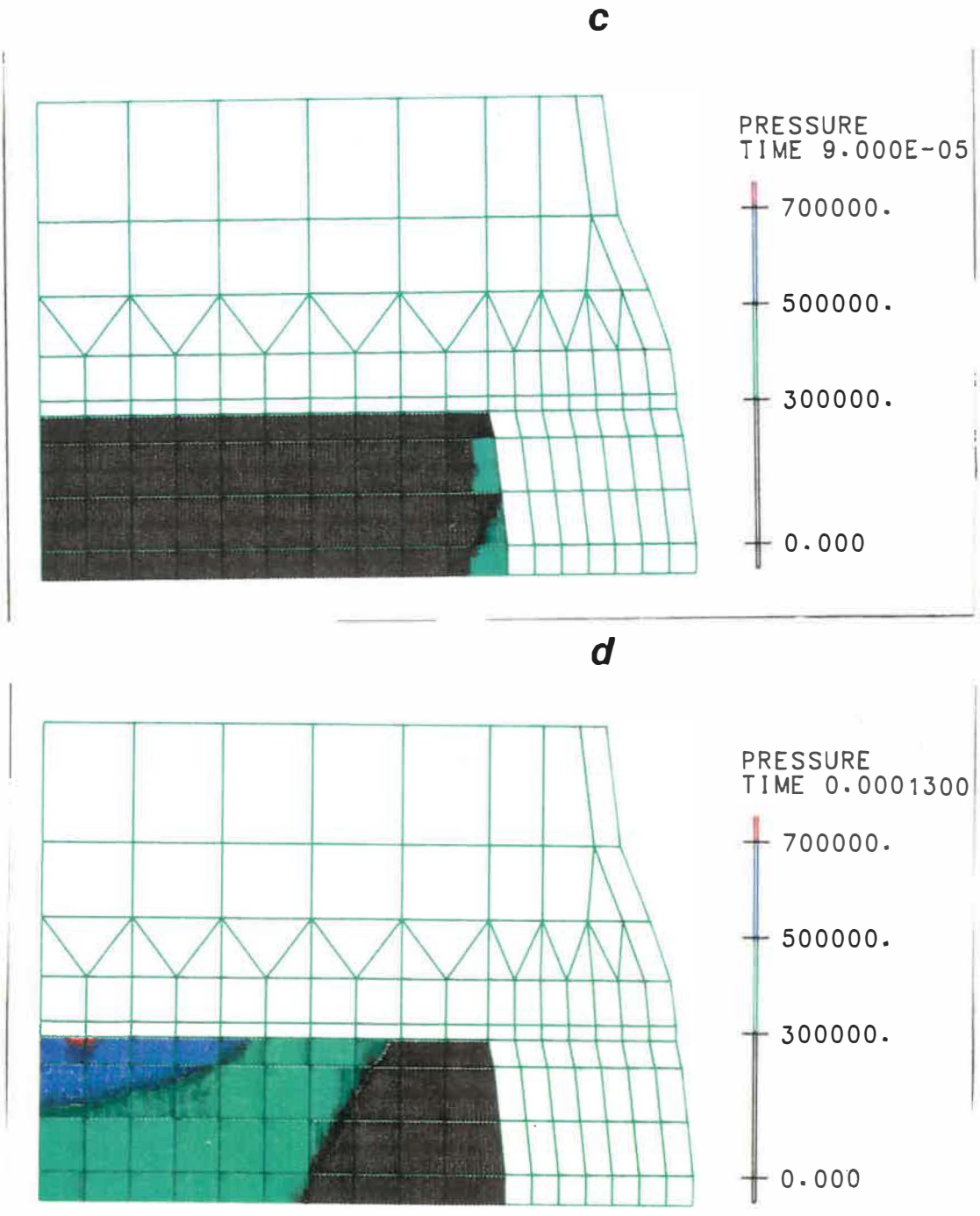

Fig. IV.5 Band plots of the pressure (Pa) distribution in the nucleus of the axisymmetric model, under a step load of 400 N with a rising time of 1.E-05 Sec. (a-h) for different time steps (Sec).

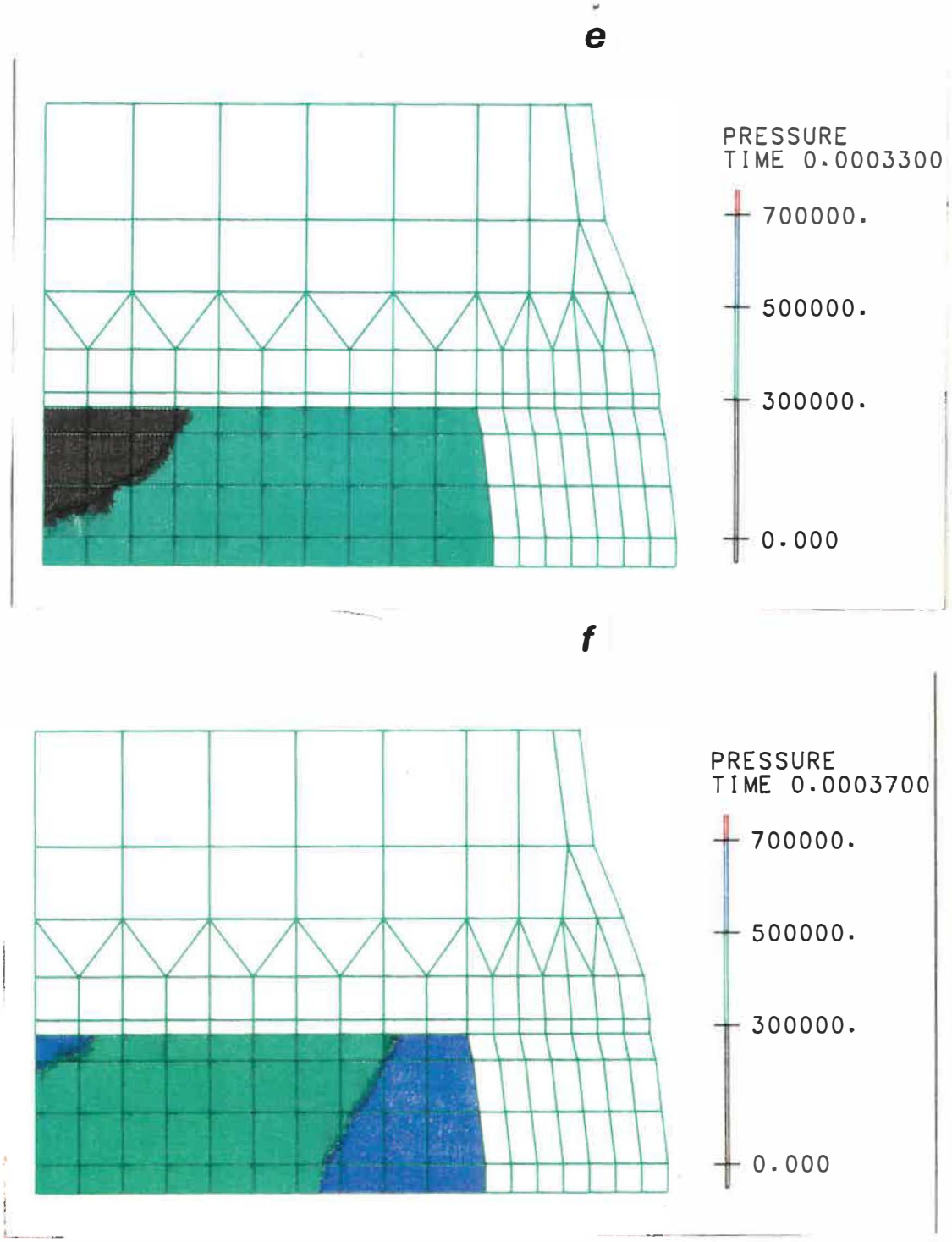

Fig. IV.5 Band plots of the pressure (Pa) distribution in the nucleus of the axisymmetric model, under a step load of 400 N with a rising time of 1.E-05 Sec. (a-h) for different time steps (Sec).

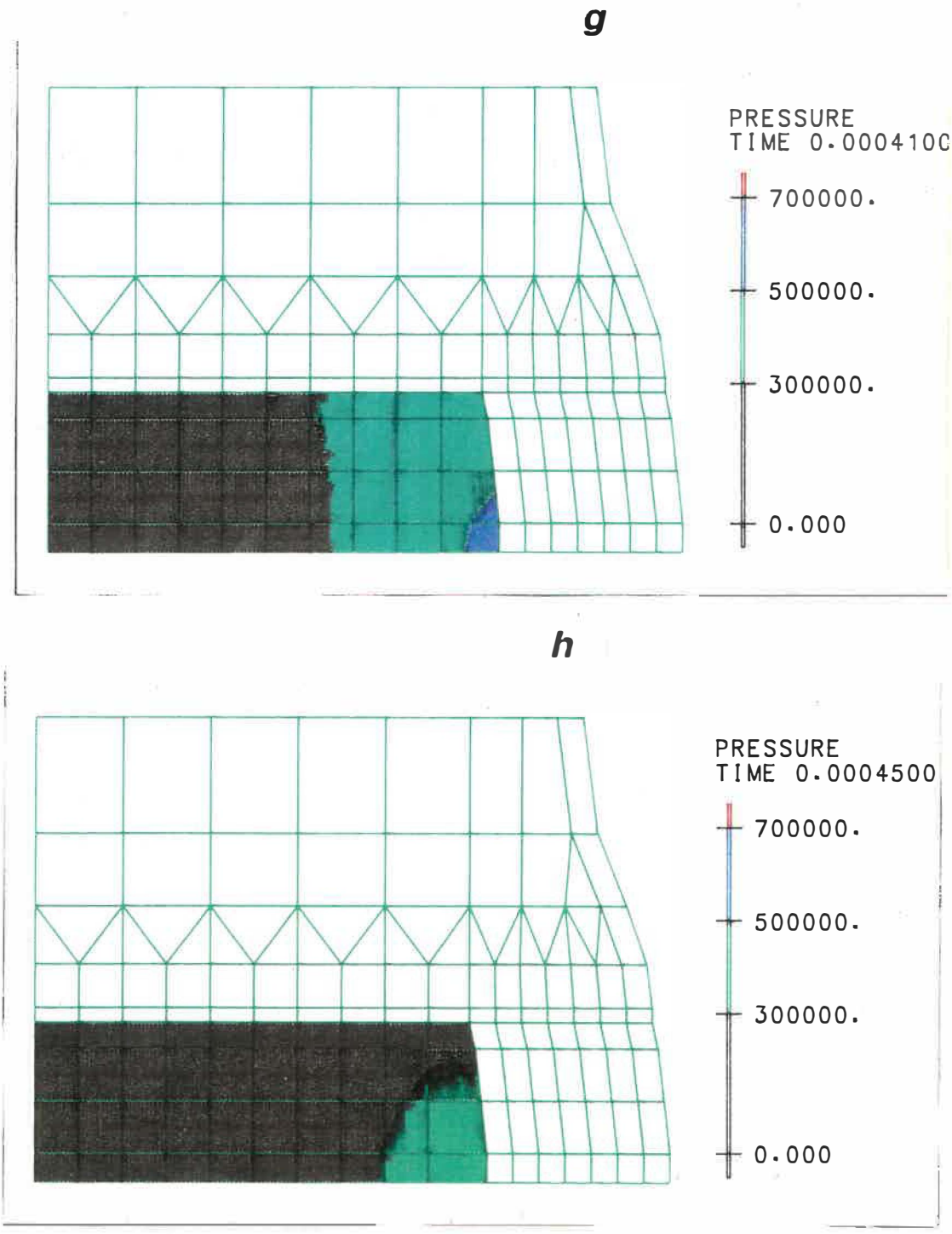

Fig. IV.5 Band plots of the pressure (Pa) distribution in the nucleus of the axisymmetric model, under a step load of 400 N with a rising time of 1.E-05 Sec. (a-h) for different time steps (Sec).

APPENDIX V: Some of the mode shapes of the finite element models.

(Figs. V.1-V.4)

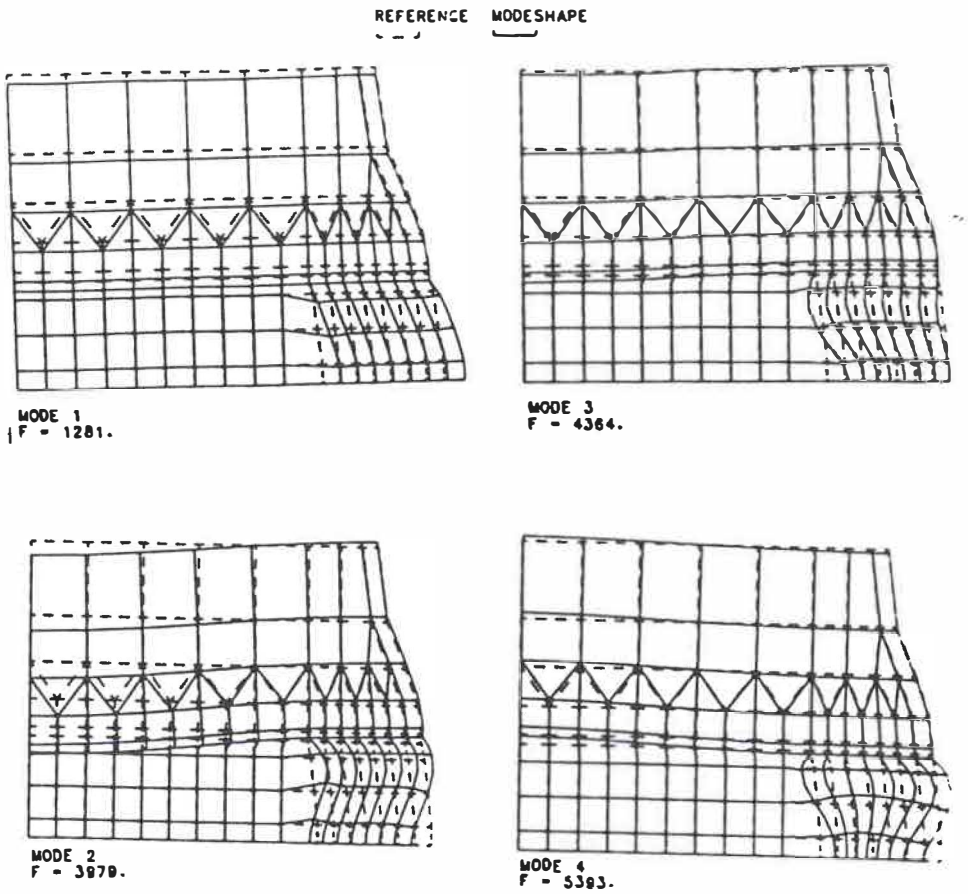

Fig. V.1 The first four mode shapes of the potential-based axisymmetric model without the added mass. (F = frquency)

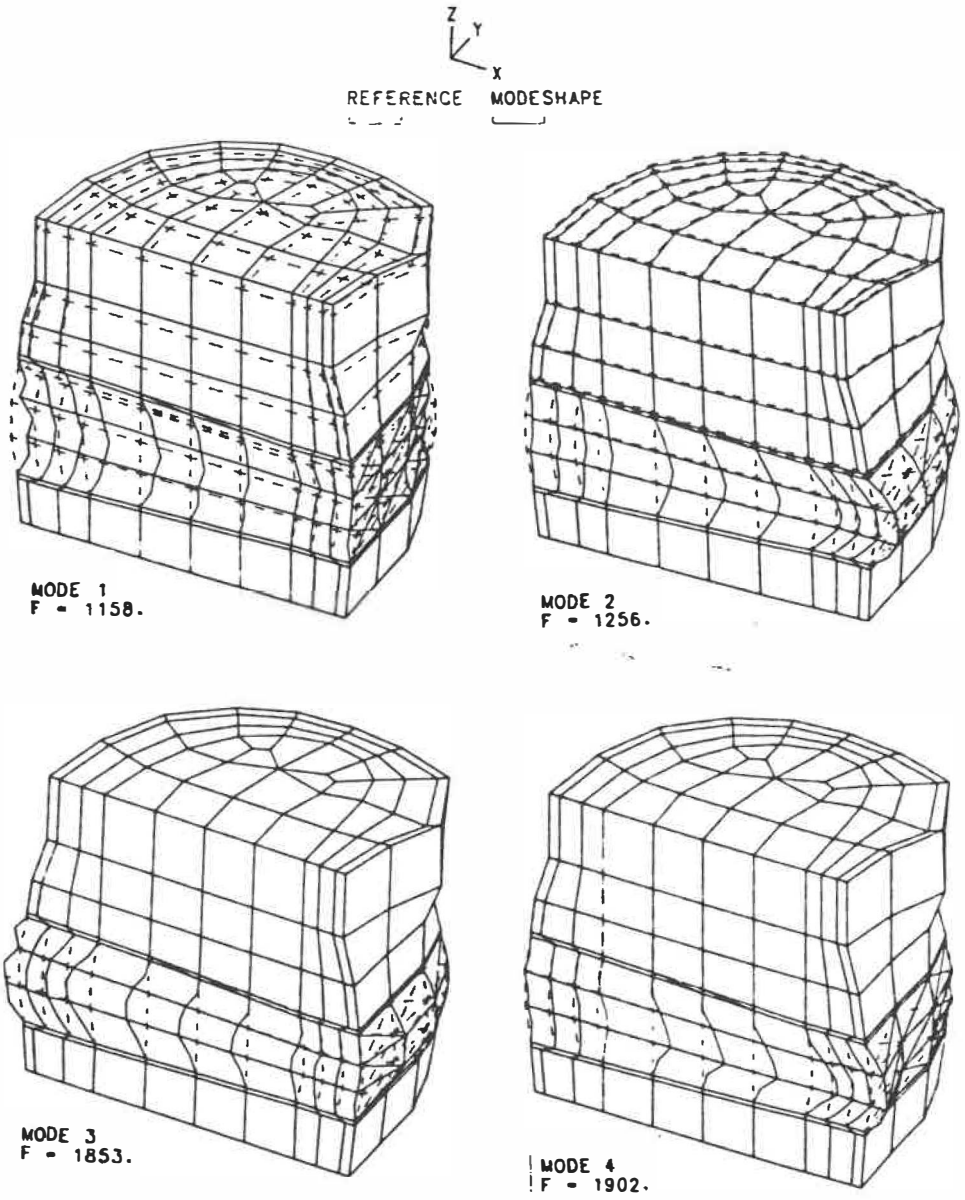

Fig. V.2 The first four mode shapes of the top constrained 3-D model without the added mass. (F = Frequency)

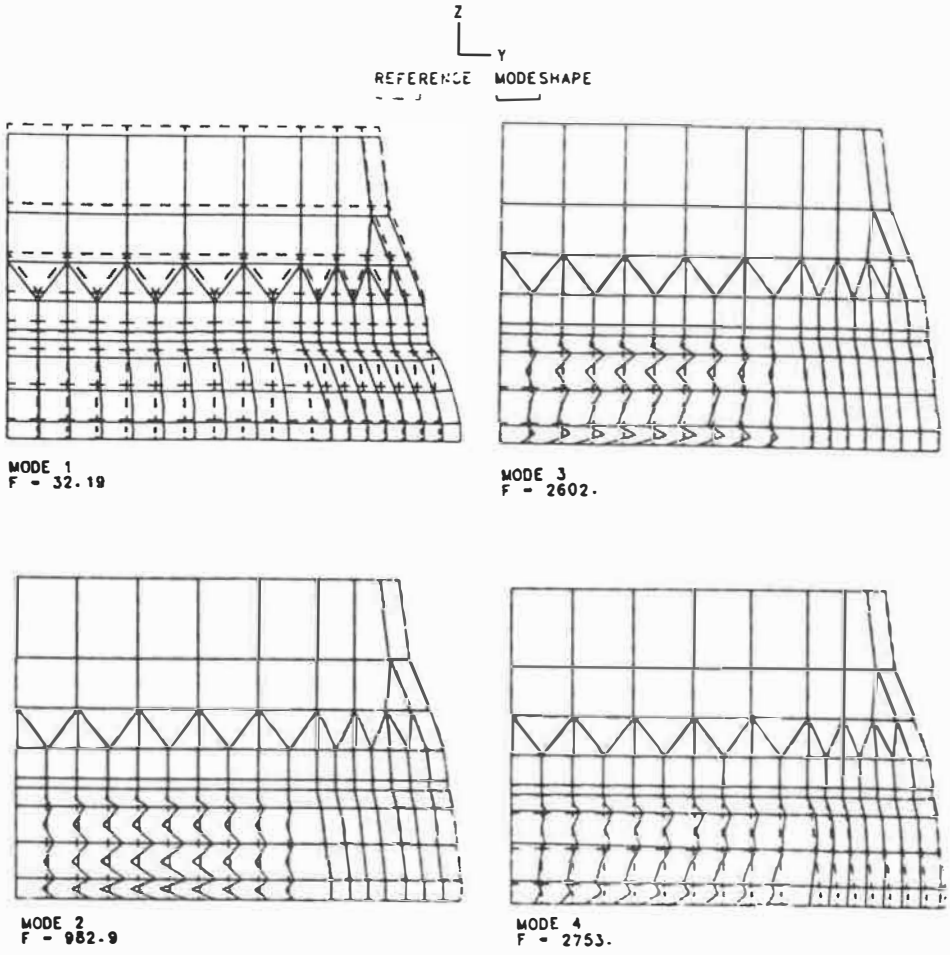

Fig. V.3 The first four mode shapes of the displacement-based axisymmetric model with the added mass. (F = Frequency)

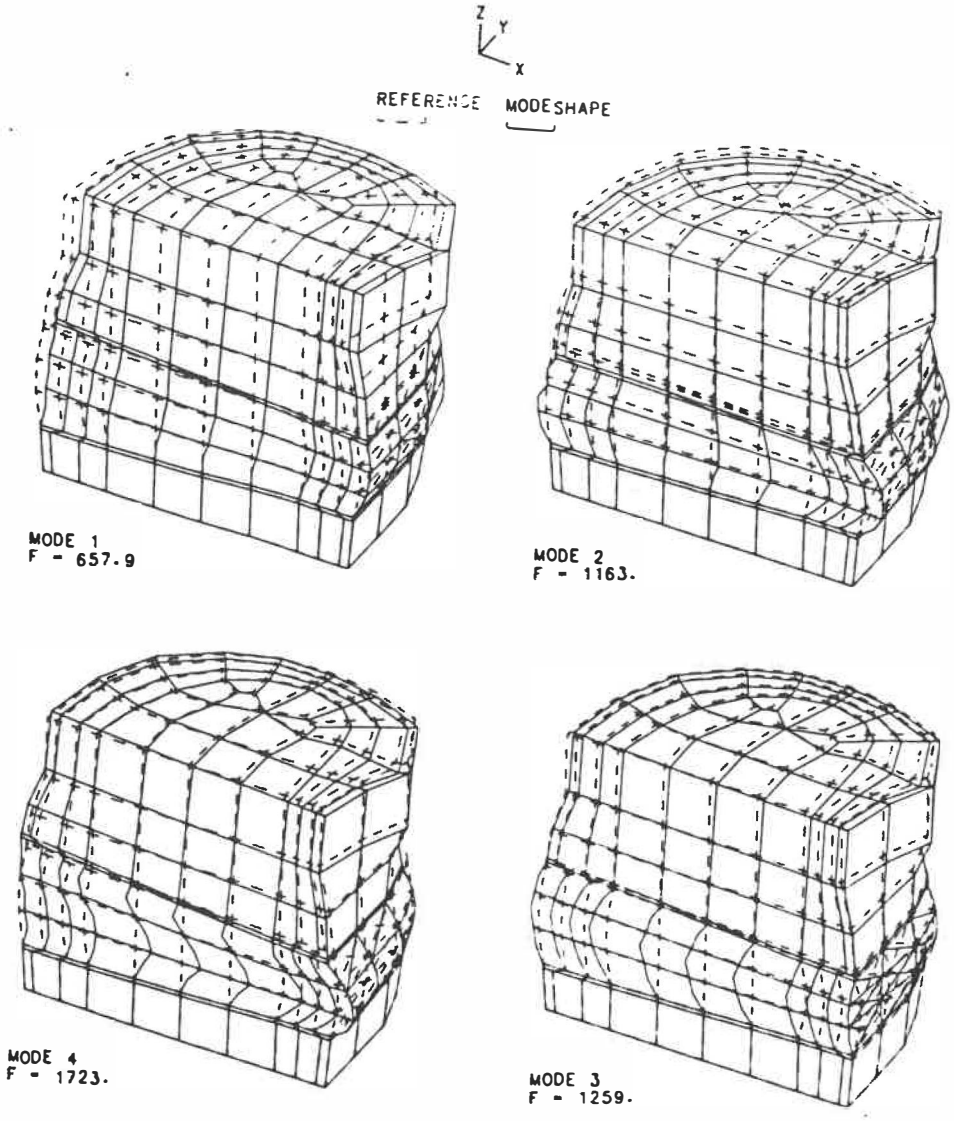

Fig. V.4 The first four mode shapes of the unconstrained 3-D model without the upper body mass (no pre-load). (F = Frequency)